

1-1-2018

Addressing The Proton Radius Puzzle Using Qed-Nrqed Effective Field Theory

Steven Patrick Dye
Wayne State University,

Follow this and additional works at: https://digitalcommons.wayne.edu/oa_dissertations



Part of the [Other Physics Commons](#)

Recommended Citation

Dye, Steven Patrick, "Addressing The Proton Radius Puzzle Using Qed-Nrqed Effective Field Theory" (2018). *Wayne State University Dissertations*. 1922.

https://digitalcommons.wayne.edu/oa_dissertations/1922

This Open Access Dissertation is brought to you for free and open access by DigitalCommons@WayneState. It has been accepted for inclusion in Wayne State University Dissertations by an authorized administrator of DigitalCommons@WayneState.

**ADDRESSING THE PROTON RADIUS PUZZLE USING QED-NRQED
EFFECTIVE FIELD THEORY**

by

STEVEN DYE

DISSERTATION

Submitted to the Graduate School
of Wayne State University,
in partial fulfillment of the requirements
for the degree of

DOCTOR OF PHILOSOPHY

2018

MAJOR: Physics

Approved By:

Advisor

ACKNOWLEDGEMENTS

First and foremost, I would like to thank Gil Paz for being a tremendous advisor throughout my time here at Wayne State. His constant guidance and patience has made me the scientist I am today, and I am eternally grateful for that. I would like to thank the members of my committee Abhijit Majumder, Alexey Petrov, and Paul Pancella, all of whom had mentored me throughout my physics career. I would like to thank Ratna Naik and David Cinabro for their roles as Chair of the Department during my time here. Both had gone above and beyond their responsibilities as Chairs in order to help me succeed. I would like to give a special thank you to Scott Payson who played a pivotal role in shaping my early teaching career. I would like to thank Matthew Gonderinger for his contributions to this work. Finally, I would like to thank my classmates Derek Hazard, Joydeep Roy, Ayesh Gunawardana, Renae Conlin, and Cody Grant for their friendship and comradery during my tenure as a graduate student at Wayne State.

TABLE OF CONTENTS

DEDICATION	ii
ACKNOWLEDGEMENTS	ii
LIST OF FIGURES	vii
LIST OF TABLES	ix
CHAPTER 1: INTRODUCTION	1
1.1 For the Non-Physicist	1
1.2 For the Physicist	2
1.3 Structure of this Dissertation.	2
CHAPTER 2: BACKGROUND	4
2.1 Derivation of the Charge Radius.	4
2.2 Spectroscopy Background.	5
2.3 Spectroscopy Experiment	7
2.3.1 Hydrogen Spectroscopy	7
2.3.2 Muonic Hydrogen Spectroscopy	8
2.4 Scattering Background	12
2.5 Scattering Experiment.	13
2.5.1 Electron-Proton Scattering	13
2.5.2 Muon-Proton Scattering.	14
2.6 Proton Charge Radius Results and Summary	15

CHAPTER 3: THE FIELD THEORIES	17
3.1 QED	17
3.1.1 QED Lagrangian	17
3.1.2 QED Feynman Rules	17
3.2 NRQED	18
3.2.1 NRQED Lagrangian	18
3.2.2 NRQED Feynman Rules	20
3.3 QED-NRQED.	20
CHAPTER 4: ESTABLISHING QED-NRQED	24
4.1 One Photon Exchange and Proven Results.	24
4.1.1 One Photon QED-NRQED Coulomb Gauge.	24
4.1.2 One Photon QED-NRQED Feynman Gauge.	27
4.2 Two Photon Results at Leading Order	28
4.2.1 Two Photon QED-NRQED at Leading Order	28
4.2.2 Two Photon QED at Leading Order	29
4.2.3 Classical Potential	30
4.2.4 Cross Section	31
4.2.5 Anti-lepton Cross Section	34
4.3 Establishing QED-NRQED Summary.	36
CHAPTER 5: TWO PHOTON EXCHANGE RESULTS AT ORDER $1/M^2$	37
5.1 Two Photon Exchange: Feynman Gauge.	37
5.1.1 QED Point Particle	37

5.1.2	Effective Field Theory	41
5.1.2.1	Leading Power	41
5.1.2.2	Order $1/M$: $iD_t - D^2$ interference.	44
5.1.2.3	Order $1/M$: $iD_t - \sigma \cdot B$ interference	45
5.1.2.4	Order $1/M$: D^2 two-photon term	45
5.1.2.5	Order $1/M^2$: $D^2 - D^2$ interference	46
5.1.2.6	Order $1/M^2$: $\sigma \cdot B - \sigma \cdot B$ interference	47
5.1.2.7	Order $1/M^2$: $D^2 - \sigma \cdot B$ interference	48
5.1.2.8	Order $1/M^2$: $iD_t - \nabla \cdot E$ interference	49
5.1.2.9	Order $1/M^2$: $iD_t - \sigma \cdot (D \times E - E \times D)$ interference: Time derivative Feynman rule	50
5.1.2.10	Order $1/M^2$: $iD_t - \sigma \cdot (D \times E - E \times D)$ interference: Seagull Feynman rule	51
5.1.2.11	Order $1/M^2$: $iD_t - \sigma \cdot (D \times E - E \times D)$ interference: Two-photon-time-derivative Feynman rule.	52
5.1.2.12	Order $1/M^2$: $iD_t - D^4$ interference	52
5.1.2.13	Total Result	54
5.1.3	Extraction of b_1 and b_2	54
5.2	Two Photon Exchange: Coulomb Gauge	55
5.2.1	QED Point Particle	55
5.2.2	Effective Field Theory	56
5.2.2.1	Leading Power	56
5.2.2.2	Order $1/M$: $iD_t - D^2$ interference.	57
5.2.2.3	Order $1/M$: $iD_t - \sigma \cdot B$ interference	58

5.2.2.4	Order $1/M$: D^2 two-photon term	59
5.2.2.5	Order $1/M^2$: $D^2 - D^2$ interference	59
5.2.2.6	Order $1/M^2$: $\sigma \cdot B - \sigma \cdot B$ interference	60
5.2.2.7	Order $1/M^2$: $D^2 - \sigma \cdot B$ interference	61
5.2.2.8	Order $1/M^2$: $iD_t - \nabla \cdot E$ interference	62
5.2.2.9	Order $1/M^2$: $iD_t - \sigma \cdot (D \times E - E \times D)$ interference: Time derivative Feynman rule	63
5.2.2.10	Order $1/M^2$: $iD_t - \sigma \cdot (D \times E - E \times D)$ interference: Seagull Feynman rule	64
5.2.2.11	Order $1/M^2$: $iD_t - \sigma \cdot (D \times E - E \times D)$ interference: Two-photon-time-derivative Feynman rule.	65
5.2.2.12	Order $1/M^2$: $iD_t - D^4$ interference	65
5.2.2.13	Total Result	67
5.2.3	Extraction of b_1 and b_2	68
5.3	Two Photon Exchange Results at Order $1/M^2$ Conclusion	68
CHAPTER 6: CONCLUSIONS AND OUTLOOK		70
6.1	Conclusion.	70
6.2	Future Work	70
APPENDIX: A1		73
BIBLIOGRAPHY		75
ABSTRACT		82
AUTOBIOGRAPHICAL STATEMENT		83

LIST OF FIGURES

Figure 2.1	A photon interacting with a proton.	4
Figure 2.2	Plot from the 2010 Pohl paper showing their results [1]. Displayed is the number of events as a function of the laser frequency.	9
Figure 2.3	Plots from [3]. Muonic hydrogen resonances for singlet and triplet transitions. 10	
Figure 2.4	Plots from [16]. Shown here are the measured frequencies from each transition, the expected deuteron radius, the CODATA-2010 result, and the $\mu p + \text{iso}$ result, which is obtained by combining the proton radius from muonic hydrogen and the electronic isotope shift.	11
Figure 2.5	Plot from [33]. Ratio of electric to magnetic form factor as extracted by Rosenbluth measurements (squares) and from the JLab measurements of recoil polarization (circles). The dashed line is the fit to the polarization transfer data.	13
Figure 2.6	Plot from Ref. [53] which highlights the discrepancy between the atomic and muonic results. The Proton charge radius from muonic hydrogen is marked as red while hydrogen spectroscopy is marked as blue, and electron-proton scattering as green. The CODATA value accounts for e-p scattering, H and deuterium (D) spectroscopy but does not consider the muonic results.. . . .	15
Figure 2.7	Plot from Ref. [53] which highlights the discrepancy between the atomic and muonic results. The Proton charge radius from muonic hydrogen is marked as red while hydrogen spectroscopy is marked as blue, and electron-proton scattering as green. The CODATA value accounts for e-p scattering, H and deuterium (D) spectroscopy but does not consider the muonic results.. . . .	15
Figure 2.8	Plot from Ref. [53]. Deuteron charge radii as obtained from μd spectroscopy (red), by combining μp spectroscopy and the H-D iso-shift measurement (brown), from electron scattering (green) and only D spectroscopy (blue). The CODATA value does not account for the muonic results but considers both proton and deuteron data from Ref. [16]	16

Figure 4.1	QED-NRQED Feynman diagrams that give a non-zero contribution to elastic lepton-proton scattering at $\mathcal{O}(Q_p\alpha)$ up to power m^2/M^2 . The double line denotes the NRQED field. The dashed (curly) line represents Coulomb (transverse) photon. The dot, circle, and cross vertices represent the Coulomb, Fermi, and Darwin terms, respectively, see Ref. [61] for details.	25
Figure 4.2	QED-NRQED Feynman diagrams that give a non-zero contribution to elastic lepton-proton scattering at $\mathcal{O}(Q_p\alpha)$ up to power m^2/M^2 . The double line denotes the NRQED field. The dashed (curly) line represents Coulomb (transverse) photon. See Ref. [61] for details.	27
Figure 4.3	QED-NRQED Feynman diagrams contributing to elastic lepton-proton scattering at $\mathcal{O}(Q_p^2\alpha^2)$ at leading power in m/M . The double line denotes the NRQED field.	28
Figure 4.4	The leptonic part of the $\mathcal{O}(Q_p^2\alpha^2)$ amplitude at leading power in m/M for a lepton (left) and an anti-lepton (right).	35

LIST OF TABLES

Table 3.1	QED Feynman Rules	18
Table 3.2	NRQED Propagators	20
Table 3.3	NRQED Vertices.	21
Table 3.4	Possible interactions in the QED-NRQED EFT	22
Table 3.5	Possible interactions for the experiments	22

CHAPTER 1: INTRODUCTION

1.1 For the Non-Physicist

Everything in the visible universe is made up of particles. Learning and understanding the properties of these particles and how they interact with each other is the goal that scientists in the field of physics strives to achieve. The properties of these particles can include their mass, electric charge, spin, among many others.

The particle I am most interested in is the proton. Including the neutron and the electron, these three particles make up all matter in our everyday lives. The property that most interests me is called the charge radius. The proton has an electric charge and some finite size, so it is reasonable to assume that this electric charge is distributed throughout the volume of the proton. Intuitively the charge radius is defined as the average distance the electric charge is from the center of the proton. In the past, the charge radius has been measured through two different kinds of experiments; electron-proton scattering, which is when an electron interacts electromagnetically with a proton at high energies, and electron spectroscopy, which is when an electron pairs up with a proton to create a hydrogen atom by interacting electromagnetically at low energies. The charge radius of the proton calculated from these experiments were found to be in reasonable agreement with each other.

In 2010 however an experiment was performed to measure the proton charge radius using muonic hydrogen spectroscopy. The experiment was the similar to spectroscopy experiments performed in the past, except that the electron was replaced with a muon, an exotic particle that is very similar to the electron, except for being much heavier. The result of this experiment showed that the proton charge radius was much smaller than what was measured in previous experiments. This has led to a proposal for a new experiment, consisting of muon-proton scattering, to see if the charge radius is consistent with the muonic hydrogen result, or with the already established electron-proton and hydrogen spectroscopy results. My project has been to come up with a new way to calculate the charge radius from the data from this future experiment. This paper establishes the properties of this new method, and presents

calculated results.

1.2 For the Physicist

In 2010 the first measurement of the proton charge radius from spectroscopy of muonic hydrogen was found to be 0.84184(67) fm by the Charge Radius Experiment with Muonic Atoms (CREMA) collaboration [1]. This measurement puts the proton charge radius five standard deviations away from the regular hydrogen spectroscopy result of 0.8768(69) fm [2]. In the seven years since there has been a large interest in the physics field to solve this puzzle to no avail, and in fact the puzzle has only gotten worse. A reanalysis performed by CREMA of the charge radius from muonic hydrogen obtained a result of 0.84087(39) fm [3], while the latest combined atomic hydrogen and electron elastic scattering results obtain a result of 0.8751(61) fm, increasing the discrepancy to 5.6 standard deviations [4].

Contained within this dissertation is the establishment of a new Effective Field Theory (EFT). This EFT is a hybrid between Quantum Electrodynamics (QED) and Non-Relativistic Quantum Electrodynamics (NRQED), and describes the electromagnetic interactions between a relativistic particle and a non-relativistic one. In particular, we are interested in the one photon exchange (1PE) and two photon exchange (TPE) between a relativistic lepton (specifically either an electron or a muon), and a non-relativistic proton. This QED-NRQED EFT is motivated by the MUon proton Scattering Experiment (MUSE), which will examine e^+p , e^-p , μ^+p , and μ^-p elastic scattering [5]. MUSE is essential to solving the proton charge radius puzzle, as calculations of the radius has not performed from muonic elastic scattering thus far. The experiment is scheduled to begin dating data in 2018/2019.

1.3 Structure of this Dissertation

This dissertation is structured as follows: in section 2 the background of the proton charge radius and how it is extracted from experiment is discussed. Section 3 will present the field theories QED and NRQED and illustrate how they are combined to create QED-

NRQED. In section 4 we present 1PE calculations and TPE calculations at leading order in QED-NRQED and compare them to related calculation methods, thereby establishing this new EFT. In section 5 we present TPE calculations to higher orders in order to determine values for the Wilson coefficients of interest. In section 6 we present the conclusions and outlook for the EFT, followed by the Appendix.

CHAPTER 2: BACKGROUND

While the proton charge radius puzzle is relatively new, the methodology for measuring and calculating the charge radius is well established. This chapter contains the derivation of the proton charge radius, as well as background information on the two types of experiments used to calculate the charge radius, spectroscopy and lepton-proton scattering. This background will include theoretical calculations and experimental results. It should be noted that all calculations presented in this document and in particle physics in general are performed using “natural units”, where $\hbar = c = 1$.

2.1 Derivation of the Charge Radius

Electromagnetic interactions between particles are described through the matrix element of the electromagnetic current

$$\langle N(p') | J_\mu^{em} | N(p) \rangle = \bar{u}(p') \left[\gamma_\mu F_1(q^2) + \frac{i\sigma_{\mu\nu}}{2M} F_2(q^2) q^\nu \right] u(p), \quad (2.1)$$

where $F_1(q^2)$ and $F_2(q^2)$ are the Pauli and Dirac form factors, and $q = p' - p$. Form factors

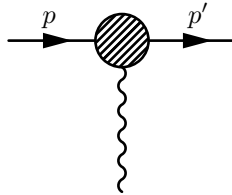


Figure 2.1: A photon interacting with a proton.

describe the physical properties of the particle. These form factors can be written in a different basis as the electric and magnetic form factors through the relations

$$G_E(q^2) = F_1(q^2) + \frac{q^2}{4M^2} F_2(q^2) \quad G_M(q^2) = F_1(q^2) + F_2(q^2). \quad (2.2)$$

It is with these form factors that charge radius of a particle can be defined as

$$\langle r_E^2 \rangle^{1/2} = \frac{6}{G_E(0)} \left. \frac{dG_E(q^2)}{dq^2} \right|_{q^2=0}. \quad (2.3)$$

Since the charge radius is defined as the slope of $G_E(q^2)$ evaluated at $q^2 = 0$, one might naively think that only data of G_E at low q^2 would be required. This is not the case however as this data cannot achieve the required precision without additional information [6]. Ref. [7] suggests supplementing the low Q^2 ($Q^2 = -q^2$) scattering data with constraints on the curvature and higher-order derivatives of the form factor from chiral perturbation theory.

2.2 Spectroscopy Background

One method that the proton charge radius is measured through is spectroscopy, which is the study of emitted electromagnetic radiation. This section contains information on how the charge radius is calculated.

The proton charge radius can be measured through the Lamb shift, which is the difference in energy between the $2S_{\frac{1}{2}}$ and $2P_{\frac{1}{2}}$ states [8]. Note that the Dirac equation predicts that these two states have the same energy. There are two sources for this energy shift, one being the radiative corrections to the interaction of a lepton-proton pair, such as vacuum polarization, and the other being through the different interactions that the orbits have with the proton. The $2S_{\frac{1}{2}}$ state wave function is spherical in its distribution and has a maximum probability of being at the center of the atomic nucleus, meaning that the lepton has a finite probability of being inside the proton. When the lepton is inside the proton, there is some shielding of the electromagnetic field, reducing the strength of the interaction. The $2S_{\frac{1}{2}}$ state probability distribution is described by squaring its wave function, ($|\Psi_{2,0,0}|^2$). The $2P_{\frac{1}{2}}$ state wave function has a distribution similar to a figure eight, meaning that as the wave function approaches the center of the proton, the probability of the lepton being there approaches zero. This means that the $2S_{\frac{1}{2}}$ orbital has a greater chance of being inside the proton than the $2P_{\frac{1}{2}}$ orbital does, leading to greater shielding in the $2S_{\frac{1}{2}}$ state, resulting in a shift in the

energy states between these two levels. The $2P_{\frac{1}{2}}$ probability distribution can be described by squaring its wave function, ($|\Psi_{2,1,0}|^2$). The probability distributions can be expressed through the relations

$$|\Psi_{2,0,0}|^2 = \frac{1}{32\pi a_0^3} \left(2 - \frac{r}{a_0}\right)^2 e^{-r/a_0} \quad |\Psi_{2,1,0}|^2 = \frac{1}{32\pi a_0^3} \frac{r^2}{a_0^2} e^{-r/a_0} \cos^2 \theta, \quad (2.4)$$

where r is the radius of the particle orbiting the proton, a_0 is the Bohr radius, and θ is the angle at which the lepton is currently at relative to the z-axis.

From Lamb shift measurements, the proton charge radius can be calculated by the difference in energy between a point like particle and from that measured from experiments. The Fourier transform is defined as

$$\rho(\vec{r}) = \frac{1}{(2\pi)^3} \int d^3q F(\vec{q}) e^{-i\vec{q}\cdot\vec{r}} \quad F(\vec{q}) = \int d^3r \rho(\vec{r}) e^{i\vec{q}\cdot\vec{r}}, \quad (2.5)$$

where \vec{q} is the three-dimensional momentum of the exchanged photon. Using Gauss's law, the electric potential of the proton can be written as

$$V(\vec{r}) = \frac{|e|}{(2\pi)^3} \int d^3q e^{-i\vec{q}\cdot\vec{r}} \frac{F(\vec{q})}{q^2}. \quad (2.6)$$

For small \vec{q} , we can assume that the proton charge distribution $\rho(\vec{r})$ is spherically symmetric, and therefore can use a Taylor Series expansion on the Fourier transform and write it as $F(\vec{q}) = 1 - \frac{\vec{q}^2 \langle r^2 \rangle}{6} + \dots$, where $\int d^3r \rho(\vec{r}) = 1$ and $\langle r^2 \rangle = \int d^3r \rho(\vec{r}) r^2$. Using this and the relation

$$\frac{1}{4\pi r} = \frac{1}{(2\pi)^3} \int d^3q \frac{e^{-i\vec{q}\cdot\vec{r}}}{q^2}, \quad (2.7)$$

The potential energy of the proton can be written as

$$V(\vec{r}) = \frac{|e|}{4\pi r} - \frac{\langle r^2 \rangle}{6} |e| \delta^3(\vec{r}) + \dots \quad (2.8)$$

Using this shift in potential energy and perturbation theory, the difference in energy levels

between a point particle and a particle with a finite size can be calculated to be

$$\Delta E_{\langle r^2 \rangle} = \langle \psi | \frac{\langle r^2 \rangle}{6} | e | \delta^3(\vec{r}) | \psi \rangle = \frac{2\alpha^4}{3n^3} m_r^3 \langle r^2 \rangle \delta_{\ell 0}, \quad (2.9)$$

where n is the principle quantum number of the wave function, $\alpha = e^2/4\pi$ is the fine structure constant, and m_r is the reduced mass. Since the reduced mass for muonic hydrogen is of the order 200 times larger than atomic hydrogen, the energy shift for muonic hydrogen will be of the order 200^3 times larger. Radiative effects are however still a factor in extracting the charge radius. The proton structure effects for atomic hydrogen is of the order 10^{-9} eV, while for muonic hydrogen it is of the order 10^{-3} eV. Since the effect is larger the muonic hydrogen than it is for atomic hydrogen, it allows for a better precision measurement on the charge radius of the proton, as the Lamb shift measurement itself is of the order 10^{-5} eV.

2.3 Spectroscopy Experiment

2.3.1 Hydrogen Spectroscopy

Atomic spectroscopy has been the benchmark for precision electromagnetic measurements for the past 70 years. Because of its rich history, this section will only focus on the experiments referenced by the CODATA-2014 report [4] and the newest hydrogen spectroscopy result. The CODATA value of the proton charge radius is based primarily on precision spectroscopy results from Ref [9, 10, 11, 12], and calculations of bound-state QED [13, 14].

Ref. [9] measured the absolute frequency of the hydrogen $1S - 2S$ two photon transition, and obtained a measurement of 2 466 061 413 187 103(46) Hz. This was acquired by phase coherent comparison, which used an atomic cesium fountain clock as a frequency standard. Ref. [10] measured the stability of the fine structure constant α , and concluded that $\dot{\alpha}/\alpha = (-.09 \pm 2.9) \times 10^{-15} \text{ yr}^{-1}$, which is consistent with zero. This was performed by measuring the $1S - 2S$ transition and comparing it to [9]. The same experimental setup was used in both [9] and [10]. Ref. [11] performed a reanalysis of spectroscopy data, including obtaining improved values of the $1S_{1/2}$ Lamb shift and of the $2S_{1/2} - nS_{1/2}, nD_J$ frequencies, where

n is the wave number, reducing the uncertainty in the Rydberg constant R_∞ , and to the Lamb Shift results. Ref. [12] performed an optical frequency measurement of the $2S - 12D$ two-photon transitions in hydrogen and deuterium. They obtained Lamb shift values of $L_{1S-2P} = 8172.837(22)$ MHz and $L_{2S-2P} = 1057.8446(29)$ MHz for the hydrogen atom, and $L_{1S-2P} = 8183.966(22)$ MHz and $L_{2S-2P} = 1059.2337(29)$ MHz for deuterium.

The most recent hydrogen spectroscopy experiment measured the $2S - 4P$ transition frequency in hydrogen [15]. The results of this experiment put the charge radius at $0.8335(95)$ fm, which is consistent with the muonic hydrogen results and 3.3 standard deviations away from previously established hydrogen result. This latest result has not been included in the CODATA results, nor the muonic hydrogen results.

2.3.2 Muonic Hydrogen Spectroscopy

Unlike atomic spectroscopy, which has a rich history of experiments, muonic spectroscopy currently only has three published experimental results, two muonic hydrogen experiments and one muonic deuterium experiment, all of which have been performed by the CREMA collaboration. Here we provide a summary of the experimental set-ups and the resultant measurements.

The first muonic hydrogen experiment was performed in 2010 by Pohl *et al.* at the Paul Scherrer Institute (PSI) in Switzerland [1]. Here they performed laser spectroscopy of the $(2S_{1/2}^{F=1} - 2P_{3/2}^{F=1})$ transition in muonic hydrogen, where F is the hyperfine splitting level. The experiment was set up as follows: a low energy muon beam with an energy around 5 keV is stopped in a low-pressure hydrogen gas target with a temperature of 300 K and a pressure of 1 mbar. Here highly excited muonic proton bound states are formed. About 1% of the muonic protons end up in the $2S$ -state, which has a lifetime of around $1 \mu\text{s}$ within the gas target. After a delay of $0.9 \mu\text{s}$, the muonic hydrogen is illuminated by a laser pulse at a wavelength of $6.0 \mu\text{m}$. The laser induces the $2S \rightarrow 2P$ transition, after which decays back to the ground state, emitting a photon. The frequency of these emitted photon were

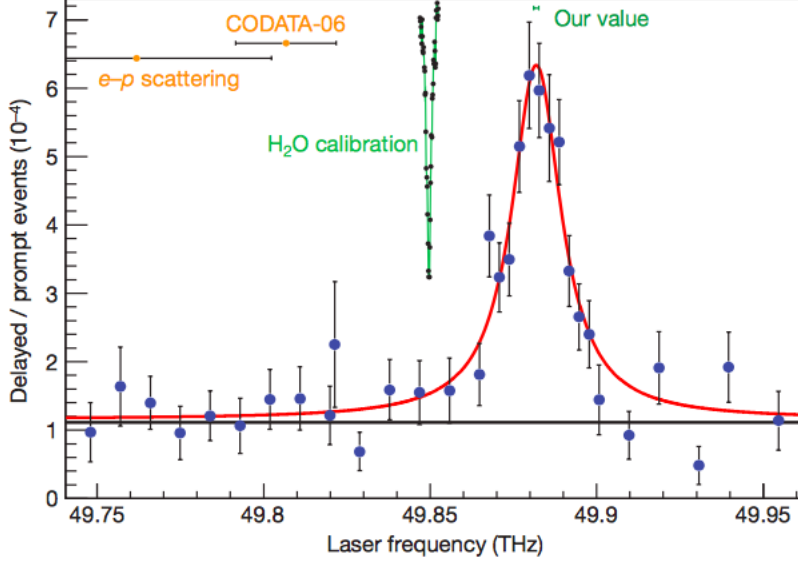


Figure 2.2: Plot from the 2010 Pohl paper showing their results [1]. Displayed is the number of events as a function of the laser frequency.

measured to be 49,881.88(76) GHz. Using this measurement, and the relation

$$\Delta E_{Lamb} = 209.9779(49) - 5.2262r_p^2 + 0.0347r_p^3, \quad (2.10)$$

the proton charge radius is calculated to be $r_p = 0.84184(67)$ fm. In Eq. 2.10, the first term accounts for bound-state QED contributions (radiative, recoils, binding, and relativistic corrections), the second term takes into account the shift of the energy levels caused by the finite size of the proton, and the third term is the two-photon exchange (TPE), which is related to the proton polarizability. Note that all of these numbers have units of meV.

The second experiment was performed by the same group in 2013 using the same experimental set-up as the experiment in 2010 [3]. Here the $2S_{1/2}^{F=0} - 2P_{3/2}^{F=1}$ transition frequency was measured, along with a reevaluation of the $2S_{1/2}^{F=1} - 2P_{3/2}^{F=2}$ transition frequency. With the addition of the $2S_{1/2}^{F=0} - 2P_{3/2}^{F=1}$ transition frequency the hyperfine splitting of the $2S_{1/2}$ state was determined to be $\Delta E_{HFS}^{exp} = 22.8089(51)$ meV, making the calculation of the proton charge radius independent of theoretical predictions for the $2S$ hyperfine splitting energy. The measured values of the $2S_{1/2}^{F=0} - 2P_{3/2}^{F=1}$ and $2S_{1/2}^{F=1} - 2P_{3/2}^{F=2}$ transition frequencies are

54,611.16(1.05) GHz. and 49,881.35(65) GHz. respectfully. The proton charge radius can now be extracted from Lamb shift measurements from the relation

$$\Delta E_{Lamb} = 206.0336(15) - 5.2275(10)r_p^2 + \Delta E_{TPE}, \quad (2.11)$$

where ΔE_{TPE} is the two-photon exchange contribution. Here all values have units of meV. The third term in Eq. 2.11 is the same as the third term in Eq. 2.10, the only difference being that Eq. 2.11 no longer is dependent on the theoretical prediction of the $2S$ hyperfine splitting energy since it was measured in [3]. With the hyperfine splitting energy result, the change in energy due to the TPE is determined to be $\Delta E_{TPE} = 0.0332(20)$ meV. With these measurements and Eq. 2.11, the proton charge radius was recalculated to be $r_p = 0.84087(39)$ fm.

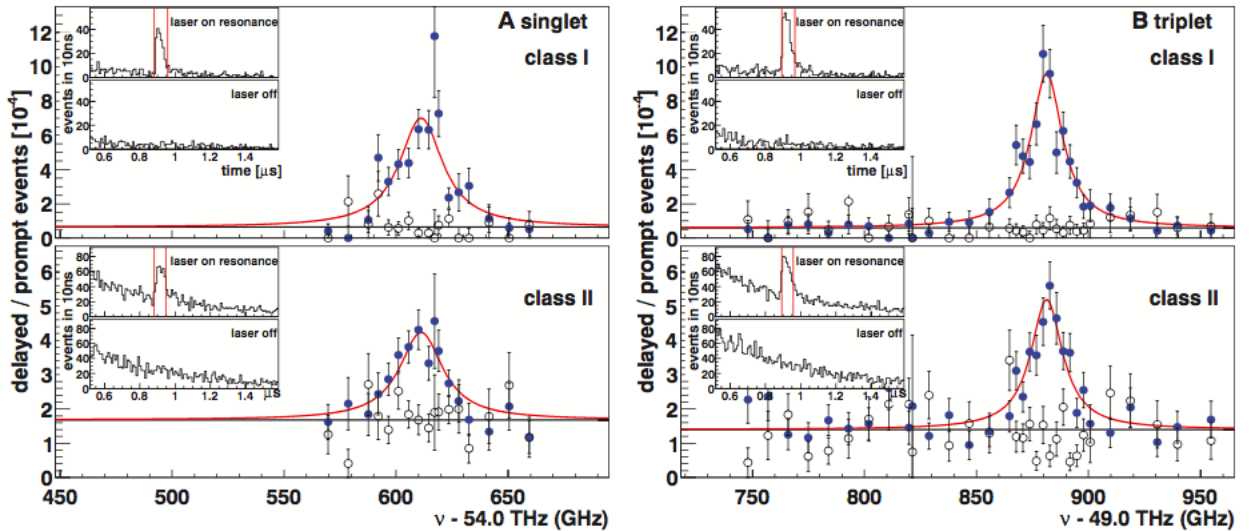


Figure 2.3: Plots from [3]. Muonic hydrogen resonances for singlet and triplet transitions.

The same experiment was performed a third time in 2016, this time using muonic deuterium instead of muonic hydrogen [16]. Using the same experimental set-up as the previous experiments, the $2S_{1/2}^{F=3/2} \rightarrow 2P_{3/2}^{F=5/2}$, $2S_{1/2}^{F=1/2} \rightarrow 2P_{3/2}^{F=3/2}$, and $2S_{1/2}^{F=1/2} \rightarrow 2P_{3/2}^{F=1/2}$ transitions were measured. The frequencies measured were 50816.27(91) GHz, 52061.2(2.03) GHz, and 52154.1(2.23) GHz, respectfully. From these measurements, the charge radius

of a deuteron is $r_d = 2.12562(78)$ fm, a 7.5σ difference from the CODATA-2010 value of $r_d = 2.1424(21)$ fm [17]. This experiment shows that the proton radius problem extends beyond just the proton itself.

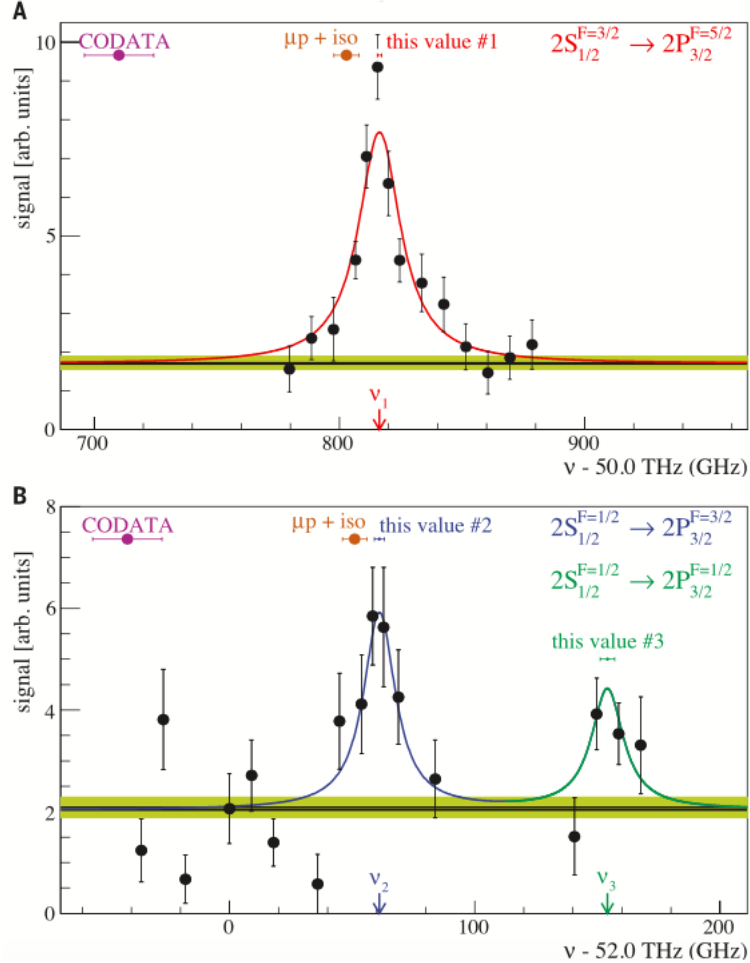


Figure 2.4: Plots from [16]. Shown here are the measured frequencies from each transition, the expected deuteron radius, the CODATA-2010 result, and the $\mu p + \text{iso}$ result, which is obtained by combining the proton radius from muonic hydrogen and the electronic isotope shift.

Future spectroscopy measurements are anticipated [18] in muonic ^3He and ^4He , where nuclear structure effects are important for interpretation [19, 20, 21, 22]. Several other experimental groups plan to measure the hyperfine splitting energy of various muonic atoms with higher precision [23, 24, 25].

2.4 Scattering Background

Information on the two form factors $G_E(Q^2)$ and $G_M(Q^2)$ are obtained from ep scattering experiments. The ratio of these two form factors are extracted from experiments through two different methods; polarization transfer technique, and Rosenbluth separation [26].

Unpolarized electron scattering experiments use the Rosenbluth separation method [27, 28, 29, 30, 31, 32], where the e^-p elastic cross section is measured at a fixed four-momentum transfer, Q^2 , while varying the electron scattering angle and the incident energy of the electron. The four-momentum is set at $Q^2 = -q^2 = 4EE' \sin^2(\theta/2)$, where E is the incident electron beam energy, E' is the scattered electron energy, and θ is the angle of the scattered electron. The form factors are then extracted from the reduced Born cross section, given by,

$$d\sigma_R = \frac{d\sigma}{d\Omega} \frac{(1 + \tau)\epsilon}{\sigma_{Mott}\tau} = \frac{\epsilon}{\tau} G_E^2(Q^2) + G_M^2(Q^2), \quad (2.12)$$

where σ_{Mott} is the cross section for elastic scattering off a point-like proton, $\epsilon = [1 + 2(1 + \tau) \tan^2(\theta/2)^{-1}]$ is the virtual photon polarization as measured in the lab frame, $\tau = Q^2/4M^2$, and M is the proton mass. $G_E^2(Q^2)$ is then proportional to the ϵ dependence of σ_R and $G_M^2(Q^2)$ is proportional to the cross section extrapolated to $\epsilon = 0$.

Recoil polarization experiments, [34, 35, 36, 37, 38] measure the polarization of the recoiling electron proton after scattering a polarized electron off an unpolarized proton target. This is referred to as the Polarization transfer technique. The ratio of the electric and magnetic form factors is proportional to the ratio of the transverse and longitudinal polarization of the recoil proton. the ratio of the form factors can be extracted from spin-dependent elastic scattering of polarized electrons from polarized proton [39]. The ratio of the electric to magnetic form factors is typically measured as, $\frac{\mu_p G_E(Q^2)}{G_M(Q^2)}$, where μ_p is the proton magnetic moment. The discrepancy between the ratios is thought to be due to the absence of TPE corrections.

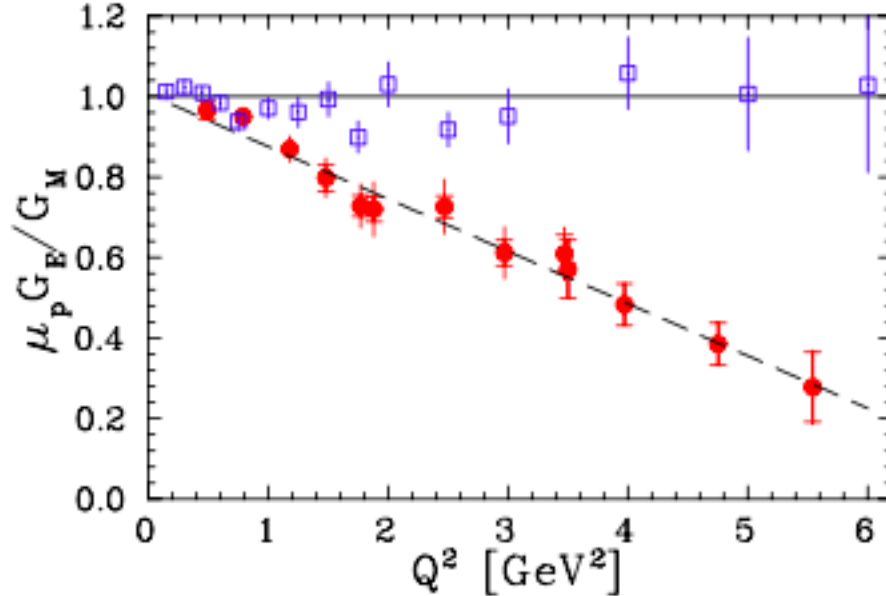


Figure 2.5: Plot from [33]. Ratio of electric to magnetic form factor as extracted by Rosenbluth measurements (squares) and from the JLab measurements of recoil polarization (circles). The dashed line is the fit to the polarization transfer data.

2.5 Scattering Experiment

2.5.1 Electron-Proton Scattering

For the past 50 years, electron scattering has been extensively used to discover information about the proton. In particular, it is used to determine the form factors, which describe the physical properties of the particle. Here we will take a look at a select few of the experiments that measured the cross sections of e^+p and e^-p , and the different methods used to extract the charge radius from these measurements.

The OLYMPUS experiment at DESY was designed to measure the ratio between e^+p and e^-p elastic scattering cross sections [40]. Data for this experiment was collected in 2012. In 2013 MAMI performed for low Q^2 (10^{-4} GeV) ep scattering experiments [41]. They did this by utilizing initial state radiation. The PRad collaboration at Jefferson Laboratory [42] looked at e^-p at low Q^2 (10^{-4} GeV). This was done by using a windowless H target and a novel non-magnetic calorimeter. The data from this experiment is currently being analyzed [43]. CLAS at Jefferson Lab measured e^+p and e^-p cross sections in order to determine the

TPE contribution to the electromagnetic form factors [44].

Since the proton charge radius can be extracted from electron-proton scattering, some of the discussion in the literature has focused on reevaluation of the extraction of proton radii from scattering, see for example the z -expansion based studies [45, 46, 47], and references therein¹. While leading to a more robust error estimate, the value for the proton charge radius of [45, 47] generally disfavors the muonic hydrogen result. It should be noted that other studies not based on the z expansion listed, e.g., in [48], find values that are consistent with the muonic hydrogen result.

2.5.2 Muon-Proton Scattering

Future proton charge radius results will be measured by elastic μ^+p and μ^-p scattering at the MUonic Scattering Experiment (MUSE) at the Paul Scherrer Institute in Switzerland [5]. The typical momentum of the muons in the experiment is of the order of the muon mass, $m \sim 100$ MeV. At these energies, the muon is relativistic but the proton can still be considered as non-relativistic. The appropriate effective field theory for such kinematics is QED-NRQED, and is the topic of this dissertation. MUSE will measure cross sections for elastic $\mu^\pm p$ and $e^\pm p$ scattering in the PSI π M1 beam line. The π M1 channel transports mixed secondary beams of electrons, muons, pions, and protons generated by interactions of the primary proton beam at the M1 production target. The primary beam identification for triggering purposes uses an array of thin scintillators with SiPM readout located upstream of the target, which are required to have <300 ps resolution along the high-rate capability and high efficiency. MUSE will test beyond standard model physics, and enhance two photon exchange effects. The beam energies for the leptons will be set at 115, 153, and 210 MeV. Data is expected to be taken in late 2018/ early 2019 [5].

¹Some other z -expansion based studies do not bound the coefficients of the z expansion [49, 50, 51] or modify it [52]. These may result in values that are lower than [45, 47]. See [45] for a discussion of the bounding of the coefficients.

2.6 Proton Charge Radius Results and Summary

Here is presented the extracted values of the proton charge radius from the different experiments. The CODATA14 value, which is the combination of the atomic spectroscopy and ep scattering is $0.8751(61)$ fm [4]. The value of the charge radius from muonic spectroscopy is $0.84087(39)$ fm [3], a discrepancy of 5.6σ from the CODATA14 result. The ep scattering in particular has many different evaluations to compare to.

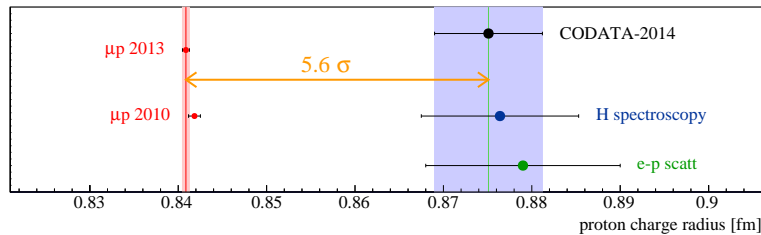


Figure 2.6: Plot from Ref. [53] which highlights the discrepancy between the atomic and muonic results. The Proton charge radius from muonic hydrogen is marked as red while hydrogen spectroscopy is marked as blue, and electron-proton scattering as green. The CODATA value accounts for e-p scattering, H and deuterium (D) spectroscopy but does not consider the muonic results.

For the past 10 years, multiple reanalyzes have been performed to the electron scattering data to determine the charge radius of the proton. Below is a table showing some of the most recent results. The proton charge radius problem also arises within the deuteron as

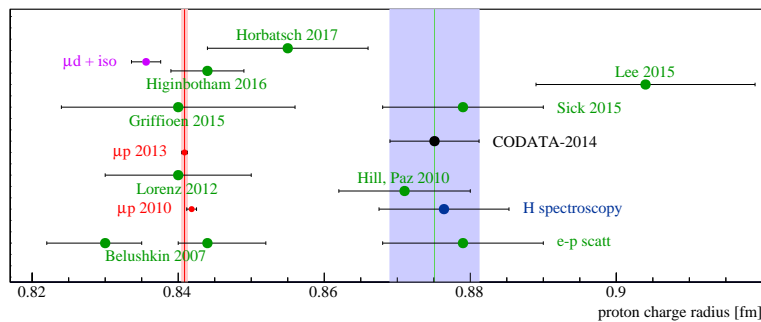


Figure 2.7: Plot from Ref. [53] which highlights the discrepancy between the atomic and muonic results. The Proton charge radius from muonic hydrogen is marked as red while hydrogen spectroscopy is marked as blue, and electron-proton scattering as green. The CODATA value accounts for e-p scattering, H and deuterium (D) spectroscopy but does not consider the muonic results.

the deuteron charge radius is highly correlated to the proton charge radius. This correlation is due to the measured isotope shift of the $1S \rightarrow 2S$ transition in atomic hydrogen and deuterium [54, 55], and contributes to the difference of the squared deuteron and proton charge radii as [56]

$$r_d^2 - r_p^2 = 3.82007(65) \text{ fm}^2. \quad (2.13)$$

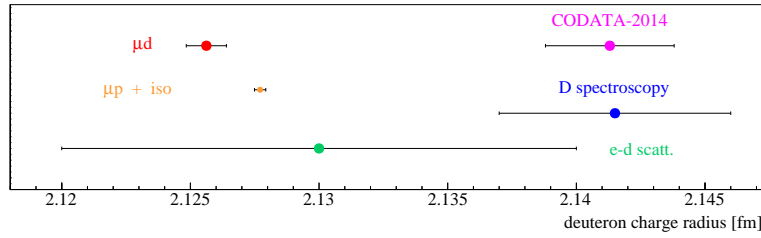


Figure 2.8: Plot from Ref. [53]. Deuteron charge radii as obtained from μd spectroscopy (red), by combining μp spectroscopy and the H-D iso-shift measurement (brown), from electron scattering (green) and only D spectroscopy (blue). The CODATA value does not account for the muonic results but considers both proton and deuteron data from Ref. [16]

Even seven years after the first mysterious results from the first CREMA experiment the proton charge radius puzzle remains unresolved. With the two different ways to measure the charge radius, scattering and spectroscopy, comes a need to compare the results of these experiments directly. Our QED-NRQED EFT hopes to make this connection in order to do just this.

CHAPTER 3: THE FIELD THEORIES

In this section, the field theories QED and NRQED are introduced and the EFT QED-NRQED is established as well. Presented here are the properties of these field theories.

3.1 QED

Quantum electrodynamics is a relativistic quantum field theory that describes the interactions between light and matter. QED was first established in 1928 [57] by Paul Dirac and is perhaps one of the most physically sound theories in science as it is able to bring full agreement between quantum mechanics and special relativity through the Dirac equation.

3.1.1 QED Lagrangian

The QED Lagrangian is can be expressed as

$$\mathcal{L} = \bar{\ell} \gamma^\mu i (\partial_\mu + ieQ_\ell A_\mu) \ell - m\bar{\ell}\ell, \quad (3.1)$$

where Q_ℓ is the electric charge of the particle (-1 for an electron or a muon). Technically QED only describes the interactions of point particles, so it cannot fully describe the interactions or more complex particles, such as the proton.

3.1.2 QED Feynman Rules

From the QED Lagrangian, the QED Feynman rules can be extracted, and are presented in Table 3.1

Here λ is the “mass” of the photon that will be used to regulate infrared divergences.

In R_Z gauge, the QED photon propagator is given by [58]

$$D^{\mu\nu}(q) = \frac{-i}{q^2 - \lambda^2 + i\epsilon} \left(g^{\mu\nu} - (1 - \xi) \frac{q^\mu q^\nu}{q^2} \right) \quad (3.2)$$

In Feynman gauge, $\xi = 1$, which reproduces the photon propagator in Table 3.1. In Coulomb

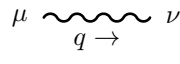
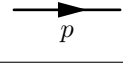
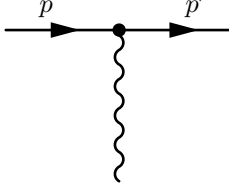
QED Feynman Rules		
Photon Propagator		$\frac{-i g_{\mu\nu}}{q^2 - \lambda^2 + i\epsilon}$
Fermion Propagator		$\frac{i(\not{p} + m)}{p^2 - m^2 + i\epsilon}$
QED vertex		$iQe\gamma^\mu$

Table 3.1: QED Feynman Rules

gauge, the photon propagator is

$$D_{\mu\nu}(q) = \begin{cases} \frac{i}{|\vec{q}|^2 + \lambda^2 + i\epsilon} & \mu, \nu = 0 \\ \frac{i}{q^2 - \lambda^2 + i\epsilon} \left(\delta_{ij} - \frac{q_i q_j}{|\vec{q}|^2} \right) & \mu = i \neq 0, \nu = j \neq 0 \\ 0 & \text{otherwise} \end{cases} \quad (3.3)$$

A derivation of this propagator, as well as background information on the gauges typically used in electromagnetism can be found in Ref [59].

3.2 NRQED

3.2.1 NRQED Lagrangian

The NRQED Lagrangian describes the interaction of non-relativistic, possibly composite, spin-half particle ψ with the electromagnetic field. Up to and including the $1/M^2$, where M is the mass of the spin-half particle, the NRQED Lagrangian is [60, 61]

$$\mathcal{L} = \psi^\dagger \left\{ iD_t + c_2 \frac{\mathbf{D}^2}{2M} + c_F Qe \frac{\boldsymbol{\sigma} \cdot \mathbf{B}}{2M} + c_D Qe \frac{[\boldsymbol{\nabla} \cdot \mathbf{E}]}{8M^2} + ic_S Qe \frac{\boldsymbol{\sigma} \cdot (\mathbf{D} \times \mathbf{E} - \mathbf{E} \times \mathbf{D})}{8M^2} \right\} \psi + \dots, \quad (3.4)$$

where $D_t = \partial/\partial t + iQeA^0$, $\mathbf{D} = \nabla - iQe\mathbf{A}$, $\boldsymbol{\sigma}$ are the Pauli matrices, Q is the electric charge of the particle (in this case, for a proton, $Q_p = 1$ and for an electron and a muon, $Q_\ell = -1$), and e is the electromagnetic coupling constant¹. Here D_t and \mathbf{D} are the components of the covariant derivative $D_\mu = \partial_\mu + iQeA_\mu$. The notation $[\nabla \cdot \mathbf{E}]$ denotes that the derivative is acting only on \mathbf{E} and not on ψ . For a review see [62]. The (hidden) Lorentz invariance of the Lagrangian implies that $c_2 = 1$ [63, 64, 65]. The other Wilson coefficients can be related to the proton electromagnetic form factors

$$\langle p(p') | J_\mu^{\text{em}} | p(p) \rangle = \bar{u}(p') \left[\gamma_\mu F_1(q^2) + \frac{i\sigma_{\mu\nu}}{2M} F_2(q^2) q^\nu \right] u(p), \quad (3.5)$$

via $c_F = F_1(0) + F_2(0)$, $c_D = F_1(0) + 2F_2(0) + 8M^2 F_1'(0)$, where $F_1' = dF_1(q^2)/dq^2$, and $c_S = 2c_F - F_1(0)$. The latter can also be determined by the hidden Lorentz invariance of the Lagrangian [63, 64, 65]. The NRQED Feynman rules can be extracted from figure 3 of [61] by multiplying the vertices by $-i$ and the propagators by i .

At $1/M^2$ there are operators that couple four spin-half fields²

$$\mathcal{L}_{\psi\chi} = \frac{d_1}{M^2} \psi^\dagger \sigma^i \psi \chi^\dagger \sigma^i \chi + \frac{d_2}{M^2} \psi^\dagger \psi \chi^\dagger \chi + \dots \quad (3.6)$$

Here χ is another NRQED field which can be different from ψ . The coefficients d_1 and d_2 start at order α^2 , see [66, 67, 68]. The $1/M^2$ NRQED Lagrangian of (3.4) and (3.6) is enough to describe the proton structure effects relevant to the current precision of muonic hydrogen spectroscopy [66, 67, 68]. In particular, χ is taken to be an NRQED field for the lepton. In the following calculations, we will only need (3.4) to describe the proton's interactions.

¹We follow the conventions of [61], although in that paper the NRQED Lagrangian describes an electron, here we take e to be positive.

²We use the convention of [65], where the operators are suppressed by $1/M^2$ instead of $1/M_\chi M$ of [61]. The two are related by a factor of M_χ/M , where M_χ is the mass of the χ field.

3.2.2 NRQED Feynman Rules

Here we present the derived Feynman rules for NRQED. The propagators are in Table 3.2 while the vertices up to order $1/M^2$ are in Table 3.3.

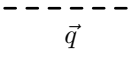
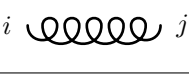
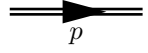
NRQED Propagators		
Coulomb Photon		$\frac{i}{\vec{q}^2 + \lambda^2}$
Transverse Photon		$\frac{i}{q^2 - \lambda^2 + i\epsilon} \left(\delta^{ij} - \frac{q^i q^j}{q^2 - \lambda^2} \right)$
Fermion		$\frac{i}{p^0 - \frac{\vec{p}^2}{2M} + i\epsilon}$

Table 3.2: NRQED Propagators

Here λ is the “mass” of the photon, which is used to regulate infrared divergences [61]. The photon contributions shown above are for Coulomb gauge. In Feynman gauge, the photon propagator is the same as Eq. 3.2 where, again $\xi = 1$.

The Two Photon Time Derivative Vertex is not presented in [61], but is included here. The dot represents that the time derivative is acting on the photon. While the Relativistic Kinetic Vertex is formally order $1/M^3$, it does contribute to amplitudes at order $1/M^2$.

3.3 QED-NRQED

The QED-NRQED EFT is the combination of the QED and NRQED field theories. The QED Feynman rules are used to describe the relativistic particle, while the NRQED rules describe the non-relativistic one. This EFT contains interactions seen in both QED and NRQED.

The NRQED interactions distinguish between the time-like (A^0) and space-like (A^i) components of A^μ . Therefore, in a photon exchange between a QED field and a NRQED field the photon polarization will be determined by the NRQED vertex. It is often convenient to use Coulomb gauge, where the photon propagator is different for time-like and space-like components. A more detailed explanation of the photon propagators can be found in [61].

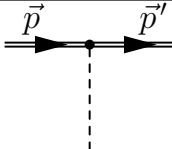
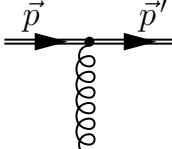
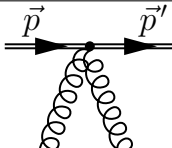
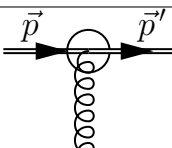
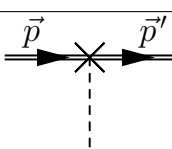
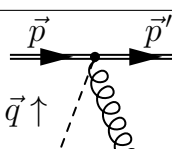
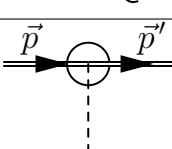
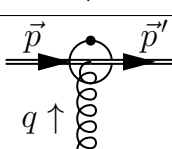
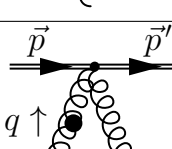
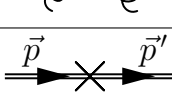
NRQED Vertices		
Coulomb		$-iQe$
Dipole		$\frac{iQec_2(\vec{p} + \vec{p}')}{2M}$
$\vec{A} \cdot \vec{A}$		$-\frac{Q^2 e^2 \delta^{ij}}{M}$
Fermi		$\frac{Qec_F(\vec{p}' - \vec{p}) \times \vec{\sigma}}{2M}$
Darwin		$\frac{iQec_D \vec{p}' - \vec{p} ^2}{8M^2}$
Seagull		$\frac{Q^2 e^2 c_S \vec{q} \times \vec{\sigma}}{4M^2}$
Spin Orbit		$\frac{Qec_S(\vec{p}' \times \vec{p}) \cdot \vec{\sigma}}{4M^2}$
Time Derivative		$-\frac{Qec_S q^0 (\vec{p}' + \vec{p}) \times \vec{\sigma}}{8M^2}$
Two Photon Time Derivative		$-\frac{Q^2 e^2 c_S \sigma^i \epsilon^{ijk} q^0}{4M^2}$
Relativistic Kinetic		$\frac{i\vec{p}^4}{8M^3}$

Table 3.3: NRQED Vertices

At $1/M^2$ we can also have contact interactions of the form $\psi^\dagger \Sigma \psi \bar{\ell} \Gamma \ell$, where ψ^\dagger is the non-relativistic proton field, ℓ is a relativistic lepton field, Γ is a 4×4 matrix and $\Sigma = 1_{2 \times 2}, \sigma^i$. The contact interactions must be even under parity and time reversal. Since both the unit matrix and the Pauli matrices are even under parity, $\bar{\ell} \Gamma \ell$ must be parity even too. This implies eight possible options for Γ , namely, $1_{4 \times 4}, \gamma^0, \sigma^{ij}, \gamma^i \gamma^5$, where the indices i, j , and k , are cycled [58]. Since $1_{2 \times 2}$ (σ^i) are even (odd) under time reversal, $1_{4 \times 4}$ and γ^0 can only be combined with $1_{2 \times 2}$, while σ^{ij} and $\gamma^i \gamma^5$ can only be combined with σ^i . We combine δ^{ij} to the former and ϵ^{ijk} to the latter.

QED-NRQED Interactions		
Spin Independent	$\psi_p^\dagger \psi_p \bar{\ell} \gamma^0 \ell$	$\psi_p^\dagger \psi_p \bar{\ell} \ell$
Spin Dependent	$\psi_p^\dagger \sigma_i \psi_p \bar{\ell} \gamma^i \gamma^5 \ell$	$\psi_p^\dagger \sigma_i \psi_p \bar{\ell} \left(\frac{i}{2} \epsilon^{ijk} \gamma_j \gamma_k \right) \ell$

Table 3.4: Possible interactions in the QED-NRQED EFT

Experiment Interactions		
Experiment	Charge Radius	Two Photon Exchange
Spectroscopy	$c_D \psi_p^\dagger \nabla \cdot \vec{E} \psi_p$	$d_2 \psi_p^\dagger \psi_p \psi_\mu^\dagger \psi_\mu$
MUSE	$c_D \psi_p^\dagger \nabla \cdot \vec{E} \psi_p$	$b_1 \psi_p^\dagger \psi_p \bar{\ell} \gamma^0 \ell$

Table 3.5: Possible interactions for the experiments

An operator of the form $\bar{\ell} \Gamma \ell$ couples the left-handed and right-handed components of the relativistic lepton field if Γ contains an even number of gamma matrices. As a result, one would expect that the Wilson coefficient of such an operator would be proportional to m . In other words, we have chiral symmetry in the $m \rightarrow 0$ limit. This implies that operators with an even number of gamma matrices should be multiplied by m/M^3 . At $1/M^2$ we therefore have only two possible contact interactions,

$$\mathcal{L}_{\ell\psi} = \frac{b_1}{M^2} \psi^\dagger \psi \bar{\ell} \gamma^0 \ell + \frac{b_2}{M^2} \psi^\dagger \sigma^i \psi \bar{\ell} \gamma^i \gamma^5 \ell + \mathcal{O}(1/M^3), \quad (3.7)$$

where our notation follows that of [65].

It is important to note that this QED-NRQED effective field theory describes electromagnetic interactions between a relativistic lepton and a non-relativistic proton. This means that the pion is not included as a dynamical degree of freedom. The effects of the strong interaction are encoded in the non-perturbative QED-NRQED Wilson coefficients c_i and b_i . For more information on the pion contributions, see [69]. Deep Inelastic Scattering is not a concern as it only contributes at energy scales above the proton mass, which is the upper energy limit of the QED-NRQED EFT.

CHAPTER 4: ESTABLISHING QED-NRQED

Here we present calculations performed in the QED-NRQED EFT and compare them to known results. The majority of this work was originally published in [70] by Dye, Gonderinger, and Paz.

4.1 One Photon Exchange and Proven Results

In order to establish the new QED-NRQED effective field theory, it must be shown that it reproduces known results. In particular, we consider $\mathcal{O}(Q_p\alpha)$ scattering up to power m^2/M^2 , where m (M) is the muon (proton) mass, $Q_p = 1$, and $\mathcal{O}(Q_p^2\alpha^2)$ scattering at leading power¹. We show how the former reproduces Rosenbluth scattering [71] and the latter reproduces scattering off of a QED “point-like” proton, and the scattering of a relativistic fermion off a static potential [72, 73].

4.1.1 One Photon QED-NRQED Coulomb Gauge

Our first application is the calculation of the QED-NRQED lepton-proton elastic scattering $\ell(k) + p(p) \rightarrow \ell(k') + p(p')$ at $\mathcal{O}(Q_p\alpha)$ (for the amplitude) and at power m^2/M^2 . We will see that the result agrees with the result of the Rosenbluth formula [71] up to power m^2/M^2 .

In the Coulomb gauge, we calculated the Feynman diagrams of Figure 4.1 for a one-photon exchange between a relativistic lepton and a non-relativistic proton up to $1/M^2$ using (3.1) and (3.4) we find

$$\mathcal{M}_{\text{QN}} = e^2 Q_p Q_\ell \left[\left(1 - c_D \frac{\vec{q}^2}{8M^2} \right) \frac{1}{\vec{q}^2} \xi_{p'}^\dagger \xi_p \bar{u}(k') \gamma^0 u(k) - i \frac{c_F}{2M} \frac{1}{q^2} \epsilon^{ijk} q^j \xi_{p'}^\dagger \sigma^k \xi_p u(k') \gamma^i u(k) \right], \quad (4.1)$$

where “QN” stands for QED-NRQED, and $\xi_{p'}$ and ξ_p are two-component spinors. There is no contribution from the operator \mathbf{D}^2 at this order. We have also omitted a contribution from c_S that is proportional to q_0 and leads to $1/M^3$ suppressed terms.

The spin-averaged square of the amplitude can be calculated by an analogue of the

¹We use the factors of Q_p to keep track of the number of proton-photon interactions.

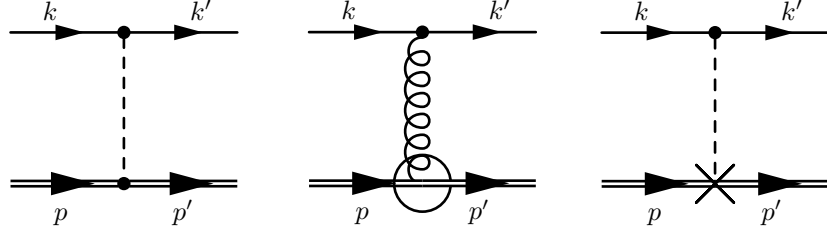


Figure 4.1: QED-NRQED Feynman diagrams that give a non-zero contribution to elastic lepton-proton scattering at $\mathcal{O}(Q_p\alpha)$ up to power m^2/M^2 . The double line denotes the NRQED field. The dashed (curly) line represents Coulomb (transverse) photon. The dot, circle, and cross vertices represent the Coulomb, Fermi, and Darwin terms, respectively, see Ref. [61] for details.

Casimir trick, see the Appendix. We find

$$\begin{aligned} \overline{|\mathcal{M}|}_{\text{QN}}^2 &= e^4 Q_p^2 Q_\ell^2 \left[\frac{1}{\vec{q}^4} \left(1 - c_D \frac{\vec{q}^2}{8M^2} \right)^2 (4EE' + q^2) + \frac{c_F^2}{M^2} \frac{1}{q^4} \vec{q}^2 \left(EE' - m^2 - \frac{\vec{k} \cdot \vec{q} \vec{k}' \cdot \vec{q}}{\vec{q}^2} \right) \right] \\ &= \frac{e^4 Q_p^2 Q_\ell^2}{\vec{q}^2} \left[\frac{1}{\vec{q}^2} (4E^2 - \vec{q}^2) - \frac{2E}{M} + \frac{\vec{q}^2 + c_F^2 (\vec{q}^2 + 4E^2 - 4m^2) + c_D (\vec{q}^2 - 4E^2)}{4M^2} \right], \quad (4.2) \end{aligned}$$

where E (E') is the energy of the initial (final) lepton. In the second line, we have expanded the kinematical variables in powers of $1/M$ and retained only terms up to $1/M^2$, for details see the Appendix.

We can compare this result to Rosenbluth scattering, i.e. the one-photon interaction between a proton, described by the form-factors, and a lepton. Without a considerable increase in complexity, we can introduce form-factors for the lepton too, since some of the radiative corrections modify the lepton form-factors from the tree-level value of $F_1 = 1, F_2 = 0$. We thus have for the lepton-photon vertex

$$\langle \ell(k') | J_\mu^{\text{em}} | \ell(k) \rangle = \bar{u}(k') \left[\gamma_\mu F_1^\ell(q^2) - \frac{i\sigma_{\mu\nu}}{2m} F_2^\ell(q^2) q^\nu \right] u(k). \quad (4.3)$$

The spin averaged square of the amplitude is given by

$$\begin{aligned} \overline{|\mathcal{M}|}^2 &= \frac{4\pi^2\alpha^2 Q_p^2 Q_\ell^2}{q^4} \text{Tr} \left\{ (\not{p}' + M) \left(\gamma_\mu F_1^p + \frac{i\sigma_{\mu\alpha}}{2M} F_2^p q^\alpha \right) (\not{p}' + M) \left(\gamma_\nu F_1^p - \frac{i\sigma_{\nu\beta}}{2M} F_2^p q^\beta \right) \right\} \\ &\times \text{Tr} \left\{ (\not{k}' + m) \left(\gamma^\mu F_1^\ell - \frac{i\sigma^{\mu\rho}}{2m} F_2^\ell q_\rho \right) (\not{k}' + m) \left(\gamma^\nu F_1^\ell + \frac{i\sigma^{\nu\lambda}}{2m} F_2^\ell q_\lambda \right) \right\}. \end{aligned} \quad (4.4)$$

Collecting the terms by their powers of q^2 we have,

$$\begin{aligned} \frac{\overline{|\mathcal{M}|}^2}{\pi^2\alpha^2} &= \frac{256E^2(F_1^\ell)^2(F_1^p)^2M^2}{q^4} + \frac{64}{q^2} \left[(F_1^\ell)^2(F_1^p + F_2^p)^2m^2 + (F_1^p)^2(F_1^\ell + F_2^\ell)^2M^2 + \right. \\ &+ 2(F_1^\ell)^2(F_1^p)^2ME - \left. \frac{E^2 \left((F_1^\ell)^2 (F_2^p)^2 m^2 + (F_1^p)^2 (F_2^\ell)^2 M^2 \right)}{m^2} \right] \\ &+ 16 \left[\left((F_1^p)^2 + 4F_1^p F_2^p + (F_2^p)^2 \right) \left((F_1^\ell)^2 + 4F_1^\ell F_2^\ell + (F_2^\ell)^2 \right) + F_1^\ell F_1^p (F_1^\ell F_1^p - 4F_2^\ell F_2^p) \right. \\ &- \left. \frac{2E \left((F_1^\ell)^2 (F_2^p)^2 m^2 + (F_1^p)^2 (F_2^\ell)^2 M^2 \right)}{m^2 M} + \frac{E^2 (F_2^\ell)^2 (F_2^p)^2}{m^2} \right] \\ &+ 4q^2 \left[\frac{F_2^\ell F_2^p \left((2F_1^\ell + F_2^\ell) F_2^p m^2 + (2F_1^p + F_2^p) F_2^\ell M^2 \right)}{m^2 M^2} + \frac{2E (F_2^\ell)^2 (F_2^p)^2}{m^2 M} \right] \\ &+ q^4 \left[\frac{(F_2^\ell)^2 (F_2^p)^2}{m^2 M^2} \right], \end{aligned} \quad (4.5)$$

where we have suppressed the dependence of the form factors on q^2 . Inserting this expression into (6) and taking the limit $F_1^\ell \rightarrow 1$, $F_2^\ell \rightarrow 0$ reproduces similar expressions in the literature [74, 75].

As explained in the Appendix, in the rest frame of the initial proton, $\overline{|\mathcal{M}|}^2 = 4ME_{p'} \overline{|\mathcal{M}|}_{\text{QN}}^2$. Multiplying (4.2) by $4ME_{p'}$, using the relations $c_F = F_1(0) + F_2(0)$, $c_D = F_1(0) + 2F_2(0) + 8M^2 F_1'(0)$, and expanding in powers of $1/M$, we find that the result agrees with the expansion of (4.5) in powers of $1/M$ in the $F_1^\ell \rightarrow 1$, $F_2^\ell \rightarrow 0$ limit. In particular, there is no contribution to the Wilson coefficients of the contact interactions, b_1 and b_2 at this order, but at $\mathcal{O}(Q_p^2\alpha^2)$.

4.1.2 One Photon QED-NRQED Feynman Gauge

As a further check of Sec. 4.1.1, the one-photon exchange between a relativistic lepton and a non-relativistic proton up to $1/M^2$ has been calculated in the Feynman gauge as well. The difference between the two gauges is that four interactions contribute to the final result in this gauge instead of three. The resulting amplitude is

$$\mathcal{M}_{\text{QN}} = e^2 Q_p Q_\ell \left[\left(1 + \frac{q^4}{4M^2 \vec{q}^2} - c_D \frac{\vec{q}^2}{8M^2} + \frac{q^0 \vec{q}^2}{2M q^2} \right) \frac{1}{\vec{q}^2} \xi_{p'}^\dagger \xi_p \bar{u}(k') \gamma^0 u(k) - i \frac{c_F}{2M} \frac{1}{q^2} \epsilon^{ijk} q^j \xi_{p'}^\dagger \sigma^k \xi_p u(k') \gamma^i u(k) \right]. \quad (4.6)$$

After performing the appropriate kinematic approximations, we are able to reproduce the amplitude in Eq. 4.1,

$$\mathcal{M}_{\text{QN}} = e^2 Q_p Q_\ell \left[\left(1 - c_D \frac{\vec{q}^2}{8M^2} \right) \frac{1}{\vec{q}^2} \xi_{p'}^\dagger \xi_p \bar{u}(k') \gamma^0 u(k) - i \frac{c_F}{2M} \frac{1}{q^2} \epsilon^{ijk} q^j \xi_{p'}^\dagger \sigma^k \xi_p u(k') \gamma^i u(k) \right]. \quad (4.7)$$

These kinematic approximations can be found in the Appendix. This shows that the Feynman gauge result is the same as the Coulomb gauge result.

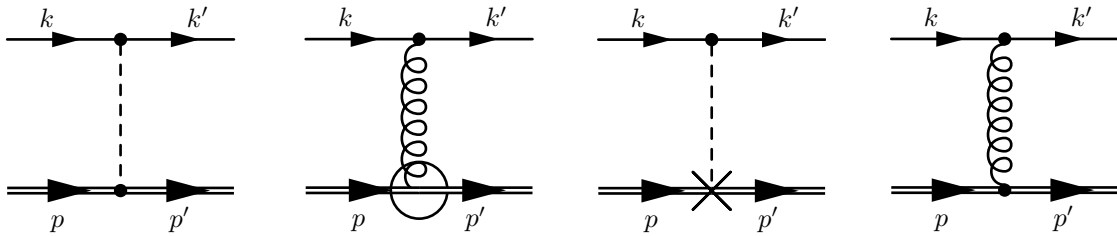


Figure 4.2: QED-NRQED Feynman diagrams that give a non-zero contribution to elastic lepton-proton scattering at $\mathcal{O}(Q_p \alpha)$ up to power m^2/M^2 . The double line denotes the NRQED field. The dashed (curly) line represents Coulomb (transverse) photon. See Ref. [61] for details.

4.2 Two Photon Results at Leading Order

We consider elastic lepton-proton scattering $\ell(k) + p(p) \rightarrow \ell(k') + p(p')$ at $\mathcal{O}(Q_p^2\alpha^2)$ at leading power in m/M . We will show that the three methods: QED-NRQED at leading power, QED for a point particle at leading power in $1/M$, and scattering off a static $1/r$ potential, give the same amplitude.

4.2.1 Two Photon QED-NRQED at Leading Order

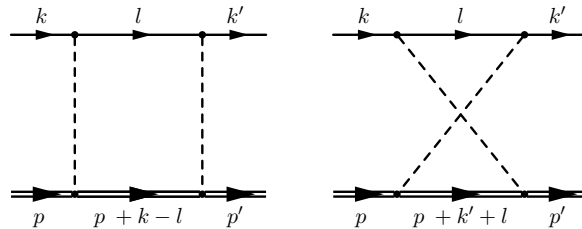


Figure 4.3: QED-NRQED Feynman diagrams contributing to elastic lepton-proton scattering at $\mathcal{O}(Q_p^2\alpha^2)$ at leading power in m/M . The double line denotes the NRQED field.

The NRQED propagator is $i(p_0 - \vec{p}^2/2M + i\epsilon)^{-1}$ [61]. At leading power in $1/M$ we can approximate² it as $i(p_0 + i\epsilon)^{-1}$. Also, at leading power the NRQED field only couples to A^0 . This means that within the Feynman gauge photon propagator, $g^{\mu\nu} \rightarrow g^{00} = 1$. Finally, in the limit of zero momentum transfer, $q^0 = 0$. This means that within these restrictions, the Feynman gauge and Coulomb gauge photon propagator are equal to each other. The resulting amplitude is therefore

$$i\mathcal{M} = Q_p^2 Q_l^2 e^4 \int \frac{d^4l}{(2\pi)^4} \frac{\bar{u}(k')\gamma^0(\not{l} + m)\gamma^0 u(k)\xi_p^\dagger \xi_p}{(l-k)^2(l-k')^2(l^2 - m^2)} \left(\frac{1}{k^0 - l^0 + i\epsilon} + \frac{1}{l^0 - k'^0 + i\epsilon} \right). \quad (4.8)$$

At the leading power in $1/M$ conservation of momentum and energy imply

$$\sqrt{\vec{k}^2 + m^2} + M = \sqrt{\vec{k}'^2 + m^2} + \sqrt{M^2 + (\vec{k}' - \vec{k})^2} \Rightarrow \sqrt{\vec{k}^2 + m^2} = \sqrt{\vec{k}'^2 + m^2} + \mathcal{O}(1/M), \quad (4.9)$$

²Note that in this approximation the propagator looks like a HQET propagator, $i(v \cdot p + i\epsilon)^{-1}$, with $v = (1, \vec{0})$. The relation between the HQET and NRQED Lagrangians is discussed in [63].

i.e. $|\vec{k}| = |\vec{k}'|$ and $k^0 = k'^0$. This also implies that $\delta^4(k' + p' - k - p) \approx \delta(k'^0 - k^0)\delta^3(\vec{k}' + \vec{p}' - \vec{k})$.

Using the identity [76] $1/(x + i\epsilon) = P(1/x) - i\pi\delta(x)$, where P is Cauchy principle value, we have at leading power in $1/M$

$$\frac{1}{k^0 - l^0 + i\epsilon} + \frac{1}{l^0 - k'^0 + i\epsilon} = \frac{1}{k^0 - l^0 + i\epsilon} + \frac{1}{l^0 - k^0 + i\epsilon} = -2\pi i\delta(l^0 - k^0). \quad (4.10)$$

Averaging over the initial proton spins and summing over the final proton spins implies $\xi_{p'}^\dagger \xi_p \rightarrow 1$. Since $\delta(l^0 - k^0)\delta(k'^0 - k^0) = \delta(l^0 - k^0)\delta(l^0 - k'^0)$, we can finally write

$$\begin{aligned} i\mathcal{M} (2\pi)^4 \delta^4(k' + p' - k - p) &= \int \frac{d^4l}{(2\pi)^4} \frac{2\pi\delta(l^0 - k^0)}{(l - k)^2 - \lambda^2} \frac{2\pi\delta(l^0 - k'^0)}{(l - k')^2 - \lambda^2} \frac{\bar{u}(k')\gamma^0(\not{l} + m)\gamma^0 u(k)}{l^2 - m^2} \\ &\times (-)iQ_p^2 Q_\ell^2 e^4 (2\pi)^3 \delta^3(\vec{k}' + \vec{p}' - \vec{k}), \end{aligned} \quad (4.11)$$

where we have introduced an IR regulator λ as the photon “mass”.

4.2.2 Two Photon QED at Leading Order

If the proton were a point particle, we could calculate the same diagrams using QED. As we will show, this toy model actually gives the same answer as the effective field theory calculation. The reason is that in the infinite proton mass limit, the only information the lepton has about the composite proton is its overall charge. Of course, once we include other properties of the proton such as its magnetic moment or charge radius, described in NRQED by operators suppressed by $1/M$ and $1/M^2$ respectively, the two calculations will differ.

Calculating the diagrams for a point particle of mass M and charge $Q_p e$ we find

$$\begin{aligned} i\mathcal{M} &= Q_p^2 Q_\ell^2 e^4 \int \frac{d^4l}{(2\pi)^4} \frac{1}{(l - k)^2 - \lambda^2} \frac{1}{(l - k')^2 - \lambda^2} \frac{\bar{u}(k')\gamma_\mu(\not{l} + m)\gamma_\nu u(k)}{(l^2 - m^2)} \\ &\times \bar{u}(p') \left(\gamma^\mu \frac{\not{p} + \not{k} - \not{l} + M}{(p + k - l)^2 - M^2} \gamma^\nu + \gamma^\nu \frac{\not{p} - \not{k}' + \not{l} + M}{(p - k' + l)^2 - M^2} \gamma^\mu \right) u(p). \end{aligned} \quad (4.12)$$

Since $p = (M, \vec{0})$, in the infinite mass limit

$$\frac{\not{p} + \not{k} - \not{l} + M}{(p+k-l)^2 - M^2} \rightarrow \frac{1 + \gamma^0}{2} \cdot \frac{1}{k^0 - l^0}, \quad \frac{\not{p}' - \not{k}' + \not{l} + M}{(p-k'+l)^2 - M^2} \rightarrow \frac{1 + \gamma^0}{2} \cdot \frac{1}{l^0 - k'^0}, \quad (4.13)$$

and $u(p) = (\xi_p, 0)$, $\bar{u}(p') = (\xi_{p'}, 0)^\dagger \gamma^0$. As a result $(1 - \gamma^0)u(p) = 0$, $\bar{u}(p')(1 - \gamma^0) = 0$. The proton matrix element can be simplified as

$$\begin{aligned} \bar{u}(p')\gamma^\alpha \left(\frac{1 + \gamma^0}{2}\right) \gamma^\beta u(p) &= \bar{u}(p')\gamma^\alpha \left(\frac{1 + \gamma^0}{2}\right) \left(\frac{1 + \gamma^0}{2}\right) \gamma^\beta u(p) \\ &= \bar{u}(p') \left[\left(\frac{1 - \gamma^0}{2}\right) \gamma^\alpha + g^{\alpha 0} \right] \left[g^{\beta 0} + \gamma^\beta \left(\frac{1 - \gamma^0}{2}\right) \right] u(p) = g^{\alpha 0} g^{\beta 0} \xi_{p'}^\dagger \xi_p. \end{aligned} \quad (4.14)$$

All together, the result is

$$i\mathcal{M} = Q_p^2 Q_\ell^2 e^4 \int \frac{d^4 l}{(2\pi)^4} \frac{\bar{u}(k')\gamma^0 (\not{l} + m) \gamma^0 u(k) \xi_{p'}^\dagger \xi_p}{(l-k)^2 (l-k')^2 (l^2 - m^2)} \left(\frac{1}{k^0 - l^0 + i\epsilon} + \frac{1}{l^0 - k'^0 + i\epsilon} \right), \quad (4.15)$$

which is the same result as from the QED-NRQED calculation, see equation (4.8). We now proceed in the same way as in the previous section to obtain equation (4.11).

4.2.3 Classical Potential

We consider a lepton scattering off a static external potential [72, 73] :

$$\vec{A} = 0, \quad A^0 = \frac{Q_p e e^{-\lambda r}}{4\pi r} = -Q_p e \int \frac{d^4 q}{(2\pi)^4} \frac{2\pi\delta(q^0)}{q^2 - \lambda^2} e^{iqx}, \quad (4.16)$$

This implies that in terms of Feynman rules we have a factor of $2\pi\delta(q^0)/(q^2 - \lambda^2)$ for each photon exchange with the potential. Calculating the transition matrix element we have

$$i\mathcal{M} (2\pi)\delta(k'^0 - k^0) = -iQ_p^2 Q_\ell^2 e^4 \int \frac{d^4 l}{(2\pi)^4} \frac{2\pi\delta(l^0 - k^0)}{(l-k)^2 - \lambda^2} \cdot \frac{2\pi\delta(l^0 - k'^0)}{(l-k')^2 - \lambda^2} \cdot \frac{\bar{u}(k')\gamma^0 (\not{l} + m) \gamma^0 u(k)}{l^2 - m^2}. \quad (4.17)$$

Up to a factor of $(2\pi)^3\delta^3(\vec{k}' + \vec{p}' - \vec{k})$ this is the same result as the QED-NRQED calculation, equation (4.11).

4.2.4 Cross Section

For completeness we also calculate the cross section. The calculation is similar to [72, 73] but the integrals are calculated using the standard Feynman parameters. We start from equation (4.11). Using

$$\frac{\delta(l^0 - k^0)\delta(l^0 - k'^0)}{[(l - k)^2 - \lambda^2][(l - k')^2 - \lambda^2][l^2 - m^2]} = \frac{\delta(l^0 - k^0)\delta(l^0 - k'^0)}{\left[(\vec{l} - \vec{k})^2 + \lambda^2\right]\left[(\vec{l} - \vec{k}')^2 + \lambda^2\right]\left[\vec{k}^2 - \vec{l}^2\right]}, \quad (4.18)$$

and

$$\delta(l^0 - k^0)\bar{u}(k')\gamma^0(\not{l} + m)\gamma^0 u(k) = \delta(l^0 - k^0)\bar{u}(k')\left(k^0\gamma^0 + m + \vec{l} \cdot \vec{\gamma}\right)u(k), \quad (4.19)$$

we get

$$\begin{aligned} i\mathcal{M}(2\pi)^4\delta^4(k' + p' - k - p) &= -2i\frac{Q_p^2 Q_\ell^2 \alpha^2}{\pi} 2\pi\delta(k^0 - k'^0)(2\pi)^3\delta^3(\vec{k}' + \vec{p}' - \vec{k}) \\ &\times \int d^3l \frac{\bar{u}(k')\left(k^0\gamma^0 + m + \vec{l} \cdot \vec{\gamma}\right)u(k)}{\left[(\vec{l} - \vec{k})^2 + \lambda^2\right]\left[(\vec{l} - \vec{k}')^2 + \lambda^2\right]\left[\vec{k}^2 - \vec{l}^2 + i\epsilon\right]}. \end{aligned} \quad (4.20)$$

We need two integrals

$$\begin{aligned} I_1 &= \int d^3l \frac{1}{\left[(\vec{l} - \vec{k})^2 + \lambda^2\right]\left[(\vec{l} - \vec{k}')^2 + \lambda^2\right]\left[\vec{k}^2 - \vec{l}^2 + i\epsilon\right]}, \\ I_2^i &= \int d^3l \frac{l^i}{\left[(\vec{l} - \vec{k})^2 + \lambda^2\right]\left[(\vec{l} - \vec{k}')^2 + \lambda^2\right]\left[\vec{k}^2 - \vec{l}^2 + i\epsilon\right]}. \end{aligned} \quad (4.21)$$

The denominators arising from the photon propagators can be combined using a Feynman parameter as

$$x\left[(\vec{l} - \vec{k})^2 + \lambda^2\right] + \bar{x}\left[(\vec{l} - \vec{k}')^2 + \lambda^2\right] = (\vec{l} - \vec{K})^2 + M^2, \quad (4.22)$$

where $0 \leq x \leq 1$, $\bar{x} = 1 - x$, $\vec{K} = x\vec{k} + \bar{x}\vec{k}'$, $M^2 = -\vec{K}^2 + \vec{k}^2 + \lambda^2$, and we have used $\vec{k}^2 = \vec{k}'^2$. Combining this with the third denominator of (4.21) using another Feynman parameter we find

$$\begin{aligned} I_1 &= -2 \int_0^1 dx \int_0^1 dy y \int d^3l \frac{1}{(\vec{l}^2 + \Delta - i\epsilon)^3} \\ I_2^i &= -2 \int_0^1 dx \int_0^1 dy y^2 \int d^3l \frac{K^i}{(\vec{l}^2 + \Delta - i\epsilon)^3}, \end{aligned} \quad (4.23)$$

where $\Delta = y\bar{y}\vec{K}^2 + yM^2 - \bar{y}\vec{k}^2$ and we have changed $\vec{l} \rightarrow \vec{l} - \vec{K}y$. It is convenient to perform the integral over $|\vec{l}|$ first and then to integrate over y . For the x integral we note that Δ is a function of $x(1-x)$. We split the integration range into two intervals, $0 \leq x \leq 1/2$ and $1/2 \leq x \leq 1$, and change variables to $z = x(1-x)$. Thus, for a function $f(x)$,

$$\int_0^1 dx f(x) = \int_0^{\frac{1}{4}} dz \frac{f\left(\frac{1}{2} - \frac{1}{2}\sqrt{1-4z}\right) + f\left(\frac{1}{2} + \frac{1}{2}\sqrt{1-4z}\right)}{\sqrt{1-4z}}. \quad (4.24)$$

After the change of variables, $\vec{K}^2 = \vec{k}^2 - 4\vec{k}^2 z \sin^2 \frac{\theta}{2}$ and $M^2 = \lambda^2 + 4\vec{k}^2 z \sin^2 \frac{\theta}{2}$. Performing the $|\vec{l}|$ and y integrations we have

$$I_1 = -2 \int_0^{\frac{1}{4}} \frac{dz}{\sqrt{1-4z}} \frac{\pi^2}{M \left[(M - i|\vec{k}|)^2 + \vec{K}^2 \right]} \quad (4.25)$$

$$\begin{aligned} I_2^i &= -2\pi^2 \left(\frac{k^i + k'^i}{2} \right) \int_0^{\frac{1}{4}} \frac{dz}{\sqrt{1-4z}} \left\{ \frac{1}{M\vec{K}^2} + \frac{iM|\vec{K}| + \vec{k}^2}{M\vec{K}^2 \left[(M - i|\vec{k}|)^2 + \vec{K}^2 \right]} + \right. \\ &\quad \left. + \frac{i}{2|\vec{K}|^3} \log \left(\frac{iM + |\vec{k}| - |\vec{K}|}{iM + |\vec{k}| + |\vec{K}|} \right) \right\}. \end{aligned} \quad (4.26)$$

The polynomial terms in I_1 and I_2^i can be integrated directly. For the logarithmic term in I_2^i it is convenient to use integration by parts. Defining $I_2^i \equiv I_2(k^i + k'^i)/2$, we find

$$\begin{aligned} I_1 &= \frac{\pi^2}{2i|\vec{k}|^3 \sin^2 \frac{\theta}{2}} \log \left(\frac{2|\vec{k}| \sin \frac{\theta}{2}}{\lambda} \right) \\ I_2 &= \frac{\pi^2}{2|\vec{k}|^3 \cos^2 \frac{\theta}{2}} \left\{ \frac{\pi}{2} \left(1 - \frac{1}{\sin \frac{\theta}{2}} \right) - i \left[\frac{1}{\sin^2 \frac{\theta}{2}} \log \left(\frac{2|\vec{k}| \sin \frac{\theta}{2}}{\lambda} \right) + \log \frac{\lambda}{2|\vec{k}|} \right] \right\}. \end{aligned} \quad (4.27)$$

This is the same result in Ref. [73]. As was pointed out in [65], [72] has the wrong sign for I_1 .

Since $\not{k}u(k) = (k^0\gamma^0 - \vec{k} \cdot \vec{\gamma})u(k) = mu(k)$, we have $\vec{k} \cdot \vec{\gamma} u(k) = (k^0\gamma^0 - m)u(k)$. Similarly $\bar{u}(k') \vec{k}' \cdot \vec{\gamma} = \bar{u}(k')(k'^0\gamma^0 - m)$. Equation (4.20) simplifies to

$$\mathcal{M}_{\text{QN}}^{(2)} = -\frac{2Q_p^2 Q_\ell^2 \alpha^2}{\pi} \bar{u}(k') [m(I_1 - I_2) + k^0\gamma^0(I_1 + I_2)] u(k), \quad (4.28)$$

where we have added the subscript ‘‘QN’’ to denote that we are using non-relativistic normalization for the proton states.

The $\mathcal{O}(Q_p\alpha)$ amplitude at leading power is obtained from equation (4.1) by keeping only the leading power term and replacing $\xi_p^\dagger \xi_p \rightarrow 1$, see section 4.2. We have

$$\mathcal{M}_{\text{QN}}^{(1)} = -4\pi\alpha Q_p Q_\ell \frac{1}{\vec{q}^2} u(k') \gamma^0 u(k). \quad (4.29)$$

At leading power in $1/M$ the relation between \mathcal{M}_{QN} and \mathcal{M} in the initial proton rest frame is just $\mathcal{M} = 2M\mathcal{M}_{\text{QN}}$, see the Appendix, and we obtain

$$\mathcal{M}^{(1+2)} = \frac{-8M\pi\alpha Q_p Q_\ell}{\vec{q}^2} \bar{u}(k') \left\{ \gamma^0 \left[1 + \alpha Q_p Q_\ell \frac{k^0 \vec{q}^2}{2\pi^2} (I_1 + I_2) \right] + \alpha Q_p Q_\ell \frac{m \vec{q}^2}{2\pi^2} (I_1 - I_2) \right\}. \quad (4.30)$$

At leading power in $1/M$ the cross section is given by $d\sigma/d\Omega = \overline{|\mathcal{M}|^2}/(64\pi^2 M^2)$. We find

$$\frac{d\sigma}{d\Omega} = \frac{4Q_p^2 \alpha^2 Q_\ell^2 E^2 (1 - v^2 \sin^2 \frac{\theta}{2})}{\vec{q}^4} \left[1 + \alpha Q_p Q_\ell \frac{\vec{q}^2 E}{\pi^2} \left(\text{Re}(I_1 + I_2) + \frac{m^2 \text{Re}(I_1 - I_2)}{E^2 (1 - v^2 \sin^2 \frac{\theta}{2})} \right) \right], \quad (4.31)$$

where $E = k^0$ and $v = |\vec{k}|/k^0$. Since I_1 is purely imaginary, only I_2 contributes to the cross section. In particular, the dependence on λ cancels. The cross section is finally

$$\frac{d\sigma}{d\Omega} = \frac{4Q_p^2 \alpha^2 Q_\ell^2 E^2 (1 - v^2 \sin^2 \frac{\theta}{2})}{\vec{q}^4} \left[1 - \alpha Q_p Q_\ell \frac{\pi v \sin \frac{\theta}{2} (1 - \sin \frac{\theta}{2})}{1 - v^2 \sin^2 \frac{\theta}{2}} \right]. \quad (4.32)$$

Taking $Q_\ell = -1$ we obtain the results³ of [72, 73].

4.2.5 Anti-lepton Cross Section

In the calculation above we have assumed that the lepton is a particle. It is instructive to see how (4.32) changes for anti-lepton-proton scattering. The answer, ‘‘Take $Q_\ell = +1$ in (4.32)’’ is correct, but since for QED the Feynman rule for the vertex is the same for leptons and anti-leptons, it is not immediately obvious why this is true. Beyond the theoretical interest, MUSE will consider both $\mu^\pm p$ and $e^\pm p$ scattering [5], so it is instructive to see how the cross section changes.

Ignoring overall minus signs, apart from sign difference between lepton and anti-leptons, the leptonic part of the $\mathcal{O}(Q_p \alpha)$ amplitude is given by

$$\begin{aligned} \mathcal{M}_{\ell^-}^{(1)} &= Q_p \alpha \bar{u}(k') \gamma^\mu u(k) A_\mu(k - k') \dots \\ \mathcal{M}_{\ell^+}^{(1)} &= -Q_p \alpha \bar{v}(k) \gamma^\mu v(k') A_\mu(k - k') \dots \end{aligned} \quad (4.33)$$

³Note that [72] uses $A^0 = Q_p e e^{-\lambda r}/r$. As a result, one needs to replace $\alpha \rightarrow e^2$ in the comparison. Also, one has to be careful about the relative sign between the lepton and the potential charges in [73].



Figure 4.4: The leptonic part of the $\mathcal{O}(Q_p^2\alpha^2)$ amplitude at leading power in m/M for a lepton (left) and an anti-lepton (right).

As seen in figure 4.4, the leptonic part of the $\mathcal{O}(Q_p^2\alpha^2)$ amplitude is

$$\begin{aligned}\mathcal{M}_{\ell^-}^{(2)} &= Q_p^2\alpha^2 \int \frac{d^4l}{(2\pi)^4} \bar{u}(k')\gamma^\mu \frac{\not{l}+m}{l^2-m^2} \gamma^\nu u(k) A_\mu(l-k') A_\nu(k-l) \dots \\ \mathcal{M}_{\ell^+}^{(2)} &= -Q_p^2\alpha^2 \int \frac{d^4l}{(2\pi)^4} \bar{v}(k)\gamma^\nu \frac{(-\not{l}+m)}{l^2-m^2} \gamma^\mu v(k') A_\mu(l-k') A_\nu(k-l) \dots\end{aligned}\quad (4.34)$$

Notice that $\mathcal{M}_{\ell^+}^{(1)}$ and $\mathcal{M}_{\ell^+}^{(2)}$ have the same overall sign. Calculating the spin-averaged leptonic part of the squared amplitude we have the following traces

$$\begin{aligned}\ell^- : & \text{Tr} \left\{ (\not{k}' + m) [\gamma^\rho + Q_p\alpha\gamma^\mu (a\not{l} + b m) \gamma^\nu] (\not{k} + m) [\gamma^{\rho'} + Q_p\alpha\gamma^{\nu'} (a^*\not{l} + b^* m) \gamma^{\mu'}] \right\} \\ \ell^+ : & \text{Tr} \left\{ (\not{k} - m) [\gamma^\rho + Q_p\alpha\gamma^\nu (-a\not{l} + b m) \gamma^\mu] (\not{k}' - m) [\gamma^{\rho'} + Q_p\alpha\gamma^{\mu'} (-a^*\not{l} + b^* m) \gamma^{\nu'}] \right\},\end{aligned}\quad (4.35)$$

where a and b contain integrals over d^4l and we ignore overall factors common to the two traces. Collecting the terms arising from the interference between $\mathcal{M}^{(1)}$ and $\mathcal{M}^{(2)}$, i.e. the $\mathcal{O}(Q_p^3\alpha^3)$ terms in the cross section, we always pick up even number of gamma matrices which imply we always get an extra minus sign for the anti-leptons. The order of the gamma matrices also changes, but because of the symmetries of trace, this has no effect. The cross section is therefore,

$$\frac{d\sigma_{\ell^\mp}}{d\Omega} = \frac{4Q_p^2\alpha^2 E^2 (1 - v^2 \sin^2 \frac{\theta}{2})}{\vec{q}^4} \left[1 \pm \alpha Q_p \frac{\pi v \sin \frac{\theta}{2} (1 - \sin \frac{\theta}{2})}{1 - v^2 \sin^2 \frac{\theta}{2}} \right]. \quad (4.36)$$

4.3 Establishing QED-NRQED Summary

QED-NRQED lepton-proton scattering at $\mathcal{O}(Q_p\alpha)$ and power m^2/M^2 reproduces the known Rosenbluth scattering formula, i.e. the one-photon exchange cross section expressed in terms of the proton form factors [71], up to power m^2/M^2 . It requires just the Dirac Lagrangian and the NRQED Lagrangian up to $1/M^2$. In particular, there is no contribution at this order from $1/M^2$ corrections to the Dirac Lagrangian [65] and more importantly from the lepton-proton contact interactions. This implies that the coefficients of these operators start at a higher order in α . In particular, one would expect that the first non-zero contribution to b_1 and b_2 in equation (3.7) would be at $\mathcal{O}(Q_p^2\alpha^2)$. For that, one has to calculate an appropriate amplitude to $\mathcal{O}(Q_p^2\alpha^2)$ and power m^2/M^2 and is done in Chapter 5.

QED-NRQED lepton-proton scattering at $\mathcal{O}(Q_p^2\alpha^2)$ and at leading power reproduces the $\mathcal{O}(Q_p^2\alpha^2)$ terms in the scattering of a lepton off a static $1/r$ potential [72, 73]. Interestingly it also reproduces the lepton scattering off a “point particle” proton at leading power in $1/M$. It is easy to understand why. In the $M \rightarrow \infty$ limit the only information the lepton has about the proton is the proton’s charge $Q_p e$. Effects such as the proton magnetic moment and the proton charge radius arise only at $1/M$ and $1/M^2$ respectively, see equation (3.4). QED-NRQED can naturally incorporate such effects. For completeness, we have also calculated the cross section, but unlike [72, 73] we used the standard technique of Feynman parameters. Still, these leading power integrals are not representative of the typical integrals one would obtain in calculating QED-NRQED diagrams at higher powers. These integrals will be seen in the two-photon exchange sections. Finally, we have also commented on the change in the cross section when we consider anti-lepton scattering.

CHAPTER 5: TWO PHOTON EXCHANGE RESULTS AT ORDER $1/M^2$

Information about the Wilson coefficient c_D , which is equivalent to the proton charge radius, only becomes relevant at $\mathcal{O}(1/M^2)$. This means that information about the $\mathcal{O}(1/M^2)$ contact interaction coefficients b_1 and b_2 are needed. This information can be obtained through the two-photon exchange calculations using the QED-NRQED EFT, presented here in this chapter. The calculations here are four-fold. The first calculation is performed on a “point-like” proton in Feynman gauge in QED while the second is performed on a physical proton also in Feynman gauge in QED-NRQED. The differences between these two calculations is what gives us information about the Wilson coefficients b_1 and b_2 . These calculations are then repeated in the Coulomb gauge for comparison. When calculating the EFT integrals in the TPE, two methods were used. The first is a method of regions similar to what is used in Soft-Collinear Effective Theory [78], the second uses an expansion of the photon propagator. The simplest way to determine these coefficients is to use the zero momentum exchange reference frame.

5.1 Two Photon Exchange: Feynman Gauge

For the two photon exchange calculations, we have set the proton incoming (\vec{p}) and outgoing (\vec{p}') to zero.

5.1.1 QED Point Particle

We consider the toy example of a point-particle “proton”. In this calculation, the lepton line is kept the same, but the proton line is taken to the non-relativistic limit. For this case, the amplitude of the direct and cross Feynman diagrams for a relativistic lepton and a non-relativistic point-like proton is

$$i\mathcal{M} = e^4 Q_p^2 Q_l^2 \int \frac{d^4 l}{(2\pi)^4} \frac{1}{(l^2 - \lambda^2)^2} \frac{1}{l^2 + 2mv \cdot l} \left[\frac{A^{\mu\nu}(l) B_{\mu\nu}(-l)}{l^2 - 2Mv \cdot l} + \frac{A^{\mu\nu}(l) B_{\nu\mu}(l)}{l^2 + 2Mv \cdot l} \right] \quad (5.1)$$

where

$$\begin{aligned} A^{\mu\nu}(l) &= \bar{u}(k)\gamma^\mu [\not{l} + m(1 + \gamma^0)] \gamma^\nu u(k) \\ B^{\mu\nu}(l) &= \bar{u}(p)\gamma^\mu [\not{l} + M(1 + \gamma^0)] \gamma^\nu u(p), \end{aligned} \quad (5.2)$$

and $v = (1, \vec{0})$, $k = mv$, $p = Mv$.

We use non-relativistic normalization for the proton spinors $u(p)^\dagger u(p) = 1$, where $u(p) = (\chi \ 0)$ and the Dirac representation of the γ matrices

$$\gamma^0 = \begin{pmatrix} 1 & 0 \\ 0 & -1 \end{pmatrix}, \quad \gamma^i = \begin{pmatrix} 0 & \sigma^i \\ -\sigma^i & 0 \end{pmatrix}.$$

The components of $A^{\mu\nu}$ are

$$\begin{aligned} A^{00}(l) &= \bar{u}(k) [\gamma^0 (l^0 + m) + l^i \gamma^i + m] u(k) \\ A^{0i}(l) &= \bar{u}(k) [\gamma^i (l^0 + m) + m\gamma^0 \gamma^i + l^j (\delta^{ij} \gamma^0 - i\epsilon^{ijk} \gamma^k \gamma^5)] u(k) \\ A^{i0}(l) &= \bar{u}(k) [\gamma^i (l^0 + m) + m\gamma^i \gamma^0 + l^j (\delta^{ij} \gamma^0 + i\epsilon^{ijk} \gamma^k \gamma^5)] u(k) \\ A^{ij}(l) &= \bar{u}(k) [(\delta^{ij} \gamma^0 + i\epsilon^{ijk} \gamma^k \gamma^5) (l^0 + m) - l^k \gamma^i \gamma^k \gamma^j + m\gamma^i \gamma^j] u(k), \end{aligned} \quad (5.3)$$

where we have used the identity $\gamma^0 \gamma^i \gamma^j = -(\delta^{ij} \gamma^0 + i\epsilon^{ijk} \gamma^k \gamma^5)$. The components of $B^{\mu\nu}$ are

$$\begin{aligned} B^{00}(l) &= \chi^\dagger \chi (2M + l^0), & B^{0i} &= \chi^\dagger (l^i - i\epsilon^{ijk} l^j \sigma^k) \chi \\ B^{i0}(l) &= \chi^\dagger (l^i + i\epsilon^{ijk} l^j \sigma^k) \chi, & B^{ij} &= l^0 \chi^\dagger (\delta^{ij} + i\epsilon^{ijk} \sigma^k) \chi. \end{aligned} \quad (5.4)$$

Neglecting terms linear in \vec{l} we find

$$\begin{aligned}
A^{\mu\nu}(l)B_{\nu\mu}(l) &= \bar{u}(k)u(k)\chi^\dagger\chi 2m(M - l^0) + \bar{u}(k)\gamma^0 u(k)\chi^\dagger\chi \left[2(m + l^0)(M + 2l^0) - 2\vec{l}^2 \right] \\
+ \bar{u}(k) \left(\frac{i}{2}\epsilon^{ijk}\gamma^j\gamma^k \right) u(k)\chi^\dagger\sigma^i\chi(-2ml^0) &+ \bar{u}(k)\gamma^i\gamma^5 u(k)\chi^\dagger\sigma^i\chi \left[-\frac{4}{3}\vec{l}^2 + 2l^0(m + l^0) \right] \\
A^{\mu\nu}(l)B_{\mu\nu}(-l) &= \bar{u}(k)u(k)\chi^\dagger\chi 2m(M + l^0) + \bar{u}(k)\gamma^0 u(k)\chi^\dagger\chi \left[2(m + l^0)(M - 2l^0) + 2\vec{l}^2 \right] \\
+ \bar{u}(k) \left(\frac{i}{2}\epsilon^{ijk}\gamma^j\gamma^k \right) u(k)\chi^\dagger\sigma^i\chi(-2ml^0) &+ \bar{u}(k)\gamma^i\gamma^5 u(k)\chi^\dagger\sigma^i\chi \left[-\frac{4}{3}\vec{l}^2 + 2l^0(m + l^0) \right], \quad (5.5)
\end{aligned}$$

where we have used that for integrals over $l^i l^j$ we can replace $l^i l^j \rightarrow \vec{l}^2/3$. We need the following integrals.

$$I(M), I^0(M), I^{00}(M), \tilde{I}(M) = (-i)(4\pi)^2 \int \frac{d^4 l}{(2\pi)^4} \frac{\{1, l^0, l^0 l^0, \vec{l}^2\}}{(l^2 - \lambda^2)^2 (l^2 + 2mv \cdot l)(l^2 + 2Mv \cdot l)}. \quad (5.6)$$

To calculate the integrals, we note the partial fractioning identity

$$\frac{1}{l^2 + 2mv \cdot l} \cdot \frac{1}{l^2 + 2Mv \cdot l} = \frac{1}{2(M - m)} \frac{1}{v \cdot l} \left(\frac{1}{l^2 + 2mv \cdot l} - \frac{1}{l^2 + 2Mv \cdot l} \right). \quad (5.7)$$

We define

$$i(m), i^0(m), i^{00}(m), \tilde{i}(m) = (-i)(4\pi)^2 \int \frac{d^4 l}{(2\pi)^4} \frac{\{1, l^0, l^0 l^0, \vec{l}^2\}}{(l^2 - \lambda^2)^2 (v \cdot l)(l^2 + 2mv \cdot l)}, \quad (5.8)$$

and express $I, I^0, I^{00}, \tilde{I}$ in terms of $i, i^0, i^{00}, \tilde{i}$:

$$I(M) = \frac{i(m) - i(M)}{2(M - m)}, I^0(M) = \frac{i^0(m) - i^0(M)}{2(M - m)}, I^{00}(M) = \frac{i^{00}(m) - i^{00}(M)}{2(M - m)}, \tilde{I}(M) = \frac{\tilde{i}(m) - \tilde{i}(M)}{2(M - m)}. \quad (5.9)$$

In calculating the i integrals it is convenient to combine denominators via

$$\frac{1}{l^2 + 2mv \cdot l} \cdot \frac{1}{v \cdot l} = \int_0^\infty \frac{2 dy}{(l^2 + 2mv \cdot l + 2yv \cdot l)^2}. \quad (5.10)$$

Calculating $i, i^0, i^{00}, \tilde{i}$ we find

$$\begin{aligned}
i(m) &= \frac{\pi(m - \sqrt{m^2})}{m\lambda^3} + \frac{1}{m\lambda^2} - \frac{\sqrt{m^2}\pi}{8m^3\lambda} + \frac{1}{6m^3} \\
i^0(m) &= -\frac{\pi}{2\sqrt{m^2}\lambda} + \frac{1 + \log m^2 - \log \lambda^2}{2m^2} \\
i^{00}(m) &= \frac{-2 + \log m^2 - \log \lambda^2}{2m} \\
\tilde{i}(m) &= \frac{\pi(m - \sqrt{m^2})}{m\lambda} + \frac{3 \log m^2 - 3 \log \lambda^2}{2m}.
\end{aligned} \tag{5.11}$$

In terms of the I functions we have

$$\begin{aligned}
\frac{\mathcal{M}_{p.p.}}{Q_i^2 Q_p^2 e^4} &= \bar{u}(k)u(k)\chi^\dagger\chi \left\{ 2Mm [I(-M) + I(M)] + 2m [I^0(-M) - I^0(M)] \right\} + \\
&+ \bar{u}(k)\gamma^0 u(k)\chi^\dagger\chi \left\{ 2Mm [I(-M) + I(M)] - 4m [I^0(-M) - I^0(M)] + \right. \\
&+ 2M [I^0(-M) + I^0(M)] - 4 [I^{00}(-M) - I^{00}(M)] + 2 [\tilde{I}(-M) - \tilde{I}(M)] \left. \right\} \\
&+ \bar{u}(k) \left(\frac{i}{2} \epsilon^{ijk} \gamma^j \gamma^k \right) u(k)\chi^\dagger \sigma^i \chi \left\{ -2m [I^0(-M) + I^0(M)] \right\} \\
&+ \bar{u}(k)\gamma^i \gamma^5 u(k)\chi^\dagger \sigma^i \chi \left\{ 2m [I^0(-M) + I^0(M)] + 2 [I^{00}(-M) + I^{00}(M)] - \frac{4}{3} [\tilde{I}(-M) + \tilde{I}(M)] \right\}.
\end{aligned} \tag{5.12}$$

All together, the result is

$$\begin{aligned}
\frac{\mathcal{M}_{p.p.}}{Q_i^2 Q_p^2 \alpha^2} &= \bar{u}(k)u(k)\chi^\dagger\chi \left[\frac{2mM\pi}{(m+M)\lambda^3} + \frac{3\pi}{4(m+M)\lambda} + \frac{2}{mM} \left(\log \lambda - \frac{1}{3} - \frac{m^2 \log M - M^2 \log m}{m^2 - M^2} \right) \right] \\
&+ \bar{u}(k)\gamma^0 u(k)\chi^\dagger\chi \left[\frac{2mM\pi}{(m+M)\lambda^3} - \frac{5\pi}{4(m+M)\lambda} + \frac{2}{mM} \left(-2 \log \lambda - \frac{1}{3} + \frac{2(m^2 \log M - M^2 \log m)}{m^2 - M^2} \right) \right] \\
&+ \bar{u}(k) \left(\frac{i}{2} \epsilon^{ijk} \gamma^j \gamma^k \right) u(k)\chi^\dagger \sigma^i \chi \left[\frac{m\pi}{M(m+M)\lambda} + \frac{2 \log \lambda - 1}{M^2} + \frac{2(M^2 \log m - m^2 \log M)}{M^2(m^2 - M^2)} \right] \\
&+ \bar{u}(k)\gamma^i \gamma^5 u(k)\chi^\dagger \sigma^i \chi \left[-\frac{\pi}{M\lambda} - \frac{\pi}{3(m+M)\lambda} + \frac{1 + 2 \log M - 2 \log \lambda}{M^2} \right].
\end{aligned} \tag{5.13}$$

In the non-relativistic limit $\bar{u}u, \bar{u}\gamma^0 u \rightarrow \chi_\ell^\dagger \chi_\ell$, and $\bar{u} \left(\frac{i}{2} \epsilon^{ijk} \gamma^j \gamma^k \right) u, \bar{u} \gamma^i \gamma^5 u \rightarrow \chi_\ell^\dagger \sigma^i \chi_\ell$ and we obtain

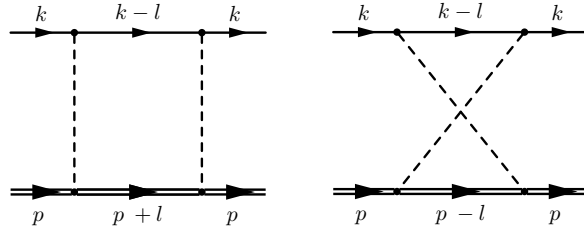
$$\begin{aligned} \frac{\mathcal{M}_{p.p.}^{NR}}{Q_l^2 Q_p^2 \alpha^2} &= \chi_\ell^\dagger \chi_\ell \chi_p^\dagger \chi_p \left[\frac{4mM\pi}{(m+M)\lambda^3} - \frac{\pi}{2(m+M)\lambda} + \frac{2}{mM} \left(-\log \lambda - \frac{2}{3} + \frac{m^2 \log M - M^2 \log m}{m^2 - M^2} \right) \right] \\ &+ \chi_\ell^\dagger \sigma^i \chi_\ell \chi_p^\dagger \sigma^i \chi_p \left[-\frac{4\pi}{3(m+M)\lambda} + \frac{2 \log(m/M)}{m^2 - M^2} \right], \end{aligned} \quad (5.14)$$

which is the NRQED-NRQED result [79].

5.1.2 Effective Field Theory

In the following calculations, $k = (m, \vec{0})$, and everything at order $1/M^3$ and above is omitted. The integrals in this section are solved using two methods, the method of regions and expanding the non-relativistic proton propagator in powers of $1/M$.

5.1.2.1 Leading Power



Calculating the direct and cross Coulomb photon exchange diagrams, we find

$$\mathcal{M}_{\text{Direct+Crossed}} = \alpha^2 Q_l^2 Q_p^2 \chi_\ell^\dagger \chi_\ell [\bar{u} \gamma^0 u (I_0^D + I_0^C) + \bar{u} u (I_m^D + I_m^C)],$$

where

$$I_{m,0}^{D,C} = (-i)(4\pi)^2 \int \frac{d^4 l}{(2\pi)^4} \frac{\{m, m - l^0\}}{[(l-k)^2 - m^2] (l^2 - \lambda^2)^2 \left[\pm l^0 - \frac{\vec{l}^2}{2M} \right]}.$$

We present two methods for performing these sets of integrals. The first method uses method of regions approach. The integrals has three mass scales, the photon “mass” λ , the lepton mass m , and the proton mass M . Our method takes the ratios of these regions with respect

to M , i.e. $\delta = \lambda/M$ and $\epsilon = m/M$. From here the integral is broken up into two regions, the first being where the photon momentum l is of the order δ , while the second region is when $l > \delta$. The residue theorem is used to integrate over l^0 . From here, an intermediate energy cut-off is used to separate these two regions, at which point they are integrated over \vec{l} . The intermediate energy cut-off cancels in the sum of the two regions. This serves as a check for the calculation. Finally, the terms independent of λ were expanded with respect to ϵ . From this method, the results of these integrals are

$$I_m^D = \frac{2\pi m M}{(m+M)\lambda^3} - \frac{1}{\lambda^2} + \frac{\pi(3m^3 + 5m^2M - mM^2 + M^3)}{8mM(m+M)^2\lambda} + \frac{(5m-2M)\log(\lambda/m)}{4mM^2} - \frac{(5m^2 - 5mM + 2M^2)}{12m^2M^2}$$

$$I_m^C = \frac{1}{\lambda^2} - \frac{(3m+M)\pi}{8mM\lambda} - \frac{(5m+2M)\log(\lambda/m)}{4mM^2} + \frac{(5m^2 + 5mM + 2M^2)}{12m^2M^2}$$

$$I_0^D = \frac{2mM\pi}{(m+M)\lambda^3} - \frac{1}{\lambda^2} + \frac{(3m^3 + m^2M - mM^2 + 5M^3)\pi}{8mM(m+M)^2\lambda} + \frac{(5m^2 - 8mM + 4M^2)}{4m^2M^2} \log(\lambda/m) \\ - \frac{15}{8M^2} \log(m/M) + \frac{15 \log 2}{4M^2} - \frac{(161m^2 - 20mM + 32M^2)}{48m^2M^2}$$

$$I_0^C = \frac{1}{\lambda^2} - \frac{(3m+5M)\pi}{8mM\lambda} - \frac{(5m^2 + 8mM + 4M^2)}{4m^2M^2} \log(\lambda/m) \\ + \frac{15}{8M^2} \log(m/M) - \frac{15 \log 2}{4M^2} + \frac{(161m^2 + 20mM + 32M^2)}{48m^2M^2}$$

In total,

$$\frac{\mathcal{M}_{D+C}}{Q_l^2 Q_p^2 \alpha^2} = \bar{u}u\chi^\dagger\chi \left[\frac{2mM\pi}{(m+M)\lambda^3} - \frac{(m+3M)\pi}{4(m+M)\lambda} - \frac{\log(\lambda/m)}{mM} + \frac{5}{6mM} \right] \\ + \bar{u}\gamma^0 u\chi^\dagger\chi \left[\frac{2mM\pi}{(m+M)\lambda^3} - \frac{(5m+7M)\pi}{4(m+M)\lambda} - \frac{4\log(\lambda/m)}{mM} + \frac{5}{6mM} \right]. \quad (5.15)$$

The second method involves expanding the non-relativistic proton propagator in terms

of $1/M$. The proton propagator now takes the form

$$\frac{i}{p^0 - \frac{\vec{p}^2}{2M} + i\epsilon} \rightarrow i \left(\frac{1}{p^0} + \frac{\vec{p}^2}{2(p^0)^2 M} + \frac{\vec{p}^4}{4(p^0)^3 M^2} + \dots \right) \quad (5.16)$$

where only terms of up to $1/M^2$ are kept. Here we integrate over l^0 using the residue theorem and integrate over \vec{l} . From this method, the solutions to the integrals are

$$I_m^D = \frac{2\pi m}{\lambda^3} - \frac{1}{\lambda^2} + \frac{\pi}{8\lambda m} - \frac{1}{6m^2} - \frac{2\pi m^2}{\lambda^3 M} - \frac{3\pi}{8\lambda M} + \frac{5}{12mM} - \frac{\log(\lambda/m)}{2mM} \\ + \frac{2\pi m^3}{\lambda^3 M^2} + \frac{5\pi m}{4\lambda M^2} - \frac{5}{12M^2} + \frac{5\log(\lambda/m)}{4M^2}$$

$$I_m^C = \frac{1}{\lambda^2} - \frac{\pi}{8\lambda m} + \frac{1}{6m^2} - \frac{3\pi}{8\lambda M} + \frac{5}{12mM} - \frac{\log(\lambda/m)}{2mM} + \frac{5}{12M^2} - \frac{5\log(\lambda/m)}{4M^2}$$

$$I_0^D = \frac{2\pi m}{\lambda^3} - \frac{1}{\lambda^2} + \frac{5\pi}{8\lambda m} - \frac{2}{3m^2} + \frac{\log(\lambda/m)}{m^2} - \frac{2\pi m^2}{\lambda^3 M} - \frac{11\pi}{8\lambda M} + \frac{5}{12mM} - \frac{2\log(\lambda/m)}{mM} \\ + \frac{2\pi m^3}{\lambda^3 M^2} + \frac{9\pi m}{4\lambda M^2} - \frac{113}{48M^2} + \frac{5\log(\lambda/m)}{4M^2} + \frac{15\log(2\Lambda/m)}{8M^2}$$

$$I_0^C = \frac{1}{\lambda^2} - \frac{5\pi}{8\lambda m} + \frac{2}{3m^2} - \frac{\log(\lambda/m)}{m^2} - \frac{3\pi}{8\lambda M} + \frac{5}{12mM} - \frac{2\log(\lambda/m)}{mM} \\ + \frac{113}{48M^2} - \frac{5\log(\lambda/m)}{4M^2} - \frac{15\log(2\Lambda/m)}{8M^2}$$

where Λ is a UV cutoff regulator. In total

$$\frac{\mathcal{M}_{D+C}}{Q_i^2 Q_p^2 \alpha^2} = \bar{u} u \chi^\dagger \chi \left[\frac{2m\pi}{\lambda^3} \left(1 - \frac{m}{M} + \frac{m^2}{M^2} \right) + \frac{\pi}{4M\lambda} \left(-3 + \frac{5m}{M} \right) + \frac{5}{6mM} - \frac{\log(\lambda/m)}{mM} \right] \\ + \bar{u} \gamma^0 u \chi^\dagger \chi \left[\frac{2m\pi}{\lambda^3} \left(1 - \frac{m}{M} + \frac{m^2}{M^2} \right) - \frac{\pi}{4M\lambda} \left(7 - \frac{9m}{M} \right) + \frac{5}{6mM} - \frac{4\log(\lambda/m)}{mM} \right]. \quad (5.17)$$

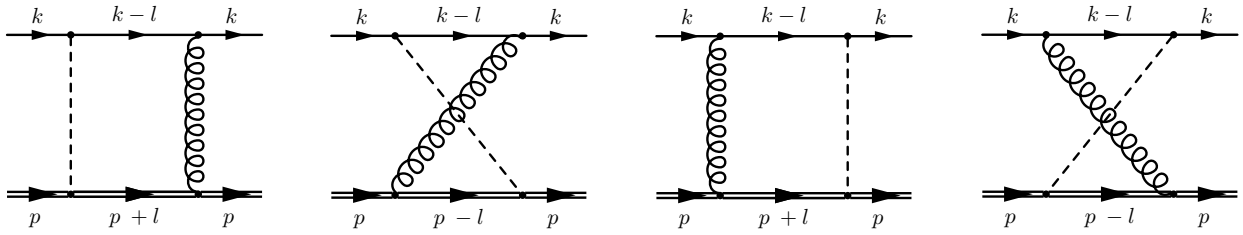
As a comparison, the NRQED-NRQED calculation of the analogous diagrams gives

$$\frac{\mathcal{M}^{NN}}{Q_l^2 Q_p^2 \alpha^2} = \chi_\mu^\dagger \chi_\mu \chi_p^\dagger \chi_p \frac{4mM\pi}{(m+M)\lambda^3}, \quad (5.18)$$

i.e. the sum of the two $1/\lambda^3$ terms in (5.15) agrees with (5.18). More importantly, (5.17) clearly is the $1/M$ expanded result of (5.15).

Since the expanded results are simpler to check numerically, the rest of the calculations only the expanded results will be presented.

5.1.2.2 Order $1/M$: $iD_t - D^2$ interference



The amplitude of the resulting diagrams is

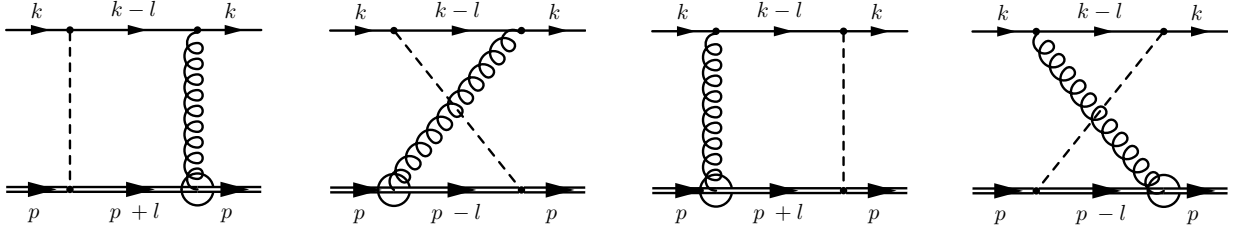
$$\mathcal{M}_{D,C} = (-i) \pm e^4 Q_l^2 Q_p^2 \bar{u} \gamma^0 u \chi^\dagger \chi \frac{1}{M} \int \frac{d^4 l}{(2\pi)^4} \frac{1}{(l-k)^2 - m^2} \frac{\vec{l}^2}{(l^2 - \lambda^2)^2} \frac{1}{\pm l^0 - \frac{\vec{l}^2}{2M}}, \quad (5.19)$$

where

$$\begin{aligned} \mathcal{M}_D &= +\alpha^2 Q_l^2 Q_p^2 \bar{u} \gamma^0 u \chi^\dagger \chi \left(\frac{2\pi}{\lambda M} + \frac{3 \log(\lambda/m)}{mM} - \frac{2\pi m}{\lambda M^2} + \frac{31}{8M^2} - \frac{15 \log(2\Lambda/m)}{4M^2} \right) \\ \mathcal{M}_C &= -\alpha^2 Q_l^2 Q_p^2 \bar{u} \gamma^0 u \chi^\dagger \chi \left(-\frac{3 \log(\lambda/m)}{mM} + \frac{31}{8M^2} - \frac{15 \log(2\Lambda/m)}{4M^2} \right). \end{aligned}$$

Thus,

$$\mathcal{M}_{D+C} = \alpha^2 Q_l^2 Q_p^2 \bar{u} \gamma^0 u \chi^\dagger \chi \left(\frac{2\pi}{\lambda M} + \frac{6 \log(\lambda/m)}{mM} - \frac{2\pi m}{\lambda M^2} \right).$$



5.1.2.3 Order $1/M$: $iD_t - \sigma \cdot B$ interference

We find

$$\mathcal{M}_{D,C} = -(-i) \left(\frac{2}{3} \right) e^4 Q_l^2 Q_p^2 c_F \bar{u} \gamma^i \gamma^5 u \chi^\dagger \sigma^i \chi \frac{1}{M} \int \frac{d^4 l}{(2\pi)^4} \frac{1}{(l-k)^2 - m^2} \frac{\vec{l}^2}{(l^2 - \lambda^2)^2} \frac{1}{\pm l^0 - \frac{\vec{l}^2}{2M}}$$

$$\begin{aligned} \frac{\mathcal{M}_D}{\alpha^2 Q_l^2 Q_p c_F} &= -\frac{2}{3} \bar{u} \gamma^i \gamma^5 u \chi^\dagger \sigma^i \chi \left(\frac{2\pi}{\lambda M} + \frac{3 \log(\lambda/m)}{mM} - \frac{2\pi m}{\lambda M^2} + \frac{31}{8M^2} - \frac{15 \log(2\Lambda/m)}{4M^2} \right) \\ \frac{\mathcal{M}_C}{\alpha^2 Q_l^2 Q_p c_F} &= -\frac{2}{3} \bar{u} \gamma^i \gamma^5 u \chi^\dagger \sigma^i \chi \left(-\frac{3 \log(\lambda/m)}{mM} + \frac{31}{8M^2} - \frac{15 \log(2\Lambda/m)}{4M^2} \right) \end{aligned}$$

Thus,

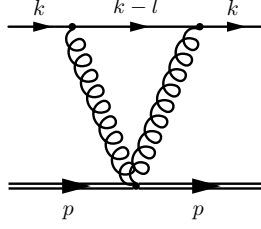
$$\mathcal{M}_{D+C} = -\frac{2}{3} \alpha^2 Q_l^2 Q_p c_F \bar{u} \gamma^i \gamma^5 u \chi^\dagger \sigma^i \chi \left(\frac{2\pi}{\lambda M} - \frac{2\pi m}{\lambda M^2} + \frac{31}{4M^2} - \frac{15 \log(2\Lambda/m)}{2M} \right).$$

As a comparison, the NRQED-NRQED calculation of the analogous diagrams gives

$$\mathcal{M}^{NN} = \frac{2}{3} \alpha^2 c_F^p c_F^\mu \chi_\mu^\dagger \sigma_\mu^i \chi_\mu \chi_p^\dagger \sigma_p^i \chi_p \left(-\frac{2\pi}{(m+M)\lambda} \right). \quad (5.20)$$

5.1.2.4 Order $1/M$: D^2 two-photon term

For the D^2 two-photon interaction, only one diagram contributes.



The amplitude of this diagram is expressed as

$$\begin{aligned}
\mathcal{M} &= (-i)3e^4 Q_l^2 Q_p^2 \bar{u}[\gamma^0(m-l^0) - m]u \chi^\dagger \chi \frac{1}{M} \int \frac{d^4 l}{(2\pi)^4} \frac{1}{[l^2 - \lambda^2]^2} \frac{1}{(l-k)^2 - m^2} \\
&= 3\alpha^2 Q_l^2 Q_p^2 \bar{u} \gamma^0 u \chi^\dagger \chi \left(-\frac{\pi}{2\lambda M} - \frac{1}{2mM} - \frac{2 \log(\lambda/m)}{mM} \right) \\
&\quad - 3\alpha^2 Q_l^2 Q_p^2 \bar{u} u \chi^\dagger \chi \left(-\frac{\pi}{2\lambda M} + \frac{1}{2mM} - \frac{\log(\lambda/m)}{mM} \right). \tag{5.21}
\end{aligned}$$

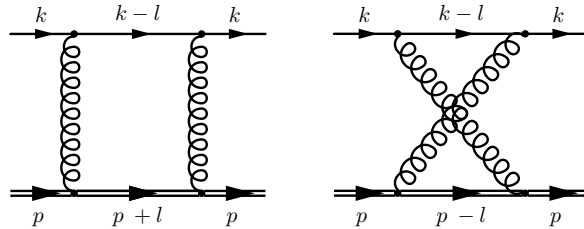
The non-relativistic limit of (5.21) is

$$\mathcal{M}^{NR} = \alpha^2 Q_l^2 Q_p^2 \chi_\mu^\dagger \chi_\mu \chi_p^\dagger \chi_p \left(\frac{2 \log m - 2 \log \lambda}{mM} - \frac{28}{15} \cdot \frac{1}{mM} \right). \tag{5.22}$$

As a comparison, the NRQED-NRQED calculation of the analogous diagram gives

$$\mathcal{M}^{NN} = \alpha^2 Q_l^2 Q_p^2 \chi_\mu^\dagger \chi_\mu \chi_p^\dagger \chi_p \left(\frac{2 \log(2\Lambda) - 2 \log \lambda}{mM} - \frac{28}{15} \cdot \frac{1}{mM} \right). \tag{5.23}$$

5.1.2.5 Order $1/M^2$: $D^2 - D^2$ interference



The amplitude of these two diagrams is

$$\mathcal{M}_{D,C} = (-i) \frac{e^4 Q_l^2 Q_p^2}{4M^2} \bar{u} [\gamma^0(m - l^0) - m] u \chi^\dagger \chi \int \frac{d^4 l}{(2\pi)^4} \frac{1}{(l-k)^2 - m^2} \frac{\vec{l}^2}{(l^2 - \lambda^2)^2} \frac{1}{\pm l^0 - \frac{l^2}{2M}},$$

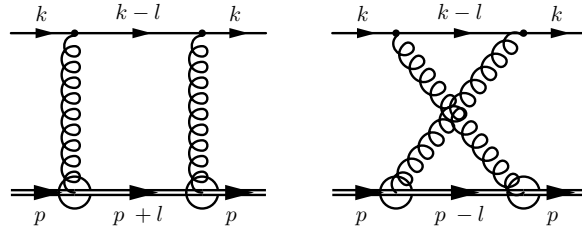
where

$$\begin{aligned} \mathcal{M}_D &= \frac{\alpha^2 Q_l^2 Q_p^2}{4M^2} \left[\chi^\dagger \chi \bar{u} \gamma^0 u \left(\frac{2\pi m}{\lambda} + 3 \log(\lambda/m) + \frac{3 \log(2\Lambda/m)}{2} + \frac{1}{4} \right) - \chi^\dagger \chi \bar{u} u \left(\frac{2\pi m}{\lambda} + 3 \log(\lambda/m) \right) \right] \\ \mathcal{M}_C &= \frac{\alpha^2 Q_l^2 Q_p^2}{4M^2} \left[\chi^\dagger \chi \bar{u} \gamma^0 u \left(-3 \log(\lambda/m) - \frac{3 \log(2\Lambda/m)}{2} - \frac{1}{4} \right) - \chi^\dagger \chi \bar{u} u (-3 \log(\lambda/m)) \right]. \end{aligned}$$

Thus,

$$\mathcal{M}_{D+C} = \frac{\alpha^2 Q_l^2 Q_p^2}{4M^2} (\bar{u} \gamma^0 u - \bar{u} u) \left(\frac{2\pi m}{\lambda} \right).$$

5.1.2.6 Order $1/M^2$: $\sigma \cdot B - \sigma \cdot B$ interference



The resulting amplitude is

$$\begin{aligned} \mathcal{M}_C + \mathcal{M}_D &= \frac{\alpha^2 Q_l^2 c_F^2}{2M^2} \left[\bar{u} \gamma^0 u \chi^\dagger \chi (I_0^C + I_0^D) - \bar{u} u \chi^\dagger \chi (I_m^C + I_m^D) \right. \\ &\quad \left. + \bar{u} \left(\frac{i}{2} \epsilon^{ijk} \gamma^j \gamma^k \right) u \chi^\dagger \sigma^i \chi \frac{1}{3} (I_m^D - I_m^C) + \bar{u} \gamma^i \gamma^5 u \chi^\dagger \sigma^i \chi \frac{1}{3} (I_0^C - I_0^D) \right], \end{aligned}$$

where

$$I_{m,0}^{D,C} = (-i) (4\pi)^2 \int \frac{d^4 l}{(2\pi)^4} \frac{\{m, m - l^0\} \vec{l}^2}{[(l-k)^2 - m^2] [(l^2 - \lambda^2)^2] \left[\pm l^0 - \frac{l^2}{2M} \right]},$$

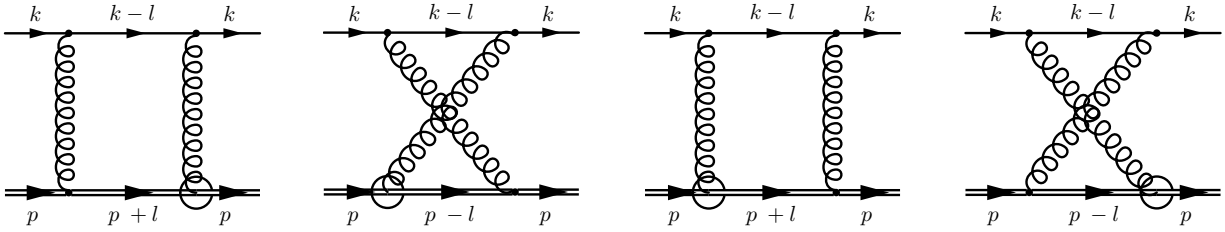
and

$$\begin{aligned}
I_m^D &= \frac{2\pi m}{\lambda} + 3 \log(\lambda/m) \\
I_0^D &= \frac{2\pi m}{\lambda} + 3 \log(\lambda/m) + \frac{1}{4} + \frac{3}{2} \log(2\Lambda/m) \\
I_m^C &= -3 \log(\lambda/m) \\
I_0^C &= -3 \log(\lambda/m) - \frac{1}{4} - \frac{3}{2} \log(2\Lambda/m).
\end{aligned}$$

Thus,

$$\begin{aligned}
\mathcal{M}_{D+C} &= \frac{\alpha^2 Q_l^2 c_F^2}{2M^2} \left[\bar{u} \gamma^0 u \chi^\dagger \chi \left(\frac{2\pi m}{\lambda} \right) - \bar{u} u \chi^\dagger \chi \left(\frac{2\pi m}{\lambda} \right) \right. \\
&\quad \left. + \bar{u} \left(\frac{i}{2} \epsilon^{ijk} \gamma^j \gamma^k \right) u \chi^\dagger \sigma^i \chi \left(\frac{2\pi m}{3\lambda} + 2 \log(\lambda/m) \right) \right. \\
&\quad \left. + \bar{u} \gamma^i \gamma^5 u \chi^\dagger \sigma^i \chi \left(-\frac{2\pi m}{3\lambda} - \frac{1}{6} - 2 \log(\lambda/m) - \log(2\Lambda/m) \right) \right].
\end{aligned}$$

5.1.2.7 Order $1/M^2$: $D^2 - \sigma \cdot B$ interference



$$\mathcal{M}_{D+C} = \frac{\alpha^2 Q_l^2 Q_p c_F}{M^2} \frac{1}{3} \chi^\dagger \sigma^i \chi \left[\bar{u} \left(\frac{i}{2} \epsilon^{ijk} \gamma^j \gamma^k \right) u (I_m^D - I_m^C) - \bar{u} \gamma^i \gamma^5 u (I_0^D - I_0^C) \right]$$

where

$$I_{m,0}^{D,C} = (-i)(4\pi)^2 \int \frac{d^4l}{(2\pi)^4} \frac{\{m, m-l^0\} \vec{l}^2}{[(l-k)^2 - m^2] [(l^2 - \lambda^2)^2] \left[\pm l^0 - \frac{\vec{l}^2}{2M} \right]}$$

$$I_m^D = \frac{2\pi m}{\lambda} + 3 \log(\lambda/m)$$

$$I_0^D = \frac{2\pi m}{\lambda} + \frac{1}{4} + 3 \log(\lambda/m) + \frac{3 \log(2\Lambda/m)}{2}$$

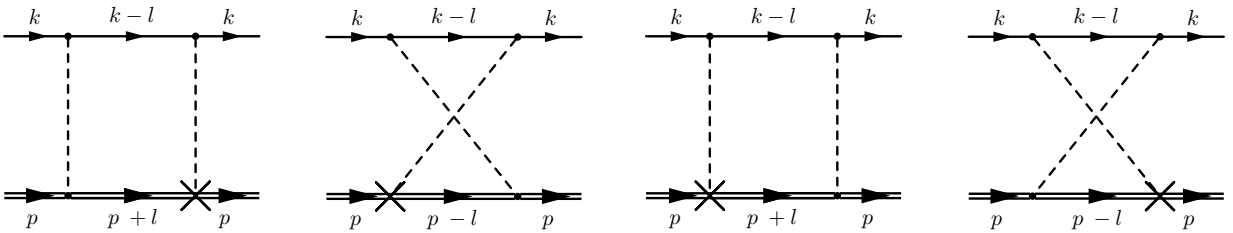
$$I_m^C = -3 \log(\lambda/m)$$

$$I_0^C = -\frac{1}{4} - 3 \log(\lambda/m) - \frac{3 \log(2\Lambda/m)}{2}.$$

Thus

$$\begin{aligned} \mathcal{M}_{D+C} = \frac{\alpha^2 Q_l^2 Q_p^{CF}}{M^2} \frac{1}{3} \chi^\dagger \sigma^i \chi \left[\bar{u} \left(\frac{i}{2} \epsilon^{ijk} \gamma^j \gamma^k \right) u \left(\frac{2\pi m}{\lambda} + 6 \log(\lambda/m) \right) \right. \\ \left. - \bar{u} \gamma^i \gamma^5 u \left(\frac{2\pi m}{\lambda} + \frac{1}{2} + 6 \log(\lambda/m) + 3 \log(2\Lambda/m) \right) \right]. \quad (5.24) \end{aligned}$$

5.1.2.8 Order $1/M^2$: $iD_t - \nabla \cdot E$ interference



$$\mathcal{M}_{D+C} = -\frac{\alpha^2 Q_l^2 Q_p^{CD}}{4M^2} \chi^\dagger \chi \left[\bar{u} u (I_m^D + I_m^C) + \bar{u} \gamma^0 u (I_0^D + I_0^C) \right]$$

where

$$I_{m,0}^{D,C} = (-i)(4\pi)^2 \int \frac{d^4l}{(2\pi)^4} \frac{\{m, m - l^0\} \vec{l}^2}{[(l-k)^2 - m^2] [l^2 - \lambda^2]^2 \left[\pm l^0 - \frac{\vec{l}^2}{2M} \right]}$$

$$I_m^D = \frac{2\pi m}{\lambda} + 3 \log(\lambda/m)$$

$$I_0^D = \frac{2\pi m}{\lambda} + 3 \log(\lambda/m) + \frac{1}{4} + \frac{3}{2} \log(2\Lambda/m)$$

$$I_m^C = -3 \log(\lambda/m)$$

$$I_0^C = -3 \log(\lambda/m) - \frac{1}{4} - \frac{3}{2} \log(2\Lambda/m).$$

Thus

$$\mathcal{M}_{D+C} = -\frac{\alpha^2 Q_l^2 Q_p c_D}{4M^2} \chi^\dagger \chi \left[\bar{u} u \left(\frac{2\pi m}{\lambda} \right) + \bar{u} \gamma^0 u \left(\frac{2\pi m}{\lambda} \right) \right]. \quad (5.25)$$

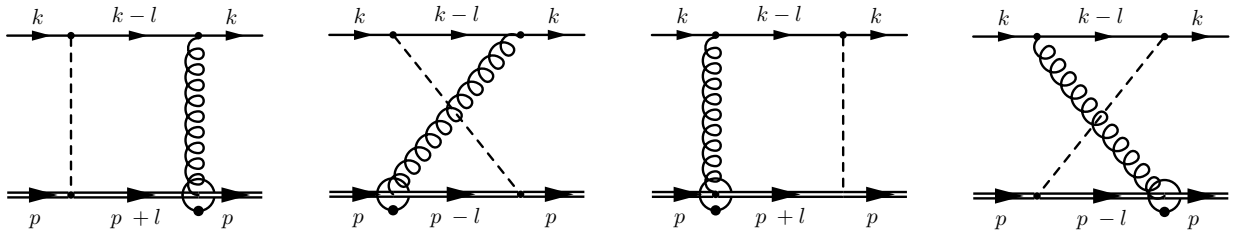
As a comparison, the NRQED-NRQED calculation of the analogous diagrams for the proton gives

$$\mathcal{M}^{NN} = \alpha^2 Q_l^2 Q_p^2 c_D^p \chi_\mu^\dagger \chi_\mu \chi_p^\dagger \chi_p \left(-\frac{\pi m}{M(M+m)\lambda} \right), \quad (5.26)$$

which is the sum of the terms in (5.25).

5.1.2.9 Order $1/M^2$: $iD_t - \sigma \cdot (D \times E - E \times D)$ interference:

Time derivative Feynman rule



$$\mathcal{M}_{D+C} = \frac{\alpha^2 Q_l^2 Q_p c_S}{6M^2} \chi^\dagger \sigma^k \chi \bar{u} \gamma^k \gamma^5 u (I^D - I^C)$$

where

$$I^{D,C} = (-i)(4\pi)^2 \int \frac{d^4 l}{(2\pi)^4} \frac{l^0 \vec{l}^2}{[(l-k)^2 - m^2] [l^2 - \lambda^2]^2} \left[\pm l^0 - \frac{\vec{l}^2}{2M} \right]$$

$$I^D = -\frac{3}{2} \log(2\Lambda/m)$$

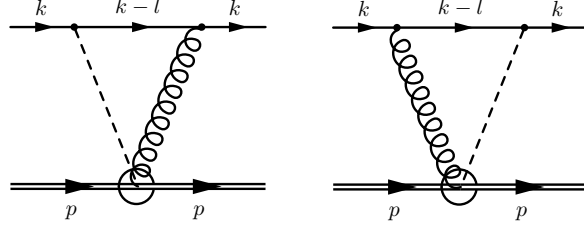
$$I^C = \frac{3}{2} \log(2\Lambda/m).$$

Thus

$$\mathcal{M}_{D+C} = \frac{\alpha^2 Q_l^2 Q_p c_S}{6M^2} \chi^\dagger \sigma^k \chi \bar{u} \gamma^k \gamma^5 u (-3 \log(2\Lambda/m)).$$

5.1.2.10 Order $1/M^2$: $iD_t - \sigma \cdot (D \times E - E \times D)$ interference:

Seagull Feynman rule



$$\mathcal{M} = \frac{\alpha^2 Q_l^2 c_S}{3M^2} \chi^\dagger \sigma^k \chi \bar{u} \gamma^k \gamma^5 u \cdot I$$

where

$$I = (-i)(4\pi)^2 \int \frac{d^4 l}{(2\pi)^4} \frac{\vec{l}^2}{[(l-k)^2 - m^2] [l^2 - \lambda^2]^2}$$

$$I = -\frac{1}{4} - \frac{3}{2} \log(2\Lambda/m),$$

where Λ is a UV cutoff regulator.

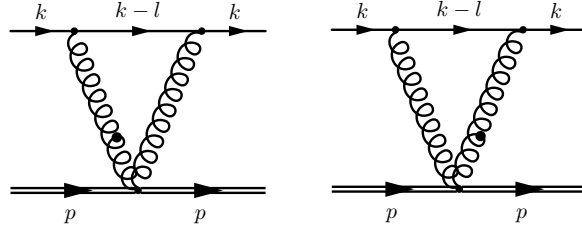
Thus

$$\mathcal{M} = \frac{\alpha^2 Q_l^2 c_S}{3M^2} \chi^\dagger \sigma^k \chi \bar{u} \gamma^k \gamma^5 u \left(-\frac{1}{4} - \frac{3}{2} \log(2\Lambda/m) \right).$$

5.1.2.11 Order $1/M^2$: $iD_t - \sigma \cdot (D \times E - E \times D)$ interference:

Two-photon-time-derivative Feynman rule

The diagrams that contribute to this interaction are



The amplitude from these diagrams is

$$\mathcal{M} = \frac{\alpha^2 Q_l^2 c_S}{M^2} \chi^\dagger \sigma^i \chi \left[\bar{u} \gamma^i \gamma^5 u \cdot I_0 - \bar{u} \left(\frac{i}{2} \epsilon^{ijk} \gamma^j \gamma^k \right) u \cdot I_m \right],$$

where

$$I_{m,0} = (-i)(4\pi)^2 \int \frac{d^4 l}{(2\pi)^4} \frac{\{m, m - l^0\} l^0}{[(l-k)^2 - m^2] [(l^2 - \lambda^2)^2]}$$

$$I_0 = \frac{\log(\lambda/m)}{2} - \frac{\log(2\Lambda/m)}{2} + \frac{5}{4}$$

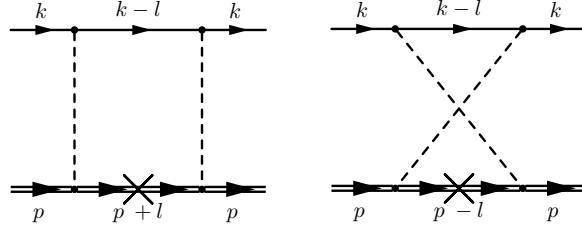
$$I_m = \log(\lambda/m) + 1,$$

where Λ is a UV cutoff regulator.

5.1.2.12 Order $1/M^2$: $iD_t - D^4$ interference

The resulting amplitude is

$$\mathcal{M}_{D+C} = -\frac{\alpha^2 Q_l^2 Q_p^2}{8M^3} \chi^\dagger \chi \left[\bar{u} u (I_m^D + I_m^C) + \bar{u} \gamma^0 u (I_0^D + I_0^C) \right],$$



where

$$I_{m,0}^{D,C} = (-i)(4\pi)^2 \int \frac{d^4l}{(2\pi)^4} \frac{\{m, m-l^0\} \vec{l}^4}{[(l-k)^2 - m^2] [l^2 - \lambda^2]^2 \left[\pm l^0 - \frac{\vec{l}^2}{2M} \right]^2}$$

$$I_m^D = \mathcal{O}(1)$$

$$I_0^D = \mathcal{O}(1)$$

$$I_m^C = 0$$

$$I_0^C = 0.$$

Thus,

$$\mathcal{M}_{D+C} = \mathcal{O}\left(\frac{1}{M^3}\right). \quad (5.27)$$

As a comparison, the NRQED-NRQED calculation of the analogous diagrams for the proton gives

$$\mathcal{M}^{NN} = \alpha^2 Q_t^2 Q_p^2 \chi_\mu^\dagger \chi_\mu \chi_p^\dagger \chi_p \left(\frac{\pi m^2}{M(M+m)^2 \lambda} \right), \quad (5.28)$$

which is the sum of the terms in (5.27).

5.1.2.13 Total Result

The total EFT result in Feynman gauge from the expanded proton propagator method is

$$\begin{aligned}
\mathcal{M}_{EFT} = & \alpha^2 Q_\ell^2 \left[\left(\frac{2Q_p^2 \pi m}{\lambda^3} - \frac{2Q_p^2 \pi m^2}{\lambda^3 M} + \frac{3Q_p^2 \pi}{4\lambda M} - \frac{2Q_p^2}{3mM} + \frac{2Q_p^2 \log(\lambda/m)}{mM} \right. \right. \\
& \left. \left. + \frac{2Q_p^2 \pi m^3}{\lambda^3 M^2} + \frac{3Q_p^2 \pi m}{4\lambda M^2} - \frac{Q_p c_D \pi m}{2\lambda M^2} - \frac{c_F^2 \pi m}{\lambda M^2} \right) \bar{u} u \chi^\dagger \chi \right. \\
+ & \left(\frac{2Q_p^2 \pi m}{\lambda^3} - \frac{2Q_p^2 \pi m^2}{\lambda^3 M} - \frac{5Q_p^2 \pi}{4\lambda M} - \frac{2Q_p^2}{3mM} - \frac{4Q_p^2 \log(\lambda/m)}{mM} + \frac{2Q_p^2 \pi m^3}{\lambda^3 M^2} + \frac{3Q_p^2 \pi m}{4\lambda M^2} - \frac{Q_p c_D \pi m}{2\lambda M^2} + \frac{c_F^2 \pi m}{\lambda M^2} \right) \bar{u} \gamma^0 u \chi^\dagger \chi \\
& + \left(-\frac{4Q_p^2 \pi}{3\lambda M} + \frac{4Q_p^2 \pi m}{3\lambda M^2} - \frac{2Q_p c_F \pi m}{3\lambda M^2} - \frac{c_F^2 \pi m}{3\lambda M^2} - \frac{31Q_p^2}{6M^2} + \frac{13Q_p c_S}{12M^2} - \frac{Q_p c_F}{6M^2} - \frac{c_F^2}{12M^2} \right. \\
+ & \left. \left(\frac{Q_p c_S}{M^2} - \frac{2Q_p c_F}{M^2} - \frac{c_F^2}{M^2} \right) \log(\lambda/m) + \left(\frac{5}{M^2} - \frac{3c_S}{2M^2} - \frac{c_F}{M^2} - \frac{c_F^2}{2M^2} \right) \log(2\Lambda/m) \right) \bar{u} \gamma^i \gamma^5 u \chi^\dagger \sigma^i \chi \\
+ & \left. \left(\frac{2Q_p c_F \pi m}{3\lambda M^2} + \frac{c_F^2 \pi m}{3\lambda M^2} - \frac{Q_p c_S}{M^2} + \left(-\frac{Q_p c_S}{M^2} + \frac{2Q_p c_F}{M^2} + \frac{c_F^2}{M^2} \right) \log(\lambda/m) \right) \bar{u} \left(\frac{i}{2} \epsilon^{ijk} \gamma^j \gamma^k \right) u \chi^\dagger \sigma^i \chi \right].
\end{aligned} \tag{5.29}$$

When this result is taken to the non-relativistic limit, i.e. $\bar{u}u, \bar{u}\gamma^0 u \rightarrow \chi_\ell^\dagger \chi_\ell, \bar{u} \left(\frac{i}{2} \epsilon^{ijk} \gamma^j \gamma^k \right) u, \bar{u} \gamma^i \gamma^5 u \rightarrow \chi_\ell^\dagger \sigma^i \chi_\ell$, and the proton Wilson coefficients are set to Q_p , the result is

$$\begin{aligned}
\frac{\mathcal{M}_{EFT}^{NR}}{Q_\ell^2 Q_p^2 \alpha^2} = & \chi_\ell^\dagger \chi_\ell \chi_p^\dagger \chi_p \left[\frac{4m\pi}{\lambda^3} - \frac{4}{3mM} - \frac{4m^2\pi}{M\lambda^3} - \frac{\pi}{2M\lambda} + \frac{2\log(m/\lambda)}{mM} + \frac{4m^3\pi}{M^2\lambda^3} + \frac{m\pi}{2M^2\lambda} \right] \\
& + \chi_\ell^\dagger \sigma^i \chi_\ell \chi_p^\dagger \sigma^i \chi_p \left[-\frac{4\pi}{3M\lambda} - \frac{16}{3M^2} + \frac{4m\pi}{3M^2\lambda} - \frac{2\log(m/2\Lambda)}{M^2} \right],
\end{aligned} \tag{5.30}$$

which is the same as Eq. 5.14 once it has been expanded in $1/M$, and the M in the logarithmic term has been replaced by a cut-off energy 2Λ .

5.1.3 Extraction of b_1 and b_2

With the amplitude of the point particle and the EFT calculations, we can now determine the Wilson coefficients b_1 and b_2 by taking difference of the two amplitudes. After expanding the $1/\lambda$ terms in the point particle solution, and the proton Wilson coefficients to Q_p , the

difference between the point particle and EFT results is

$$\mathcal{M}_{p.p.} - \mathcal{M}_{EFT} = \frac{\alpha^2 Q_\ell^2 Q_p^2}{M^2} \left(\frac{16}{3} - 2 \log(2\Lambda/M) \right) \bar{u} \gamma^i \gamma^5 u \chi^\dagger \sigma^i \chi, \quad (5.31)$$

where Λ is the UV cutoff of QED-NRQED.

5.2 Two Photon Exchange: Coulomb Gauge

For the two photon exchange calculations, we have set the proton incoming (\vec{p}) and outgoing (\vec{p}') to zero. Here we will use the same methods to solve the integrals as we have done before and only terms up to $1/M^2$ are kept.

5.2.1 QED Point Particle

The amplitude of the point particle in Coulomb gauge is calculated using the same method that was used for the Feynman gauge. The total amplitude is

$$\begin{aligned} \frac{\mathcal{M}_{p.p.}}{\alpha^2 Q_\ell^2 Q_p^2} = & \left(\frac{2\pi m M}{\lambda^3(m+M)} + \frac{17\pi}{16\lambda(m+M)} + \frac{2 \log(\lambda/m)}{mM} + \frac{2m \log(m/M)}{M(m^2 - M^2)} - \frac{247}{105mM} \right) \bar{u} u \chi^\dagger \chi \\ & + \left(\frac{2\pi m M}{\lambda^3(m+M)} - \frac{25\pi}{16\lambda(m+M)} - \frac{4 \log(\lambda/m)}{mM} - \frac{4m \log(m/M)}{M(m^2 - M^2)} + \frac{107}{105mM} \right) \bar{u} \gamma^0 u \chi^\dagger \chi \\ & + \left(-\frac{\pi(8M+3m)}{6\lambda M(m+M)} - \frac{2 \log(\lambda/m)}{3M^2} - \frac{2(m^2 - 3M^2) \log(m/M)}{3M^2(m^2 - M^2)} + \frac{23}{45M^2} \right) \bar{u} \gamma^i \gamma^5 u \chi^\dagger \sigma^i \chi \\ & + \left(\frac{\pi m}{2\lambda M(m+M)} + \frac{2 \log(\lambda/m)}{3M^2} + \frac{2m^2 \log(m/M)}{3M^2(m^2 - M^2)} - \frac{23}{45mM} \right) \bar{u} \left(\frac{i}{2} \epsilon^{ijk} \gamma^j \gamma^k \right) u \chi^\dagger \sigma^i \chi. \end{aligned} \quad (5.32)$$

Notice that this is not the same as the amplitude in the Feynman gauge, as seen in Eq. 5.13.

In the non-relativistic limit $\bar{u} u, \bar{u} \gamma^0 u \rightarrow \chi_\ell^\dagger \chi_\ell$, and $\bar{u} \left(\frac{i}{2} \epsilon^{ijk} \gamma^j \gamma^k \right) u, \bar{u} \gamma^i \gamma^5 u \rightarrow \chi_\ell^\dagger \sigma^i \chi_\ell$ and we obtain

$$\begin{aligned} \frac{\mathcal{M}_{p.p.}^{NR}}{Q_\ell^2 Q_p^2 \alpha^2} = & \chi_\ell^\dagger \chi_\ell \chi_p^\dagger \chi_p \left[\frac{4mM\pi}{(m+M)\lambda^3} - \frac{\pi}{2(m+M)\lambda} + \frac{2}{mM} \left(\frac{m^2 \log M - M^2 \log m}{m^2 - M^2} - \log \lambda - \frac{2}{3} \right) \right] \\ & + \chi_\ell^\dagger \sigma^i \chi_\ell \chi_p^\dagger \sigma^i \chi_p \left[-\frac{4\pi}{3(m+M)\lambda} + \frac{2 \log(m/M)}{m^2 - M^2} \right], \end{aligned} \quad (5.33)$$

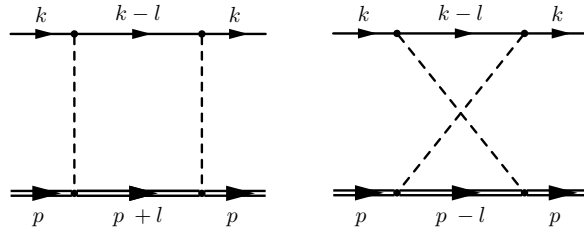
which is the same as Feynman gauge result in Eq. 5.14 and the NRQED-NRQED result [79].

5.2.2 Effective Field Theory

In the following calculations, $k = (m, \vec{0})$, and everything at order $1/M^3$ and above is omitted. The method used in this section is the same as in Sec 5.1.2. Only the expanded solutions are presented.

5.2.2.1 Leading Power

Here are the two diagrams that contribute to the Leading Power interaction.



Calculating the direct and cross Coulomb photon exchange diagrams, we find

$$\mathcal{M}_{\text{Direct+Crossed}} = \alpha^2 Q_l^2 Q_p^2 \chi^\dagger \chi [\bar{u} \gamma^0 u (I_0^D + I_0^C) + \bar{u} u (I_m^D + I_m^C)],$$

where

$$I_{m,0}^{D,C} = (-i)(4\pi)^2 \int \frac{d^4 l}{(2\pi)^4} \frac{\{m, m - l^0\}}{[(l - k)^2 - m^2] (\vec{l}^2 + \lambda^2)^2 \left[\pm l^0 - \frac{\vec{l}^2}{2M} \right]},$$

and

$$\begin{aligned} I_m^D &= \frac{2m\pi}{\lambda^3} - \frac{\pi}{2m\lambda} + \frac{8}{3m^2} - \frac{2}{3mM} - \frac{2m^2\pi}{M\lambda^3} - \frac{1}{3M^2} + \frac{2m^3\pi}{M^2\lambda^3} + \frac{m\pi}{2M^2\lambda} \\ I_m^C &= \frac{\pi}{2m\lambda} - \frac{8}{3m^2} - \frac{2}{3mM} + \frac{1}{3M^2} \\ I_0^D &= \frac{2m\pi}{\lambda^3} + \frac{\pi}{2m\lambda} - \frac{4}{3m^2} + \frac{4}{3mM} - \frac{2m^2\pi}{M\lambda^3} - \frac{\pi}{M\lambda} - \frac{7}{3M^2} + \frac{2m^3\pi}{M^2\lambda^3} + \frac{3m\pi}{2M^2\lambda} + \frac{2 \log(2\Lambda/m)}{M^2} \\ I_0^C &= -\frac{\pi}{2m\lambda} + \frac{4}{3m^2} + \frac{4}{3mM} + \frac{7}{3M^2} - \frac{2 \log(2\Lambda/m)}{M^2}, \end{aligned}$$

where Λ is a UV cutoff regulator. In total

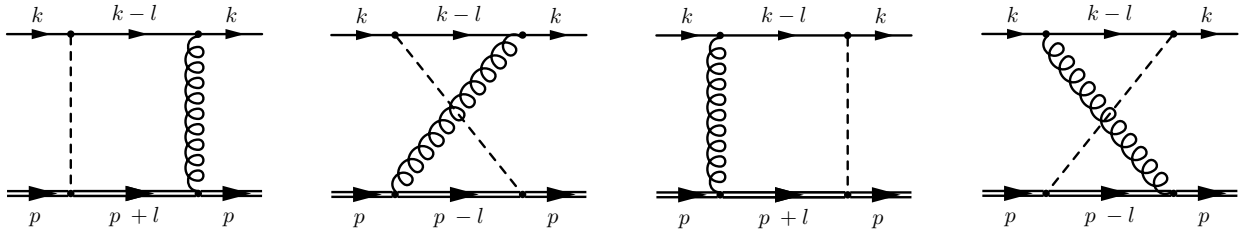
$$\begin{aligned} \frac{\mathcal{M}_{D+C}}{Q_l^2 Q_p^2 \alpha^2} &= \bar{u} u \chi^\dagger \chi \left[\frac{2m\pi}{\lambda^3} \left(1 - \frac{m}{M} + \frac{m^2}{M^2} \right) + \frac{m\pi}{2M^2\lambda} - \frac{4}{3mM} \right] \\ &+ \bar{u} \gamma^0 u \chi^\dagger \chi \left[\frac{2m\pi}{\lambda^3} \left(1 - \frac{m}{M} + \frac{m^2}{M^2} \right) - \frac{\pi}{M\lambda} \left(1 - \frac{3m}{2M} \right) + \frac{8}{3mM} \right]. \end{aligned} \quad (5.34)$$

As a comparison, the NRQED-NRQED calculation of the analogous diagrams gives

$$\frac{\mathcal{M}^{NN}}{Q_l^2 Q_p^2 \alpha^2} = \chi_\mu^\dagger \chi_\mu \chi_p^\dagger \chi_p \frac{4mM\pi}{(m+M)\lambda^3}, \quad (5.35)$$

i.e. the sum of the two $1/\lambda^3$ terms in (5.34) agrees with the $1/M$ expansion of this result, as expected.

5.2.2.2 Order $1/M$: $iD_t - D^2$ interference



We find

$$\mathcal{M}_{D,C} = (-i) \mp e^4 Q_l^2 Q_p^2 \bar{u} \gamma^0 u \chi^\dagger \chi \frac{1}{M} \int \frac{d^4 l}{(2\pi)^4} \frac{1}{(l-k)^2 - m^2} \frac{1}{l^2 - \lambda^2} \frac{1}{\pm l^0 - \frac{\vec{l}^2}{2M}} \frac{\lambda^2 \vec{l}^2}{(\vec{l}^2 + \lambda^2)^2} \quad (5.36)$$

$$\begin{aligned} \mathcal{M}_D &= -\alpha^2 Q_l^2 Q_p^2 \bar{u} \gamma^0 u \chi^\dagger \chi \left(-\frac{\pi}{2\lambda M} + \frac{2}{5mM} + \frac{\pi m}{2\lambda M^2} \right) \\ \mathcal{M}_C &= +\alpha^2 Q_l^2 Q_p^2 \bar{u} \gamma^0 u \chi^\dagger \chi \left(-\frac{2}{5mM} \right) \end{aligned}$$

Thus

$$\mathcal{M}_{D+C} = \alpha^2 Q_l^2 Q_p^2 \bar{u} \gamma^0 u \chi^\dagger \chi \left(\frac{\pi}{2\lambda M} - \frac{4}{5mM} - \frac{\pi m}{2\lambda M^2} \right)$$

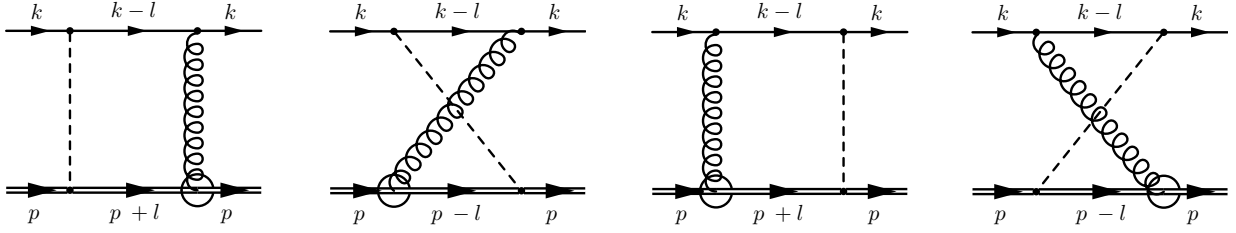
As a comparison, the NRQED-NRQED calculation of the analogous diagrams gives

$$\mathcal{M}^{NN} = \alpha^2 Q_l^2 Q_p^2 \chi_\mu^\dagger \chi_\mu \chi_p^\dagger \chi_p \left(-\frac{4}{5mM} + \frac{\pi}{2(M+m)\lambda} \right), \quad (5.37)$$

i.e. the same result.

5.2.2.3 Order $1/M$: $iD_t - \sigma \cdot B$ interference

The diagrams that contribute to this interaction are



We find

$$\mathcal{M}_{D,C} = (-i) \left(\frac{2}{3} \right) e^4 Q_l^2 Q_p c_F \bar{u} \gamma^i \gamma^5 u \chi^\dagger \sigma^i \chi \frac{1}{M} \int \frac{d^4 l}{(2\pi)^4} \frac{1}{(l-k)^2 - m^2} \frac{1}{l^2 - \lambda^2} \frac{1}{\pm l^0 - \frac{\vec{l}^2}{2M}} \frac{\vec{l}^2}{\vec{l}^2 + \lambda^2}$$

$$\begin{aligned} \frac{\mathcal{M}_D}{\alpha^2 Q_l^2 Q_p c_F} &= \frac{2}{3} \bar{u} \gamma^i \gamma^5 u \chi^\dagger \sigma^i \chi \left(-\frac{2\pi}{\lambda M} - \frac{2 \log(\lambda/m)}{mM} + \frac{4}{3mM} + \frac{2\pi m}{\lambda M^2} - \frac{4}{M^2} + \frac{3 \log(2\Lambda/m)}{M^2} \right) \\ \frac{\mathcal{M}_C}{\alpha^2 Q_l^2 Q_p c_F} &= \frac{2}{3} \bar{u} \gamma^i \gamma^5 u \chi^\dagger \sigma^i \chi \left(\frac{2 \log(\lambda/m)}{mM} - \frac{4}{3mM} - \frac{4}{M^2} + \frac{3 \log(2\Lambda/m)}{M^2} \right) \end{aligned}$$

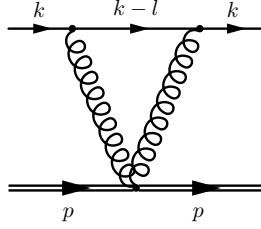
Thus

$$\mathcal{M}_{D+C} = \frac{2}{3} \alpha^2 Q_l^2 Q_p c_F \bar{u} \gamma^i \gamma^5 u \chi^\dagger \sigma^i \chi \left(-\frac{2\pi}{\lambda M} + \frac{2\pi m}{\lambda M^2} - \frac{8}{M^2} + \frac{6 \log(2\Lambda/m)}{M^2} \right)$$

As a comparison, the NRQED-NRQED calculation of the analogous diagrams gives

$$\mathcal{M}^{NN} = \frac{2}{3} \alpha^2 c_F^p c_F^\mu \chi_\mu^\dagger \sigma_\mu^i \chi_\mu \chi_p^\dagger \sigma_p^i \chi_p \left(-\frac{2\pi}{(m+M)\lambda} \right). \quad (5.38)$$

5.2.2.4 Order $1/M$: D^2 two-photon term



$$\begin{aligned}
\mathcal{M} &= (-i)e^4 Q_l^2 Q_p^2 \bar{u} [\gamma^0(m - l^0) - m] u \chi^\dagger \chi \frac{1}{M} \int \frac{d^4 l}{(2\pi)^4} \frac{1}{(l-k)^2 - m^2} \left(\frac{1}{l^2 - \lambda^2} \right)^2 \left(2 + \frac{\lambda^4}{(\vec{l}^2 + \lambda^2)^2} \right) \\
&= \alpha^2 Q_l^2 Q_p^2 \bar{u} \gamma^0 u \chi^\dagger \chi \frac{1}{M} \left(-\frac{17\pi}{16\lambda} - \frac{89}{105m} - \frac{4 \log(\lambda/m)}{m} \right) \\
&\quad - \alpha^2 Q_l^2 Q_p^2 \bar{u} u \chi^\dagger \chi \frac{1}{M} \left(-\frac{17\pi}{16\lambda} + \frac{107}{105m} - \frac{2 \log(\lambda/m)}{m} \right) \tag{5.39}
\end{aligned}$$

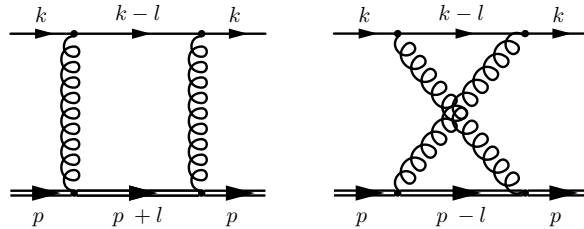
As a comparison, the NRQED-NRQED calculation of the analogous diagram gives

$$\mathcal{M}^{NN} = \alpha^2 Q_l^2 Q_p^2 \chi_\mu^\dagger \chi_\mu \chi_p^\dagger \chi_p \left(\frac{2 \log(2\Lambda) - 2 \log \lambda}{mM} - \frac{28}{15} \cdot \frac{1}{mM} \right). \tag{5.40}$$

The non-relativistic limit of (5.39) is

$$\mathcal{M}^{NR} = \alpha^2 Q_l^2 Q_p^2 \chi_\mu^\dagger \chi_\mu \chi_p^\dagger \chi_p \left(\frac{2 \log m - 2 \log \lambda}{mM} - \frac{28}{15} \cdot \frac{1}{mM} \right). \tag{5.41}$$

5.2.2.5 Order $1/M^2$: $D^2 - D^2$ interference



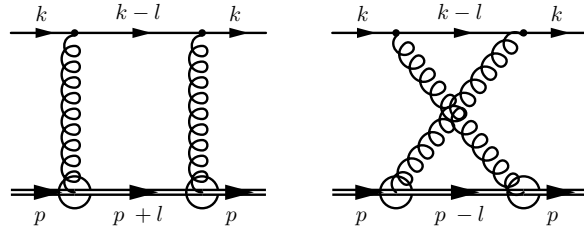
$$\mathcal{M}_{D,C} = (-i) \frac{e^4 Q_l^2 Q_p^2}{4M^2} \bar{u} [\gamma^0(m - l^0) - m] u \chi^\dagger \chi \int \frac{d^4 l}{(2\pi)^4} \frac{1}{(l - k)^2 - m^2} \frac{1}{(l^2 - \lambda^2)^2} \frac{1}{\pm l^0 - \frac{\vec{l}^2}{2M}} \frac{\vec{l}^2 \lambda^4}{(\vec{l}^2 + \lambda^2)^2}$$

$$\begin{aligned} \frac{\mathcal{M}_D}{\alpha^2 Q_l^2 Q_p^2} &= \chi^\dagger \chi (\bar{u} \gamma^0 u - \bar{u} u) \frac{1}{4M^2} \left(\frac{\pi m}{4\lambda} - \frac{6}{35} \right) \\ \frac{\mathcal{M}_C}{\alpha^2 Q_l^2 Q_p^2} &= \chi^\dagger \chi (\bar{u} \gamma^0 u - \bar{u} u) \frac{1}{4M^2} \left(\frac{6}{35} \right) \end{aligned}$$

Thus

$$\mathcal{M}_{D+C} = \frac{\alpha^2 Q_l^2 Q_p^2}{4M^2} (\bar{u} \gamma^0 u - \bar{u} u) \left(\frac{\pi m}{4\lambda} \right)$$

5.2.2.6 Order $1/M^2$: $\sigma \cdot B - \sigma \cdot B$ interference



$$\begin{aligned} \mathcal{M}_C + \mathcal{M}_D &= \frac{\alpha^2 Q_l^2 c_F^2}{2M^2} \left[\bar{u} \gamma^0 u \chi^\dagger \chi (I_0^C + I_0^D) - \bar{u} u \chi^\dagger \chi (I_m^C + I_m^D) \right. \\ &\quad \left. + \bar{u} \left(\frac{i}{2} \epsilon^{ijk} \gamma^j \gamma^k \right) u \chi^\dagger \sigma^i \chi \frac{1}{3} (I_m^D - I_m^C) + \bar{u} \gamma^i \gamma^5 u \chi^\dagger \sigma^i \chi \frac{1}{3} (I_0^C - I_0^D) \right] \end{aligned}$$

where

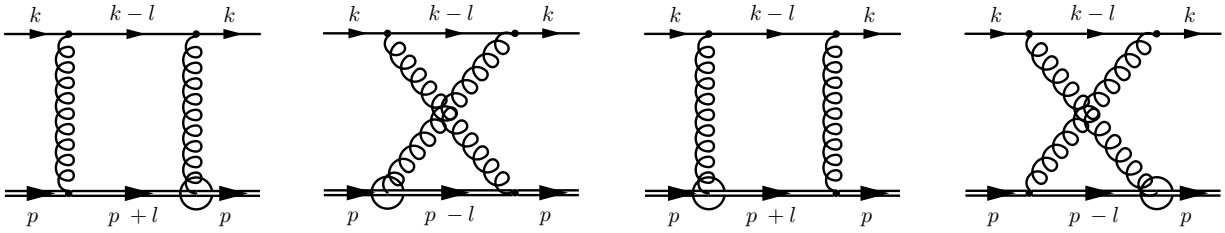
$$I_{m,0}^{D,C} = (-i)(4\pi)^2 \int \frac{d^4 l}{(2\pi)^4} \frac{\{m, m - l^0\} \vec{l}^2}{[(l - k)^2 - m^2] [(l^2 - \lambda^2)^2]} \left[\pm l^0 - \frac{\vec{l}^2}{2M} \right]$$

$$\begin{aligned}
I_m^D &= \frac{2\pi m}{\lambda} + 3 \log(\lambda/m) \\
I_0^D &= \frac{2\pi m}{\lambda} + 3 \log(\lambda/m) + \frac{1}{4} + \frac{3}{2} \log(2\Lambda/m) \\
I_m^C &= -3 \log(\lambda/m) \\
I_0^C &= -3 \log(\lambda/m) - \frac{1}{4} - \frac{3}{2} \log(2\Lambda/m).
\end{aligned}$$

Thus

$$\begin{aligned}
\mathcal{M}_C + \mathcal{M}_D &= \frac{\alpha^2 Q_l^2 c_F^2}{M^2} \left[\bar{u} \gamma^0 u \chi^\dagger \chi \left(\frac{2\pi m}{\lambda} \right) - \bar{u} u \chi^\dagger \chi \left(\frac{2\pi m}{\lambda} \right) \right. \\
&\quad + \bar{u} \left(\frac{i}{2} \epsilon^{ijk} \gamma^j \gamma^k \right) u \chi^\dagger \sigma^i \chi \left(\frac{2\pi m}{3\lambda} + 2 \log(\lambda/m) \right) \\
&\quad \left. + \bar{u} \gamma^i \gamma^5 u \chi^\dagger \sigma^i \chi \left(-\frac{2\pi m}{3\lambda} - \frac{1}{6} - 2 \log(\lambda/m) - \log(2\Lambda/m) \right) \right].
\end{aligned}$$

5.2.2.7 Order $1/M^2$: $D^2 - \sigma \cdot B$ interference



$$\mathcal{M}_C + \mathcal{M}_D = \frac{\alpha^2 Q_l^2 Q_p c_F}{M^2} \frac{1}{3} \chi^\dagger \sigma^i \chi \left[\bar{u} \left(\frac{i}{2} \epsilon^{ijk} \gamma^j \gamma^k \right) u (I_m^D - I_m^C) - \bar{u} \gamma^i \gamma^5 u (I_0^D - I_0^C) \right]$$

where

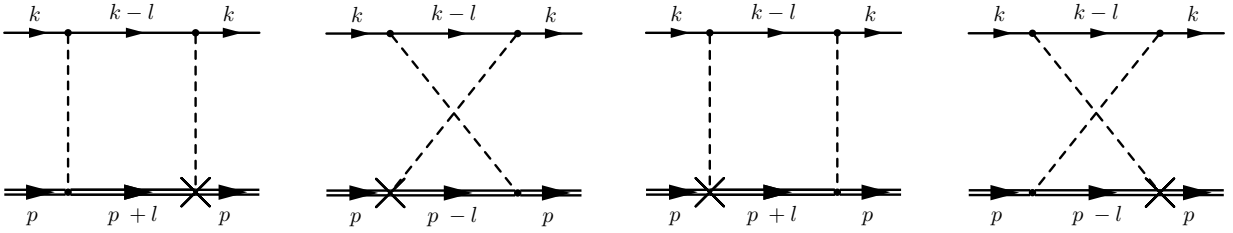
$$I_{m,0}^{D,C} = (-i)(4\pi)^2 \int \frac{d^4 l}{(2\pi)^4} \frac{\{m, m-l^0\} \vec{l}^2 \lambda^2}{[(l-k)^2 - m^2] [(l^2 - \lambda^2)^2] [\vec{l}^2 + \lambda^2] \left[\pm l^0 - \frac{\vec{l}^2}{2M} \right]}$$

$$\begin{aligned}
I_m^D &= \frac{\pi m}{2\lambda} - \frac{3}{5} \\
I_0^D &= \frac{\pi m}{2\lambda} - \frac{3}{5} \\
I_m^C &= \frac{3}{5} \\
I_0^C &= \frac{3}{5}.
\end{aligned}$$

Thus

$$\mathcal{M}_C + \mathcal{M}_D = \frac{\alpha^2 Q_l^2 Q_p c_F}{M^2} \frac{1}{3} \chi^\dagger \sigma^i \chi \left[\bar{u} \left(\frac{i}{2} \epsilon^{ijk} \gamma^j \gamma^k \right) u - \bar{u} \gamma^i \gamma^5 u \right] \left(\frac{\pi m}{2\lambda} - \frac{6}{5} \right).$$

5.2.2.8 Order $1/M^2$: $iD_t - \nabla \cdot E$ interference



$$\mathcal{M}_C + \mathcal{M}_D = -\frac{\alpha^2 Q_l^2 Q_p c_D}{4M^2} \chi^\dagger \chi \left[\bar{u} u (I_m^D + I_m^C) + \bar{u} \gamma^0 u (I_0^D + I_0^C) \right]$$

where

$$I_{m,0}^{D,C} = (-i)(4\pi)^2 \int \frac{d^4 l}{(2\pi)^4} \frac{\{m, m - l^0\} \vec{l}^2}{[(l - k)^2 - m^2] [\vec{l}^2 + \lambda^2]^2 \left[\pm l^0 - \frac{\vec{l}^2}{2M} \right]}$$

$$\begin{aligned}
I_m^D &= \frac{2\pi m}{\lambda} - 4 \\
I_0^D &= \frac{2\pi m}{\lambda} - 4 + 4 \log(2\Lambda/m) \\
I_m^C &= 4 \\
I_0^C &= 4 - 4 \log(2\Lambda/m).
\end{aligned}$$

Thus,

$$\mathcal{M}_C + \mathcal{M}_D = -\frac{\alpha^2 Q_l^2 Q_p c_D}{4M^2} \chi^\dagger \chi \left[\bar{u} u \left(\frac{2\pi m}{\lambda} \right) + \bar{u} \gamma^0 u \left(\frac{2\pi m}{\lambda} \right) \right] \quad (5.42)$$

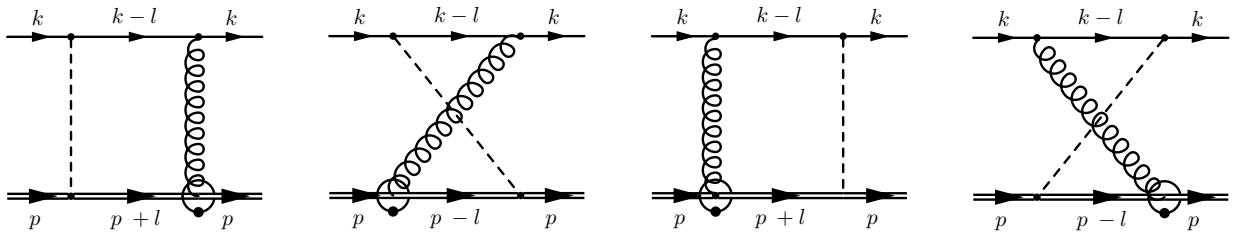
As a comparison, the NRQED-NRQED calculation of the analogous diagrams for the proton gives

$$\mathcal{M}^{NN} = \alpha^2 Q_l^2 Q_p^2 c_D^p \chi_\mu^\dagger \chi_\mu \chi_p^\dagger \chi_p \left(-\frac{\pi m}{M(M+m)\lambda} \right), \quad (5.43)$$

which is the the sum of the terms in (5.42).

5.2.2.9 Order $1/M^2$: $iD_t - \sigma \cdot (D \times E - E \times D)$ interference:

Time derivative Feynman rule



$$\mathcal{M}_C + \mathcal{M}_D = \frac{\alpha^2 Q_l^2 Q_p c_S}{6M^2} \chi^\dagger \sigma^k \chi \bar{u} \gamma^k \gamma^5 u (I^C - I^D)$$

where

$$I^{D,C} = (-i)(4\pi)^2 \int \frac{d^4 l}{(2\pi)^4} \frac{l^0 \vec{l}^2}{[(l-k)^2 - m^2] [l^2 - \lambda^2] [\vec{l}^2 + \lambda^2]} \left[\pm l^0 - \frac{\vec{l}^2}{2M} \right]$$

$$I^D = 2 \log(2\Lambda/m)$$

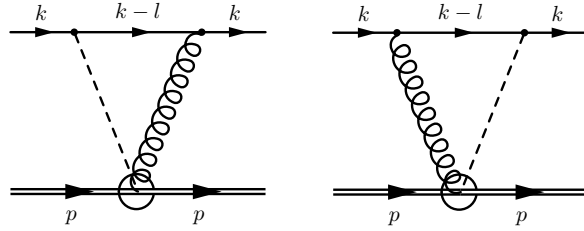
$$I^C = -2 \log(2\Lambda/m).$$

Thus,

$$\mathcal{M}_C + \mathcal{M}_D = \frac{\alpha^2 Q_l^2 Q_p c_S}{6M^2} \chi^\dagger \sigma^k \chi \bar{u} \gamma^k \gamma^5 u (-4 \log(2\Lambda/m)).$$

5.2.2.10 Order $1/M^2$: $iD_t - \sigma \cdot (D \times E - E \times D)$ interference:

Seagull Feynman rule



$$\mathcal{M} = -\frac{\alpha^2 Q_l^2 c_S}{3M^2} \chi^\dagger \sigma^k \chi \bar{u} \gamma^k \gamma^5 u \cdot I$$

where

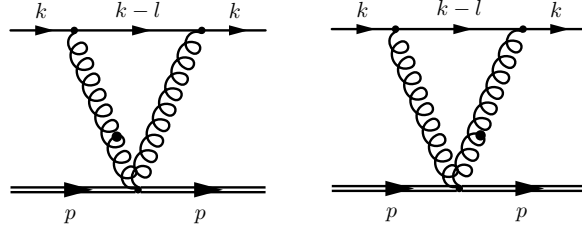
$$I = (-i)(4\pi)^2 \int \frac{d^4 l}{(2\pi)^4} \frac{\vec{l}^2}{[(l-k)^2 - m^2][l^2 - \lambda^2][\vec{l}^2 + \lambda^2]}$$

$$I = 2 \log(2\Lambda/m),$$

where Λ is a UV cutoff regulator.

Thus

$$\mathcal{M} = -\frac{\alpha^2 Q_l^2 c_S}{3M^2} \chi^\dagger \sigma^k \chi \bar{u} \gamma^k \gamma^5 u (2 \log(2\Lambda/m)).$$



5.2.2.11 Order $1/M^2$: $iD_t - \sigma \cdot (D \times E - E \times D)$ interference:

Two-photon-time-derivative Feynman rule

$$\mathcal{M} = \frac{\alpha^2 Q_l^2 c_S}{M^2} \chi^\dagger \sigma^i \chi \left[\bar{u} \gamma^i \gamma^5 u \cdot I_0 - \bar{u} \left(\frac{i}{2} \epsilon^{ijk} \gamma^j \gamma^k \right) u \cdot I_m \right]$$

where

$$I_{m,0} = (-i)(4\pi)^2 \int \frac{d^4 l}{(2\pi)^4} \frac{\{m, m - l^0\} l^0}{[(l - k)^2 - m^2] [(l^2 - \lambda^2)^2]} \left(1 - \frac{2\vec{l}^2}{3(\vec{l}^2 + \lambda^2)} \right)$$

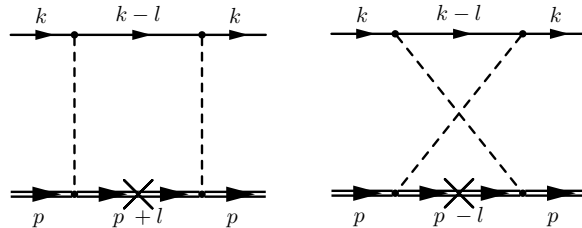
where

$$I_0 = \frac{\log(\lambda/m)}{3} - \frac{\log(2\Lambda/m)}{6} + \frac{7}{36}$$

$$I_m = \frac{\log(\lambda/m)}{3} + \frac{1}{9},$$

where Λ is a UV cutoff regulator.

5.2.2.12 Order $1/M^2$: $iD_t - D^4$ interference



$$\mathcal{M}_C + \mathcal{M}_D = -\frac{\alpha^2 Q_i^2 Q_p^2}{8M^3} \chi^\dagger \chi \left[\bar{u}u (I_m^D + I_m^C) + \bar{u}\gamma^0 u (I_0^D + I_0^C) \right]$$

where

$$I_{m,0}^{D,C} = (-i)(4\pi)^2 \int \frac{d^4l}{(2\pi)^4} \frac{\{m, m-l^0\} \vec{l}^4}{[(l-k)^2 - m^2] [\vec{l}^2 + \lambda^2]^2 \left[\pm l^0 - \frac{\vec{l}^2}{2M} \right]^2}$$

$$I_m^D = \mathcal{O}(1)$$

$$I_0^D = \mathcal{O}(1)$$

$$I_m^C = \mathcal{O}(1)$$

$$I_0^C = \mathcal{O}(1).$$

Thus,

$$\mathcal{M}_C + \mathcal{M}_D = \mathcal{O}\left(\frac{1}{M^3}\right). \quad (5.44)$$

As a comparison, the NRQED-NRQED calculation of the analogous diagrams for the proton gives

$$\mathcal{M}^{NN} = \alpha^2 Q_i^2 Q_p^2 \chi_\mu^\dagger \chi_\mu \chi_p^\dagger \chi_p \left(\frac{\pi m^2}{M(M+m)^2 \lambda} \right), \quad (5.45)$$

which is the sum of the terms in (5.44).

5.2.2.13 Total Result

The total EFT result in Coulomb gauge is

$$\begin{aligned}
\mathcal{M}_{EFT} = & \alpha^2 Q_\ell^2 \left[\left(\frac{2Q_p^2 \pi m}{\lambda^3} - \frac{2Q_p^2 \pi m^2}{\lambda^3 M} + \frac{17Q_p^2 \pi}{16\lambda M} - \frac{247Q_p^2}{105mM} + \frac{2Q_p^2 \log(\lambda/m)}{mM} \right. \right. \\
& \left. \left. + \frac{2Q_p^2 \pi m^3}{\lambda^3 M^2} + \frac{7Q_p^2 \pi m}{16\lambda M^2} - \frac{Q_p c_D \pi m}{2\lambda M^2} - \frac{c_F^2 \pi m}{\lambda M^2} \right) \bar{u} u \chi^\dagger \chi \right. \\
& + \left(\frac{2Q_p^2 \pi m}{\lambda^3} - \frac{2Q_p^2 \pi m^2}{\lambda^3 M} - \frac{25Q_p^2 \pi}{16\lambda M} + \frac{107Q_p^2}{105mM} - \frac{4Q_p^2 \log(\lambda/m)}{mM} \right. \\
& \left. + \frac{2Q_p^2 \pi m^3}{\lambda^3 M^2} + \frac{17Q_p^2 \pi m}{16\lambda M^2} - \frac{Q_p c_D \pi m}{2\lambda M^2} + \frac{c_F^2 \pi m}{\lambda M^2} \right) \bar{u} \gamma^0 u \chi^\dagger \chi \\
& + \left(-\frac{4Q_p c_F \pi}{3\lambda M} + \frac{7Q_p c_F \pi m}{6\lambda M^2} - \frac{c_F^2 \pi m}{3\lambda M^2} + \frac{7Q_p c_S}{36M^2} - \frac{74Q_p c_F}{15M^2} - \frac{c_F^2}{12M^2} + \left(\frac{Q_p c_S}{3M^2} - \frac{c_F^2}{M^2} \right) \log(\lambda/m) \right. \\
& \left. + \left(-\frac{3Q_p c_S}{2M^2} + \frac{4Q_p c_F}{M^2} - \frac{c_F^2}{2M^2} \right) \log(2\Lambda/m) \right) \bar{u} \gamma^i \gamma^5 u \chi^\dagger \sigma^i \chi \\
& \left. + \left(\frac{Q_p c_F \pi m}{6\lambda M^2} + \frac{c_F^2 \pi m}{3\lambda M^2} - \frac{Q_p c_S}{9M^2} - \frac{2Q_p c_F}{5M^2} + \left(-\frac{Q_p c_S}{3M^2} - \frac{c_F^2}{M^2} \right) \log(\lambda/m) \right) \bar{u} \left(\frac{i}{2} \epsilon^{ijk} \gamma^j \gamma^k \right) u \chi^\dagger \sigma^i \chi \right].
\end{aligned} \tag{5.46}$$

Note that as in the point-particle case, this is not the same result as the Feynman gauge as seen in Eq. 5.29.

When this result is taken to the non-relativistic limit, i.e. $\bar{u}u, \bar{u}\gamma^0 u \rightarrow \chi_\ell^\dagger \chi_\ell, \bar{u} \left(\frac{i}{2} \epsilon^{ijk} \gamma^j \gamma^k \right) u, \bar{u} \gamma^i \gamma^5 u \rightarrow \chi_\ell^\dagger \sigma^i \chi_\ell$, and the proton Wilson coefficients are set to Q_p , the result is

$$\begin{aligned}
\frac{\mathcal{M}_{EFT}^{NR}}{Q_\ell^2 Q_p^2 \alpha^2} = & \chi_\ell^\dagger \chi_\ell \chi_p^\dagger \chi_p \left[\frac{4m\pi}{\lambda^3} - \frac{4}{3mM} - \frac{4m^2\pi}{M\lambda^3} - \frac{\pi}{2M\lambda} + \frac{2\log(m/\lambda)}{mM} + \frac{4m^3\pi}{M^2\lambda^3} + \frac{m\pi}{2M^2\lambda} \right] \\
& + \chi_\ell^\dagger \sigma^i \chi_\ell \chi_p^\dagger \sigma^i \chi_p \left[-\frac{4\pi}{3M\lambda} - \frac{16}{3M^2} + \frac{4m\pi}{3M^2\lambda} - \frac{2\log(m/2\Lambda)}{M^2} \right],
\end{aligned} \tag{5.47}$$

which is the same result as the Feynman gauge calculation and the same as both point particle calculations once they been expanded in $1/M$, and the M in the logarithmic term has been replaced by a cut-off energy 2Λ .

5.2.3 Extraction of b_1 and b_2

Just as before, we can now find the Wilson coefficients b_1 and b_2 by taking the difference between the point particle and EFT amplitudes. After expanding the $1/\lambda$ terms in the point particle solution, and the proton Wilson coefficients to Q_p , the difference between the point particle and EFT result is

$$\mathcal{M}_{p.p.} - \mathcal{M}_{EFT} = \frac{\alpha^2 Q_\ell^2 Q_p^2}{M^2} \left(\frac{16}{3} - 2 \log(2\Lambda/M) \right) \bar{u} \gamma^i \gamma^5 u \chi^\dagger \sigma^i \chi, \quad (5.48)$$

This is the same result as the Feynman gauge in Eq. 5.31.

5.3 Two Photon Exchange Results at Order $1/M^2$ Conclusion

One should note that the Coulomb and Feynman do not give the same final answer in the EFT case nor for the case of the point-like proton. All four calculations do agree however once the lepton line is taken to the non-relativistic limit. In the relativistic limit, it is only the differences between the point-like proton and real proton where the different gauges agree. This shows that the QED-NRQED EFT is able to provide information about the Wilson coefficients b_1 and b_2 . Although we obtain different amplitudes in the Coulomb and Feynman gauge, the differences between the QED point particle result and the QED-NRQED real proton result are the same in both gauges, meaning that b_1 and b_2 are the same in both gauges. When matching the QED-NRQED EFT to the point particle, the value of the Wilson coefficients b_1 and b_2 are

$$b_1 = 0 + \mathcal{O}(\alpha^3) \quad b_2 = \alpha^2 Q_\ell^2 Q_p^2 \left[\frac{16}{3} - 2 \log \left(\frac{2\Lambda}{M} \right) \right] + \mathcal{O}(\alpha^3). \quad (5.49)$$

Because terms with an even number of gamma matrices are suppressed by a factor of m/M , the coefficients of the $\bar{u} u \chi^\dagger \chi$ and $\bar{u} (\epsilon^{ijk} \gamma^j \gamma^k) u \chi^\dagger \sigma^i \chi$ terms are expected to be zero, and in

fact they are. What is surprising is that b_1 , is also zero. It remains to be seen if this also the case in the matching to a real proton

CHAPTER 6: CONCLUSIONS AND OUTLOOK

6.1 Conclusion

It has been seven years since the proton charge radius puzzle was brought to light and the scientific community is no closer to solving it now. While there are many contributions that have to be taken into account when calculating the charge radius, the TPE contribution has a much higher uncertainty than many others, and is the focus of the work presented here. This dissertation has established the QED-NRQED EFT by reproducing known calculations. These calculations are the one-photon exchange which in turned reproduced Rosenbluth scattering up to $\mathcal{O}(m^2/M^2)$, and TPE at leading order in m/M , which in turned produced Mott scattering with an α correction. New results presented in Chapter 5 consisted of higher orders of TPE calculations in $\mathcal{O}(m^2/M^2)$, and showing that these calculations produce consistent results. These calculations were completed to determine the Wilson coefficients b_1 and b_2 in the QED-NRQED effective lagrangian, Eq. 3.7. Surprisingly, in the case of a point-like proton, $b_1 = 0$.

6.2 Future Work

One of the issues involved in the extraction of the proton charge radius from muonic hydrogen is the hadronic uncertainty associated with the two-photon exchange amplitude. Only its imaginary part can be directly reconstructed from experimental data. Since there is a term that needs to be subtracted in the dispersion relation, the amplitude cannot be fully reconstructed from its imaginary part. We have some information about the subtraction function, but by and large, it has to be modeled [68].

There have been several studies of this issue, see e.g. [77, 80, 81, 82, 83], but considering the far-reaching implications of the puzzle it is important to explore a variety of approaches. One such approach is to directly match onto NRQED to describe proton structure effects in hydrogen-like systems as was done in [68]¹. From such an analysis one finds that the muonic

¹See also [66, 67] for a different approach that first used NRQED for this problem.

hydrogen measurement depends on two Wilson coefficients in the NRQED Lagrangian. One is equivalent to the charge radius. The other is the coefficient of the spin-independent muon-proton contact interaction and could be determined by matching to the two-photon amplitude, if it was fully known.

The muonic hydrogen result can be tested in the planned muon-proton scattering experiment, MUSE [5]. In this experiment, the 3-momentum of the muons is of the order of the muon mass. QED-NRQED is an appropriate EFT as it combines relativistic muons and non-relativistic protons interactions, and is naturally organized as an expansion in α and m/M . This dissertation has presented three QED-NRQED calculations: $\mathcal{O}(Q_p\alpha)$ amplitude results up to and including power m^2/M^2 , $\mathcal{O}(Q_p^2\alpha^2)$ at leading power in m/M , and values for the Wilson coefficients b_1 and b_2 by matching these amplitudes onto point particle results. With the results obtained the cross section can be determined as well. In order to accomplish this, the hadronic tensor $W^{\mu\nu}$ will be needed, and is defined as

$$W^{\mu\nu}(k, s, q) = i \int d^4x e^{iq \cdot x} \langle \mathbf{k}, s | T \{ J_{\text{e.m.}}^\mu(x) J_{\text{e.m.}}^\nu(0) \} | \mathbf{k}, s \rangle, \quad (6.1)$$

where \mathbf{k} is the nucleon three-momentum, s its spin, and $J_{\text{e.m.}}^\mu$ is the electromagnetic current. Note that some authors refer to this quantity as $T^{\mu\nu}$ [84, 85].

Using current conservation, and invariance of electromagnetic interactions under parity and time-reversal, $W^{\mu\nu}$ can be expressed as

$$\begin{aligned} W^{\mu\nu} = \bar{u}_p(\mathbf{k}, s) & \left[\left(-g^{\mu\nu} + \frac{q^\mu q^\nu}{q^2} \right) W_1(\nu, Q^2) + \left(k^\mu - \frac{k \cdot q q^\mu}{q^2} \right) \left(k^\nu - \frac{k \cdot q q^\nu}{q^2} \right) W_2(\nu, Q^2) \right. \\ & + \left([\gamma^\nu, \not{q}] k^\mu - [\gamma^\mu, \not{q}] k^\nu + [\gamma^\mu, \gamma^\nu] q \cdot k \right) H_1(\nu, Q^2) \\ & \left. + \left([\gamma^\nu, \not{q}] q^\mu - [\gamma^\mu, \not{q}] q^\nu + [\gamma^\mu, \gamma^\nu] q^2 \right) H_2(\nu, Q^2) \right] u_p(\mathbf{k}, s), \quad (6.2) \end{aligned}$$

where the four scalar functions W_1 , W_2 , H_1 , and H_2 depend on the variables $\nu = 2k \cdot q$ and $Q^2 = -q^2$. For a point particle, $W_1 = 2\nu^2/(Q^4 - \nu^2)$, $W_2 = 8Q^2/(Q^4 - \nu^2)$, $H_1 =$

$-2Q^2/(Q^4 - \nu^2)$, and $H_2 = 0$. W_1 and W_2 are defined as

$$\begin{aligned}
 W_1(\nu, Q^2) &= W_1(0, Q^2) + \frac{\nu^2}{\pi} \int_0^\infty d\nu'^2 \frac{\text{Im}W_1(\nu', Q^2)}{\nu'^2(\nu'^2 - \nu^2)}, \\
 W_2(\nu, Q^2) &= \frac{1}{\pi} \int_0^\infty d\nu'^2 \frac{\text{Im}W_2(\nu', Q^2)}{\nu'^2 - \nu^2}.
 \end{aligned} \tag{6.3}$$

Future work will consist of relating the two photon exchange calculations Wilson coefficients b_1 and b_2 to the full two-photon amplitude, i.e. W_1 , W_2 , H_1 , and H_2 . This final expected result will look similar to Eq. 7 in Ref. [68]. We will also compare to the NRQED Wilson coefficients d_1 and d_2 either directly by matching, or indirectly via the full two-photon amplitude. Once this is done, one could calculate the lepton-proton cross section in QED-NRQED. Ideally this would lead to a direct model-independent relation between muon-proton scattering and muonic hydrogen spectroscopy, or in other words, use data to resolve the hadronic uncertainty.

APPENDIX: KINEMATICS

We consider lepton-proton scattering, $\ell(k) + p(p) \rightarrow \ell(k') + p(p')$ in the initial proton rest frame, i.e. $\vec{p} = 0$. We denote the lepton mass by m and the proton mass by M . The initial lepton energy is E and the final lepton energy is E' . The scattering angle, i.e. the angle between \vec{k} and \vec{k}' is θ . We define $q = k - k' = p' - p$.

For spin-averaged $2 \rightarrow 2$ scattering there are only two independent variables, so many of the kinematical variables can be related to one another:

$$\begin{aligned}
 p' &= p + q, & k' &= k - q, & p^2 &= M^2, & k^2 &= m^2, \\
 p \cdot q &= M(E - E') = Mq^0 = -q^2/2, \\
 k \cdot q &= q^2/2, & \vec{q}^2 &= -q^2 + q^4/4M^2.
 \end{aligned} \tag{4}$$

There are also several approximate relations between the various kinematic variables:

$$\begin{aligned}
 q^2 &= -\vec{q}^2 + \vec{q}^4/4M^2 + \mathcal{O}\left(\frac{1}{M^3}\right) \\
 \vec{k} \cdot \vec{q} &= \vec{q}^2/2 + \mathcal{O}\left(\frac{1}{M}\right) \\
 \vec{k}' \cdot \vec{q} &= -\vec{q}^2/2 + \mathcal{O}\left(\frac{1}{M}\right)
 \end{aligned} \tag{5}$$

The differential cross section is given by:

$$\frac{d\sigma}{d\Omega} = \frac{1}{64\pi^2 M} \frac{|\vec{k}'|}{|\vec{k}|} \frac{1}{\left| M + E - \frac{|\vec{k}|E' \cos\theta}{|\vec{k}'|} \right|} \overline{|\mathcal{M}|^2}, \tag{6}$$

where as usual $\overline{|\mathcal{M}|^2}$ is the spin-averaged amplitude squared.

Usually the Dirac spinors are normalized via $u^\dagger u = 2E$. For NRQED the spinors are

normalized as $\xi^\dagger \xi = 1$. As a result we can relate the amplitude for lepton-proton scattering in the standard normalization (\mathcal{M}) to that of QED-NRQED (\mathcal{M}_{QN}) via $\mathcal{M} = 2\sqrt{E_{p'}E_p}\mathcal{M}_{\text{QN}}$. In the rest frame of the initial proton the spin averaged amplitudes $|\overline{\mathcal{M}}|^2$ and $|\overline{\mathcal{M}}|_{\text{QN}}^2$ are related by $|\overline{\mathcal{M}}|^2 = 4ME_{p'}|\overline{\mathcal{M}}|_{\text{QN}}^2$, where $E_{p'} = \sqrt{M^2 + \vec{q}^2}$.

Spin averaged squared amplitudes in QED-NRQED can be calculated by an analogue of the Casimir trick. Thus for the amplitude of the form $\mathcal{M} = \xi_{p'}^\dagger \Sigma \xi_p \bar{u}(k') \Gamma u(k)$, where ξ is a two-component spinor, $\Sigma = \vec{\sigma}$ or $1_{2 \times 2}$, u is a Dirac spinor, and Γ part of the Dirac basis,

$$|\overline{\mathcal{M}}|_{\text{QN}}^2 = \frac{1}{4} \text{Tr} [\Sigma \Sigma^\dagger] \text{Tr} [(k + m) \Gamma (k' + m) \bar{\Gamma}], \quad (7)$$

where $\bar{\Gamma} = \gamma^0 \Gamma^\dagger \gamma^0$.

BIBLIOGRAPHY

- [1] R. Pohl *et al.*, Nature **466**, 213 (2010).
- [2] P. J. Mohr, B. N. Taylor and D. B. Newell, Rev. Mod. Phys. **80**, 633 (2008)
doi:10.1103/RevModPhys.80.633 [arXiv:0801.0028 [physics.atom-ph]].
- [3] A. Antognini *et al.*, Science **339**, 417 (2013). doi:10.1126/science.1230016
- [4] P. J. Mohr, D. B. Newell and B. N. Taylor, Rev. Mod. Phys. **88**, no. 3, 035009 (2016)
doi:10.1103/RevModPhys.88.035009 [arXiv:1507.07956 [physics.atom-ph]].
- [5] R. Gilman *et al.* [MUSE Collaboration], arXiv:1709.09753 [physics.ins-det].
- [6] R. J. Hill, EPJ Web Conf. **137**, 01023 (2017) doi:10.1051/epjconf/201713701023
[arXiv:1702.01189 [hep-ph]].
- [7] M. Horbatsch, E. A. Hessels and A. Pineda, Phys. Rev. C **95**, no. 3, 035203 (2017)
doi:10.1103/PhysRevC.95.035203 [arXiv:1610.09760 [nucl-th]].
- [8] W. E. Lamb Jr., R. C. Retherford, Phys. Rev. **72**, (1947) 339.
- [9] M. Niering *et al.*, Phys. Rev. Lett. **84**, 5496-5499 (2000).
- [10] M. Fischer *et al.*, Phys. Rev. Lett. **92**, 230802 (2004).
doi:10.1103/PhysRevLett.92.230802
- [11] B. de Beauvoir *et al.*, Eur. Phys. J. D **12**, 61-93 (2000).
- [12] C. Schwob *et al.*, Phys. Rev. Lett. **82**, 4960 (1999). doi:10.1103/PhysRevLett.82.4960
- [13] M. I. Eides, H. Grotch and V. A. Shelyuto, Phys. Rept. **342**, 63 (2001)
doi:10.1016/S0370-1573(00)00077-6 [hep-ph/0002158].
- [14] S. G. Karshenboim, Phys. Rept. **422**, 1 (2005) doi:10.1016/j.physrep.2005.08.008 [hep-ph/0509010].
- [15] A. Beyer *et al.*, Science **358**, 79 (2017)

- [16] R. Pohl *et al.* [CREMA Collaboration], *Science* **353**, no. 6300, 669 (2016).
doi:10.1126/science.aaf2468
- [17] P. J. Mohr, B. N. Taylor and D. B. Newell, *Rev. Mod. Phys.* **84**, 1527 (2012)
doi:10.1103/RevModPhys.84.1527 [arXiv:1203.5425 [physics.atom-ph]].
- [18] A. Antognini *et al.*, *Can. J. Phys.* **89**, no. 1, 47 (2011). doi:10.1139/P10-113
- [19] N. Nevo Dinur, C. Ji, S. Bacca and N. Barnea, *Phys. Lett. B* **755**, 380 (2016)
doi:10.1016/j.physletb.2016.02.023 [arXiv:1512.05773 [nucl-th]].
- [20] O. J. Hernandez, N. Nevo Dinur, C. Ji, S. Bacca and N. Barnea, *Hyperfine Interact.*
237, no. 1, 158 (2016) doi:10.1007/s10751-016-1371-9 [arXiv:1604.06496 [nucl-th]].
- [21] C. E. Carlson, M. Gorchtein and M. Vanderhaeghen, *Phys. Rev. A* **95**, no. 1, 012506
(2017) doi:10.1103/PhysRevA.95.012506 [arXiv:1611.06192 [nucl-th]].
- [22] B. Franke, J. J. Krauth, A. Antognini, M. Diepold, F. Kottmann and R. Pohl,
arXiv:1705.00352 [physics.atom-ph].
- [23] Y. Ma *et al.*, *Int. J. Mod. Phys. Conf. Ser.* **40**, 1660046 (2016).
doi:10.1142/S2010194516600466
- [24] A. Adamczak *et al.* [FAMU Collaboration], *JINST* **11**, no. 05, P05007 (2016)
doi:10.1088/1748-0221/11/05/P05007 [arXiv:1604.01572 [physics.ins-det]].
- [25] R. Pohl [CREMA Collaboration], *J. Phys. Soc. Jap.* **85**, no. 9, 091003 (2016).
doi:10.7566/JPSJ.85.091003
- [26] J. Arrington, P. G. Blunden and W. Melnitchouk, *Prog. Part. Nucl. Phys.* **66**, 782
(2011) doi:10.1016/j.ppnp.2011.07.003 [arXiv:1105.0951 [nucl-th]].
- [27] R. C. Walker *et al.*, *Phys. Rev. D* **49**, 5671 (1994). doi:10.1103/PhysRevD.49.5671
- [28] L. Andivahis *et al.*, *Phys. Rev. D* **50**, 5491 (1994). doi:10.1103/PhysRevD.50.5491
- [29] C. Berger, V. Burkert, G. Knop, B. Langenbeck and K. Rith, *Phys. Lett.* **35B**, 87
(1971). doi:10.1016/0370-2693(71)90448-5

- [30] J. Litt *et al.*, Phys. Lett. **31B**, 40 (1970). doi:10.1016/0370-2693(70)90015-8
- [31] M. E. Christy *et al.* [E94110 Collaboration], Phys. Rev. C **70**, 015206 (2004) doi:10.1103/PhysRevC.70.015206 [nucl-ex/0401030].
- [32] I. A. Qattan *et al.*, Phys. Rev. Lett. **94**, 142301 (2005) doi:10.1103/PhysRevLett.94.142301 [nucl-ex/0410010].
- [33] J. Arrington, Phys. Rev. C **68**, 034325 (2003) doi:10.1103/PhysRevC.68.034325 [nucl-ex/0305009].
- [34] V. Punjabi *et al.*, Phys. Rev. C **71**, 055202 (2005) Erratum: [Phys. Rev. C **71**, 069902 (2005)] doi:10.1103/PhysRevC.71.055202, 10.1103/PhysRevC.71.069902 [nucl-ex/0501018].
- [35] A. J. R. Puckett *et al.*, Phys. Rev. Lett. **104**, 242301 (2010) doi:10.1103/PhysRevLett.104.242301 [arXiv:1005.3419 [nucl-ex]].
- [36] A. J. R. Puckett *et al.*, Phys. Rev. C **85**, 045203 (2012) doi:10.1103/PhysRevC.85.045203 [arXiv:1102.5737 [nucl-ex]].
- [37] X. Zhan *et al.*, Phys. Lett. B **705**, 59 (2011) doi:10.1016/j.physletb.2011.10.002 [arXiv:1102.0318 [nucl-ex]].
- [38] G. Ron *et al.* [Jefferson Lab Hall A Collaboration], Phys. Rev. C **84**, 055204 (2011) doi:10.1103/PhysRevC.84.055204 [arXiv:1103.5784 [nucl-ex]].
- [39] C. B. Crawford *et al.*, Phys. Rev. Lett. **98**, 052301 (2007) doi:10.1103/PhysRevLett.98.052301 [nucl-ex/0609007].
- [40] R. Milner *et al.* [OLYMPUS Collaboration], Nucl. Instrum. Meth. A **741**, 1 (2014) doi:10.1016/j.nima.2013.12.035 [arXiv:1312.1730 [physics.ins-det]].
- [41] M. Mihovilovic *et al.* [A1 Collaboration], EPJ Web Conf. **72**, 00017 (2014). doi:10.1051/epjconf/20147200017

- [42] A. Gasparian [PRad at JLab Collaboration], EPJ Web Conf. **73**, 07006 (2014).
doi:10.1051/epjconf/20147307006
- [43] A. H. Gasparian [PRad Collaboration], JPS Conf. Proc. **13**, 020052 (2017).
doi:10.7566/JPSCP.13.020052
- [44] D. Rimal *et al.* [CLAS Collaboration], Phys. Rev. C **95**, no. 6, 065201 (2017)
doi:10.1103/PhysRevC.95.065201 [arXiv:1603.00315 [nucl-ex]].
- [45] R. J. Hill and G. Paz, Phys. Rev. D **82**, 113005 (2010) [arXiv:1008.4619 [hep-ph]].
- [46] Z. Epstein, G. Paz and J. Roy, Phys. Rev. D **90**, 074027 (2014) [arXiv:1407.5683 [hep-ph]].
- [47] G. Lee, J. R. Arrington and R. J. Hill, Phys. Rev. D **92**, 013013 (2015) [arXiv:1505.01489 [hep-ph]].
- [48] K. A. Olive *et al.* [Particle Data Group Collaboration], Chin. Phys. C **38**, 090001 (2014).
- [49] I. T. Lorenz and U. G. Meiner, Phys. Lett. B **737**, 57 (2014) [arXiv:1406.2962 [hep-ph]].
- [50] I. T. Lorenz, U. G. Meiner, H.-W. Hammer and Y.-B. Dong, Phys. Rev. D **91**, no. 1, 014023 (2015) [arXiv:1411.1704 [hep-ph]].
- [51] K. Griffioen, C. Carlson and S. Maddox, arXiv:1509.06676 [nucl-ex].
- [52] M. Horbatsch and E. A. Hessels, arXiv:1509.05644 [nucl-ex].
- [53] J. J. Krauth *et al.*, arXiv:1706.00696 [physics.atom-ph].
- [54] A. Huber, T. Udem, B. Gross, J. Reichert, M. Kourogi, K. Pachucki, M. Weitz and T. W. Hansch, Phys. Rev. Lett. **80**, 468 (1998). doi:10.1103/PhysRevLett.80.468
- [55] C. G. Parthey, A. Matveev, J. Alnis, R. Pohl, T. Udem, U. D. Jentschura, N. Kolachevsky and T. W. Hnsch, Phys. Rev. Lett. **104**, 233001 (2010).
doi:10.1103/PhysRevLett.104.233001
- [56] U. D. Jentschura, *et al.*, Phys. Rev. A **83**, 042505 (2011).

- [57] P. A. M. Dirac, Proceedings of the Royal Society of London A 114 (767): p.243-265 (1927).
- [58] M. E. Peskin and D. V. Schroeder, “An Introduction to quantum field theory,” Reading, USA: Addison-Wesley (1995)
- [59] D. TONG, [HTTP://WWW.DAMTP.CAM.AC.UK/USER/TONG/QFT/QFT.PDF](http://www.damtp.cam.ac.uk/user/tong/QFT/QFT.pdf)
- [60] W. E. Caswell and G. P. Lepage, Phys. Lett. **167B**, 437 (1986). doi:10.1016/0370-2693(86)91297-9
- [61] T. Kinoshita and M. Nio, Phys. Rev. D **53**, 4909 (1996) doi:10.1103/PhysRevD.53.4909 [hep-ph/9512327].
- [62] G. Paz, Mod. Phys. Lett. A **30**, no. 26, 1550128 (2015) doi:10.1142/S021773231550128X [arXiv:1503.07216 [hep-ph]].
- [63] A. V. Manohar, Phys. Rev. D **56**, 230 (1997) [hep-ph/9701294].
- [64] J. Heinonen, R. J. Hill and M. P. Solon, Phys. Rev. D **86**, 094020 (2012) [arXiv:1208.0601 [hep-ph]]
- [65] R. J. Hill, G. Lee, G. Paz and M. P. Solon, Phys. Rev. D **87**, 053017 (2013) [arXiv:1212.4508 [hep-ph]].
- [66] A. Pineda, Phys. Rev. C **67**, 025201 (2003) doi:10.1103/PhysRevC.67.025201 [hep-ph/0210210].
- [67] A. Pineda, Phys. Rev. C **71**, 065205 (2005) doi:10.1103/PhysRevC.71.065205 [hep-ph/0412142].
- [68] R. J. Hill and G. Paz, Phys. Rev. Lett. **107**, 160402 (2011) [arXiv:1103.4617 [hep-ph]].
- [69] O. Tomalak, B. Pasquini and M. Vanderhaeghen, Phys. Rev. D **95**, no. 9, 096001 (2017) doi:10.1103/PhysRevD.95.096001 [arXiv:1612.07726 [hep-ph]].
- [70] S. P. Dye, M. Gonderinger and G. Paz, Phys. Rev. D **94**, no. 1, 013006 (2016) doi:10.1103/PhysRevD.94.013006 [arXiv:1602.07770 [hep-ph]].

- [71] M. N. Rosenbluth, Phys. Rev. **79**, 615 (1950).
E. E. Chambers and R. Hofstadter, Phys. Rev. **103**, 1454 (1956).
- [72] R. H. Dalitz, Proc. Roy. Soc. Lond. **206**, 509 (1951).
- [73] C. Itzykson and J. B. Zuber, “Quantum Field Theory,” New York, Usa: Mcgraw-Hill (1980)
- [74] E. Borie, arXiv:1207.6651 [physics.gen-ph].
- [75] B. M. Preedom and R. Tegen, Phys. Rev. C **36**, 2466 (1987).
- [76] I.M. Gel’fand and G.E. Shilov ”Generalized functions”, New York, USA: Academic Press (1964)
- [77] D. Nevado and A. Pineda, Phys. Rev. C **77**, 035202 (2008) [arXiv:0712.1294 [hep-ph]].
C. Peset and A. Pineda, Eur. Phys. J. A **51**, 32 (2015) [arXiv:1403.3408 [hep-ph]].
C. Peset and A. Pineda, Nucl. Phys. B **887**, 69 (2014) [arXiv:1406.4524 [hep-ph]].
- [78] T. Becher, A. Broggio and A. Ferroglia, Lect. Notes Phys. **896**, pp.1 (2015)
doi:10.1007/978-3-319-14848-9 [arXiv:1410.1892 [hep-ph]].
- [79] Gil Paz, *private communication*
- [80] M. C. Birse and J. A. McGovern, Eur. Phys. J. A **48**, 120 (2012) [arXiv:1206.3030 [hep-ph]].
- [81] M. Gorchtein, F. J. Llanes-Estrada and A. P. Szczepaniak, Phys. Rev. A **87**, 052501 (2013) [arXiv:1302.2807 [nucl-th]].
- [82] J. M. Alarcon, V. Lensky and V. Pascalutsa, Eur. Phys. J. C **74**, 2852 (2014) [arXiv:1312.1219 [hep-ph]].
- [83] O. Tomalak and M. Vanderhaeghen, Phys. Rev. D **90**, 013006 (2014) [arXiv:1405.1600 [hep-ph]].
O. Tomalak and M. Vanderhaeghen, arXiv:1512.09113 [hep-ph].
- [84] J. C. Collins, Nucl. Phys. B **149**, 90 (1979) Erratum: [Nucl. Phys. B **153**, 546 (1979)].

- [85] A. Walker-Loud, C. E. Carlson and G. A. Miller, Phys. Rev. Lett. **108**, 232301 (2012).

ABSTRACT**ADDRESSING THE PROTON RADIUS PUZZLE USING QED-NRQED
EFFECTIVE FIELD THEORY**

by

STEVEN DYE**May 2018****Advisor:** Dr. Gil Paz**Major:** Physics**Degree:** Doctor of Philosophy

In 2010 the first extraction of the proton charge radius from muonic hydrogen was found to be five standard deviations away from the regular hydrogen value. Seven years later, this proton radius puzzle still persists, and challenges our understanding of the structure of the proton. An effective field theory analysis using Non-Relativistic Quantum Electrodynamics (NRQED) indicates that the muonic hydrogen result can be interpreted as a large, compared to some model estimates, muon-proton spin-independent contact interaction. The muonic hydrogen result can be tested by a muon-proton scattering experiment, MUSE, that is planned at the Paul Scherrer Institute in Switzerland. The typical momentum of the muons in this experiment is of the order of the muon mass. In this energy regime the muons are relativistic but the protons are still non-relativistic. The interaction between the muons and protons can be described by a new effective field theory QED-NRQED. This document will present elements of this effective field theory, which will include the reproduction of Rosenbluth scattering up to the second power in the inverse proton mass, relativistic scattering off of a static potential, scattering amplitudes up to the inverse proton mass squared, and the determination of the four-fermion contact interactions.

AUTOBIOGRAPHICAL STATEMENT

Name: Steven Dye

Education:

Ph.D. Physics, Wayne State University, Detroit, Michigan, 2012-2017

M.S. Physics, Wayne State University, Detroit, Michigan, 2012-2015

B.S. Physics, Western Michigan University, Kalamazoo, Michigan, 2008-2012

Professional Experience:

Graduate Research Assistant, Wayne State University Dept. of Physics and Astronomy, Detroit, Michigan, 2016-2017

Graduate Teaching Assistant, Wayne State University Dept. of Physics and Astronomy, Detroit, Michigan, 2012-2016

Undergraduate Research Assistant, Western Michigan Dept. of Physics, Kalamazoo, Michigan, 2010-2012

Publications:

Elements of QED-NRQED effective field theory: NLO scattering at leading power, S. Dye, M. Gonderinger, and G. Paz, *Physical Review D*,94 (2016) no.1, 013006